Externally Activated Cork-Shell Microcapsules

FABRICATION OF CORK-SHELL MICROCAPSULES FOR BIOMEDICAL APPLICATIONS WITH FOCUS ON ULTRASOUND TRIGGERED RELEASE

By JONATHAN DOROGIN, BASC

A Thesis Submitted to the School of Graduate Studies in Partial Fulfilment of the Requirements for the Master's Degree of Biomedical Engineering

McMaster University, Master's OF ENGINEERING (2018) Hamilton, Ontario (Biomedical Engineering)

TITLE: Fabrication of Cork-shell microcapsules for biomedical applications with focus on ultrasound triggered release

AUTHOR: Jonathan Dorogin, BASC (University of Waterloo)

SUPERVISOR: Professor Todd R. Hoare

NUMBER OF PAGES:

Lay Abstract

This thesis focuses on the fabrication of complex microcapsules that can be deliver therapeutic drugs on-demand using ultrasound waves. These microcapsules are composed of a water-based core and a biologically inert shell into which particles are embedded. Upon the application of ultrasound, these embedded particles (like corks on a bottle) are popped out to release the "corks" from the shell, creating pores from which the drug in the microcapsule core can be released. In the absence of ultrasound signals, the microcapsules do not release any of their contents, making these effective for "on-demand" release. These microcapsules are made using a modified process based on electrospraying which allows very precise control over the microcapsules' physical properties, incorporating a key modification that overcomes an inherent issue with the general technique. These microcapsules also improve on currently used ultrasound triggered drug delivery systems by requiring shorter periods of ultrasound and/or enabling better control over the dynamics of drug release following the ultrasound pulse.

Abstract

Developing a drug delivery vehicle that can control the release kinetics of a therapeutic drug on demand has great potential to improve health by allowing health care professionals to maintain the drug concentration in its therapeutic window and increase the efficiency at which treatment is administered.

On-demand release can be triggered by a range of stimuli including magnetic, radiation, and ultrasound activation. Of the three, ultrasound is the only one indiscriminate of the chemical properties of the material and is the most widely available clinically, which makes it versatile and applicable for many systems. However, existing strategies that use ultrasound as a release stimulus either pop the microcapsules altogether (enabling no subsequent effective control over the kinetics of drug release) or require continuous ultrasonic administration (typically impractical in a clinical setting), both of which are suboptimal. Overcoming at least of these shortcomings would vastly improve on the technology.

In this thesis, microcapsules with a complex shell were fabricated using a modified electrohydrodynamic approach named immersion coaxial electrospraying, which allowed for an increased polymer loading in the shell and improved manipulation of microcapsule size. The complex shell structure of the microcapsules incorporated silica microparticles that acted as corks plugging pores between the inside and outside of the microcapsule. The modified microcapsules were shown

to release their payload in the presence of a focused ultrasound signal, while uncorked microcapsules do not release. Release kinetics were shown to be adjustable based on the number of corks initially present in the shell of the microcapsule material.

Altogether, the cork-shell microcapsules fabricated in this thesis show promise as a tunable on-demand drug delivery vehicle that is able to better control release compared to conventional ultrasound triggered microcapsules.

Acknowledgements

The contents of this thesis are more than just a series of experiments and their results – the time I have spent working on this project helped me to grow as an intellectual, and to become a better person. I could not have done it alone. First and foremost, I would like to thank Dr. Todd Hoare for accepting me as a student and guiding me in this journey. He is an incredibly intelligent person who has become a role model to me in more ways than one. I have always been innovative and have found science interesting, but Dr. Hoare's passion has taught me to push through difficulties, develop creative solutions, and have fun with science. I will forever look up to you as a mentor whose kindness and trust made me a better engineer and a better human being. I would also like to thank Dr. David Koff for continuing to push me and inspire me in this project. Your insight as a medical professional about how this project will help progress the fields of radiology and oncology would re-invigorate my drive. Thank you to Jane Castelli for preparing grants and other documents that will allow this project to live on even after I finish working on it, and for making sure that Dr. Koff would be at bimonthly meetings. I would also like to thank Dr. Alfred Yu from the University of Waterloo for setting me on the right path in properly understanding ultrasound physics, and Dr. Jose Moran-Mirabel, Dr. Troy Farncombe, Dr. Alex Adronov, and Marcia Reid for letting me use your equipment. I would like to thank Paul Gatt for helping me with all of my experimental setup needs. Most of the custom equipment used in the experiments outline in this paper would not have been possible

without your help. And to the rest of the faculty and staff at McMaster University, thank you for running such a wonderfully welcoming institution.

Staff and faculty aside, I have yet to acknowledge my lab mates and my undergraduate students. To my undergraduate students Haniah Sheikh and Laura Carter, I am forever in your debt. The two of you have done work that helped this project reach the state that I am so very proud of as of this writing. Haniah, thank you for believing in this project early on. Your future is very bright and whatever field you choose to follow, I will be very proud of you. Laura, thank you for teaching me how to manage my time, and forcing me to become a better supervisor. You're both extremely smart, and you'll go really far. 19 year old me would not have been able to grasp nearly as much information as you have. To my lab-mates – many of you have become family to me. Thank you Fei and Somiraa for always helping me with my electrospraying questions. Thank you, Nicola, Kelli, Maddi, Eva, Ali A, Ali B, and everyone else in our lab for all of the fun and insightful conversations. As a team, we have all been through a lot. We've all smiled together, laughed together, cried together, and grown together.

Finally, I would like to thank my friends and family who were here with me before this entire journey started and who helped me get through all of the good times and the hard times. I never thought I would end up in grad school, but you've all been so supportive of me and my choices and I love you all. To my mom and dad, thank you so much for everything ever. I can't thank you enough for giving me the life I have. I can't imagine how hard life must have been for you to immigrate twice, start anew, struggle to succeed, and always continue smiling. The two of you have always been my biggest

inspirations and exposed me to so many things in my life, and I only hope to be as good of a parent as you one day. Thank you, mom, dad, and grandpa, for instilling a curiosity in me for engineering, and biotechnology. Thank you to both of my grandmothers for being there for me and always telling me how much you love me. Thank you to my little sister Netta who doesn't realize how proud I am of her and how much she's grown. I'm not perfect, but you're always my little sister and I'm always here for you. Thank you to all of my friends who helped me get through this master's by keeping me grounded and reminding me of the important things in life. You've all helped knowingly or unknowingly to become the person I am today that's writing this thesis.

Rest In Peace, Monika. You were an amazing student and your smile was contagious. You're in a better place now.

TABLE OF CONTENTS

Contents

LIST OF FIGURES

LIST OF TABLES

LIST OF EQUATIONS

List of Abbreviations:

APTES	(3 Aminopropyl) Triethoxysilane
ATR-FTIR	Attenuated Total Reflectance Fourier Transform Infrared Spectroscopy
BCS	Bovine Calf Serum
BSA	Bovine Serum Albumin
DCM	Dichloromethane
DMAP	4-Dimethylaminopyridine
DMEM	Dulbecco's Modified Eagle Media
DMF	N,N-Dimethyl Formamide
EDC	N-3-dimethylaminopropyl-N-ethyl carbodiimide hydrochloride
EHD	Electrohydrodynamic
FITC	Fluorescein Isothiocyanate Isomer 1
LCST	Lower Critical Solution Temperature
MRI	Magnetic Resonance Imaging
MTS	(3-(4,5-dimethylthiazol-2-yl)-5-(3-carboxymethoxyphenyl)-2-(4-sulfophenyl)-2H-tetrazolium)
PBS	Phosphate Buffered Saline
PEG	Polyethylene Glycol
PLGA	Poly (Lactic-co-Glycolic) Acid
PS	Penicillin Streptomycin
PVA	Polyvinyl Alcohol
Rhd123	Rhodamine 123
RhdB	Rhodamine B
SEM	Scanning Electron Microscopy
SPION	Superparamagnetic Iron Oxide Nanoparticle
T_g	Glass Transition Temperature
US	Ultrasound/Ultrasonic, depending on the context
UV	Ultraviolet
UV-Vis	Ultraviolet-Visible

Declaration of Academic Achievement

The majority of the written work written herein was conceived, conducted, analyzed, and written by the author of this thesis, in consultation with Dr. Todd Hoare, with the exception of the following:

Chapter 2: Haniah Sheikh, Laura Carter, and I fabricated some of the microcapsules together. Laura Carter performed the size analysis necessary to create Figure 2.12. Laura Carter and Nicola Muzzin were responsible for the cell culturing and proliferation studies, whose results are seen in Figure 2.17. Paul Gatt built the custom setups for the fabrication.

Chapter 3: Haniah Sheikh, Laura Carter, and I performed some of these release studies together. Paul Gatt built the custom waveguide and sample holders. Mandakini Jain of Dr. Troy Farncombe's lab developed the protocol for, and trained, assisted, and analysed with the ultrasound calibration equipment. Her contribution resulted in Figure 3.10 and Figure 3.11.

Chapter 1 - Introduction

1.1 Background

Until the 1960s, the delivery of medication consisted largely of pills and capsules that would dissolve in water and offer little to no control of release dynamics[1]. Since then, the fields of targeted and controlled drug delivery have been intensively investigated. A controlled drug delivery vehicle is a system that is able to more effectively moderate the rate of release of a payload, while a targeted delivery vehicle is able to release its payload in a specific location. The first proposal for a controlled drug delivery vehicle was for the use of silicone rubber to mediate zero-order (i.e. constant) drug release over time[2]; since, a range of materials and technologies have been developed (including injectables, stents, patches, inhalers, and other approaches) that offer control over drug release kinetics[3].

The initiation and control over the kinetics of release from targeted and controlled drug delivery systems may be subcategorized as endogenous or exogenous[3, 4]. Endogenous release mechanisms rely on the specific microenvironment surrounding the drug delivery vehicle (e.g. temperature, pH, and/or enzyme concentration[4-8] to control release. While in most designed vehicles these variables simply regulate the kinetics of release based on material-microenvironment interactions via a passive process, in other cases drug delivery vehicles are specifically designed to actively release drug at a particular pH or temperature (e.g. an infection site or a rapidly metabolizing tumour[7, 9-11]). Conversely, exogenous release depends on the influence of some signal from outside of

the body, most commonly by a magnetic field, various types of irradiation, and/or ultrasound[4, 12-15], and always represents an active form of release control.

Beyond the mechanisms of activation, drug delivery vehicles may be fabricated in many different geometries to serve a specific purpose. Microcapsules, microfibres, vesicles, spheres, gels, patches, cages, liposomes, and more can be made to provide therapy with different kinetics and/or degrees of localization[4, 5, 8-10, 16-22]. Alternately, clusters of multiple types of nanoparticles or fibres can be stimulated to de-cluster through thermal activation, ultrasound triggering, or pH changes[9, 21, 23]. Thermally responsive drug carriers in the form of gels, nanoparticles, membranes, nanotubes, and more[6, 8, 17, 20, 21, 24] can offer control over release kinetics and biodistribution via temperature-driven changes in swelling, colloidal stability, or conformation.

The types of fabrication methods used to create micro/nano drug delivery vehicles are also quite expansive. To create particulate-based drug delivery systems, common fabrication methods include (but are not limited to) more traditional strategies such as single or double emulsification or micellization as well as more advanced strategies such as self-assembly, electrohydrodynamics, or microfluidics [5, 12, 21, 25-34]. Although the simpler methods offer less control over the size and morphology of the delivery vehicle produced, they remain largely popular due to their ease of use. The more complex methods either require special equipment for fabrication, the combination of several simple fabrication processes, and/or the pre- or post-manipulation of chemicals to make smarter and more controlled systems.

This chapter will discuss some key concepts and developments in the fabrication, morphology, and activation mechanisms related to the design of controlled and targeted drug delivery vehicles as an introduction to the experimental work performed in this thesis. In particular, the review will focus on the design of particulate delivery vehicles that can be dispersed in water and injected into the body.

1.2Particulate Drug Delivery Vehicles

A plethora of particle-based drug delivery vehicles has been reported based on various materials fabricated with varying morphologies most appropriate to the intended function of the vehicle.

1.2.1 Materials

Most reported particulate drug delivery vehicles are fabricated from some combination of natural or synthetic polymers, lipids, and/or inorganic materials[10, 35-38]. In many cases, smart materials are incorporated into the matrix of the primary material to enable a response to an activation signal[6, 39-41]. Various stabilizers in the form of surfactants, proteins, and/or other polymers as well as targeting agents designed to bind to specific sites of interest in the body are also often co-formulated to provide improved performance[5, 10, 42-46]. Finally, and most obviously, the particle is loaded with a payload that can be a real drug, a model drug, or anything intended to be released from the vehicle.

The role of the main material constituent is to provide defined dimensions for the delivery vehicle (which play a key role in controlling its biological fate), engineer the conditions under which the vehicle will degrade, and serve as a matrix to load one or more desired drugs. For hydrophobic drug payloads, degradable and poorly water soluble polymers such as poly(lactic-co-glycolic acid) (PLGA)[36, 44, 47] and other polyesters (like polycaprolactone) [48] as well as various polyurethanes (polycarbonate-urethane) [48], polyureas (bis-chloroethylnitrosurea) [22, 48], polymethylacrylates[49] and other degradable polymers are most commonly used, either alone or fabricated in block copolymers with hydrophilic polymers such as poly(ethylene glycol) (PEG)[22, 50, 51]. Surfactant micelle [9, 52, 53] and solid lipid particle [9, 15, 37, 38, 40] delivery vehicles are also very popular for delivering more hydrophobic drugs. In contrast, hydrophilic drug payloads are typically delivered via capsular deliver vehicles that have an internal aqueous core (e.g. liposomes[15, 40] or polymersomes[21, 54, 55]) or gel-based delivery vehicles[8, 56, 57], both of which have a substantial volume into which water-soluble drugs can partition. In the latter case, various polysaccharides and variations of polyethylene glycol (PEG) such as POEGMA[8, 20, 43] are most commonly used. Some of these vehicles (e.g. liposomes or polymersomes) also have both hydrophilic (core) and hydrophobic (shell) binding sites, enabling co-delivery of both hydrophobic and hydrophilic drugs[1, 33, 48, 58-60].

Smart materials are frequently used as either the primary component of or a dopant into drug delivery vehicles to allow the system to respond to various environmental or external conditions. The most popular of these materials include materials whose bonds break down at certain pH values (e.g. polydopamine [10, 61, 62], or boronic acids[62, 63]),

materials that exhibit an lower critical solution temperature (LCST) such as poly(N-isopropylacrylamide) [20, 41], or materials that can actuate an external signal such an external magnetic field (superparamagnetic nanomaterials) or light (photosensitizers) into an actionable internal stimulus [22, 24, 64].

Surfactants, or surface-active agents, are amphiphilic molecules that are used to modify an interface to help to reduce the surface tension at the interface [65-68]. The potential of surfactants to stabilize an interface is broadly predicted based on the hydrophilic-lipophilic balance (HLB) number of the surfactant, which takes into account the ratio of hydrophilic to hydrophobic moieties in a surfactant. Table 1.1 depicts the predicted capacity of surfactants with various HLB numbers to act to stabilize interfaces[67].

Table 1.1: HLB Scale

Surfactant solubility/ Behaviour in water	HLB number	Application	
No dispersibility in water	0		–
	2		
	4		W/O emulsifier
Poor dispersibility	6		
Milky dispersion, unstable	8		Wetting agent
Milky dispersion, stable	10		
Translucent-to-clear solution	12	Detergent	O/W emulsifier
	14		
Clear solution	16	Solubilizer	
	18		

As an example of the use of the scale, if the delivery vehicle is an oil or a hydrophobic polymer like PLGA or PEG intended to be incorporated in a continuous water phase, a surfactant with a large HLB value would be preferable to provide a more favourable

surface interaction between the two phases. Surface-active molecules commonly used to formulate particulate drug delivery formulations include both naturally derived polymers and proteins (e.g. albumin, gelatin, lignin, cruciferin, biotin, fatty acid esters [5, 48, 68-70]) and synthetic materials (e.g. polyvinyl alcohol, the Span and Tween surfactant families, Tergitol, Sodium Dodecyl Benzene Sulfonate [32, 44, 65-68]). Alternately, or in addition to, surfactants, block copolymers consisting of one self-associating block and one sterically stabilizing block (e.g. PLGA-PEG) can eliminate the need for additional surfactants by incorporating the surface stabilizing agent (in this example PEG) directly into the polymer structure[71, 72].

Targeting ligands, if included in a particulate drug delivery formulation, are intended to specifically bind with one specific cellular structure on the tissue of interest. The most commonly applied targeting ligands include DNA (e.g. TAT sequences or aptamers[58]), cytokines (e.g. tumor necrosis factor α (TNF-α)), peptides[73], and antibodies [74, 75]. However, care should be taken when choosing a surface agent, as there are always positive and negative attributes to each modification. For example, increasing the number of different targeting ligands may lead to shorter circulation times in the body due to lower non-specific binding affinities[76, 77].

1.2.2 Drug Delivery Vehicle Products

Various types of particulate-based delivery systems can be fabricated depending on the materials and fabrication techniques used for formulation. [4, 9, 21, 36, 72, 78]

Micro/nano-spheres or particles can be identified as a delivery vehicle that is essentially solid throughout. Various materials such as polymers, ceramics, and metals may be used to fabricate the particles [47, 59, 72]. Relative to other vehicles, micro/nanospheres are typically more stable materials and will either not degrade or degrade over a well-defined period of time. The most common polymers used in practical drug delivery applications include PLGA, alginate, chitosan, and poly(ethylene glycol) dimethacrylate[28, 48, 53].

While drug is typically loaded within the particle, nanoparticles with high surface areas can also be used to adsorb drug on their surface and thus transport drug within the body. Graphene, a 2D sp^2-hybridized carbon analogue, has been particularly widely investigated for this purpose given its high surface area and high capacity for absorbing a variety of payloads depending on how it is surface modified[60, 79]. Carbon dots[80], carbon nanotubes[21, 81], quantum dots (with simultaneous delivery and imaging potential)[25, 81], and mesoporous silica (which can control release to some degree based on the internal mesopore size)[10, 26-28, 82], and other high surface area nanoparticles have been used in a similar context.

Recent research has expanded the compositional variability within the micro/nanoparticle area to enable simultaneous delivery of drugs requiring different microenvironments using the same particle. For example, Janus nanoparticles are particles consisting of two hemispheres, each with their own material properties. Such particles can be especially useful for drug delivery as one half of the vehicle can hold a binding agent, and the other half can contain a smart material[78, 83]; alternately, one half of the vehicle can enable drug loading while the other half can engage in another

biological function (e.g. rapid gas generation to enable particle propulsion[4, 37, 84-86]). Figure 1.1 provides an example of such a Janus particle.

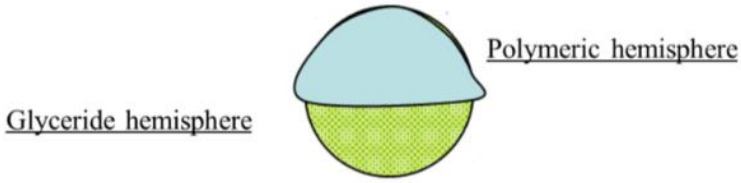

Figure 1.1: Schematic of a Janus particle. Adapted from [78]

Micro/nano-capsules are similar to micro/nano-particles in that they can be composed of a multitude of materials; however, they are a multi-phase systems that typically contain a defined core made of one material and one or more shell(s) made of a different material[9, 74, 87, 88]. These capsules can protect drugs that are soluble with the continuous phase in which the delivery vehicle is suspended. As an example, a water/oil/water (or W/O/W) delivery vehicle holds a water-soluble payload inside a hydrophobic shell that is stabilized with surfactants and is suspended in an aqueous solution. Figure 1.2 shows how the morphologies of capsules and spheres differ[72]. In this example, PLGA is the primary constituent, the surfactant is arbitrary, bone morphogenic protein-2 (BMP-2) is the payload, and BSA is a protein that stabilizes the internal aqueous cavity in the micro/nanocapsule and/or the BMP-2 protein in the hydrophobic PLGA matrix.

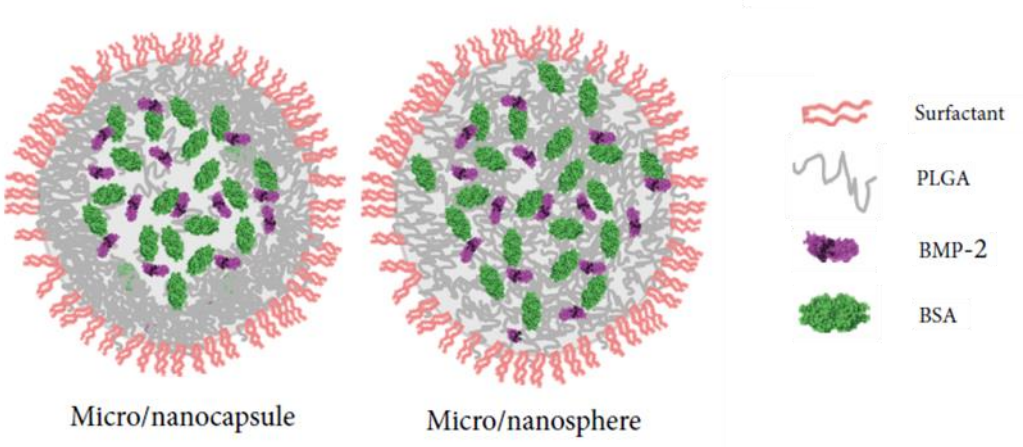

Figure 1.2: Schematic comparing micro/nanocapsules with micro/nanospheres. Adopted from [72]

Complex particle interfaces can also be fabricated using multi-component techniques. Single emulsion approaches integrating a phase change material can result in the formation of dimpled "golf-ball" morphologies when the phase change is induced (Figure 1.3A) [47]. Alternatively, one can make Janus microparticles that have different morphologies on different parts of the shell (Figure 1.3B)[78] or modify the shell material with some kind of binding complex once the surface has already been made[89]. However, all these methods require either post-processing of an already made particle or selective degradation of one or more material(s) in the shell[78].

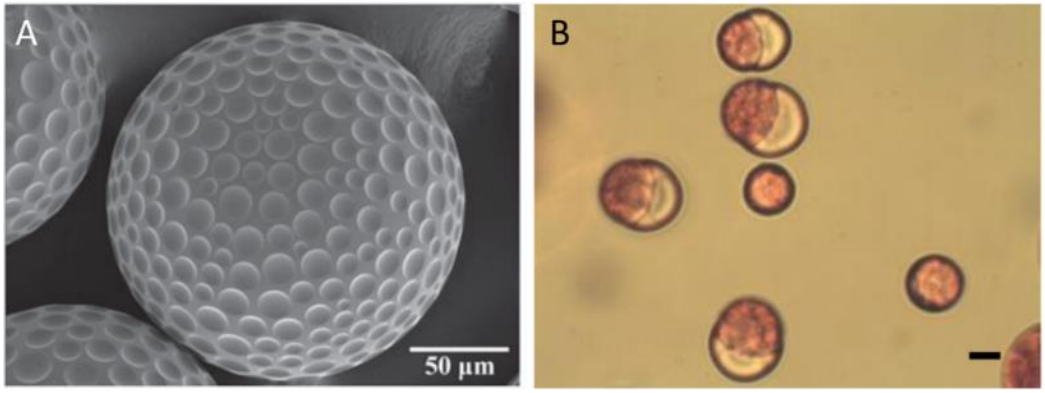

Figure 1.3: Complex microparticle structures. (A) golf ball-shaped PLGA particle fabricated by using a phase-changing material. (B) Janus particles consisting of PLGA and a hard fat . Adapted from[47, 78]

Vesicles or micelles can be formed by allowing amphiphilic materials, such as surfactants and diblock copolymers, to self-assemble[21, 36]. In these systems, the primary constituents themselves control the geometry and structure of the materials formed, with both the HLB and the relative lengths and geometries of the hydrophile and hydrophobe in each amphiphilic delivery vehicle regulating whether a vesicle or micelle is formed and the size/shape of that carrier. When the assembly material is a phospholipid, liposomes consisting of a cell membrane-like bilayer structure are formed, a type of capsule delivery vehicle with an aqueous inner layer, a lipid bilayer, and an aqueous continuous phase. Figure 1.4 depicts some drug delivery morphologies consisting of amphiphilic materials.

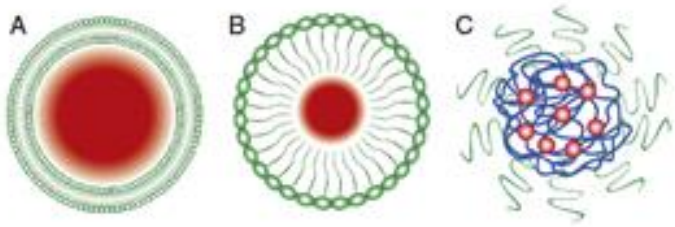

Figure 1.4: Schematic comparing amphiphilic-material-based drug delivery vehicles. (A) liposomes, (B) a surfactant micelle, (C) a amphiphilic polymeric micelle. Adopted from [21]

Coacervates are formed based on the physical interaction and subsequent phase separation of different components, typically driven by ionic or supramolecular interactions[20, 36, 39, 56, 57].

Dendrimers are also widely used for delivering more hydrophilic payloads. Dendrimers are systematically branched nanoparticles formed by conjugating repeated generations of branches from a common core. Their highly branched nature has been applied to uptake drugs such as paclitaxel and doxorubicin and release them over controlled periods of time via either simple diffusion or more active means[22, 49, 53]. Some examples of dendritic drug delivery vehicles include dendritic polydopamine[16, 49], propanoic acid derivatives[90], and dendritic PEG derivatives such as tacopherol polyethylene glycol succinate (TPGS)[91].

Nanogels/microgels are hydrogel-based nanoparticles/microparticles and are also attractive for delivering water-soluble drugs as a function of swelling[92] , degradation[92], and/or active release[8, 49]. While nanogels can in principle be made

from any water-soluble polymer, nanogels based on poly(ethylene glycol)[49], poly(oligoethylene glycol methacrylate)[8], or pectin[92] have been particularly investigated for drug delivery.

1.3 Fabrication Processes

Depending on the type of particulate drug delivery vehicle targeted, there are multiple different approaches for fabricating the different delivery vehicles ranging from very simple processes that only require stirring to more complex methods requiring specialized equipment.

1.3.1 Emulsions

Emulsion-based fabrication techniques are simple, scalable, and adapted across many fields. An emulsion consists of a material dissolved in one phase that is dispersed in a different (and immiscible) continuous phase. For drug delivery systems, these are typically oil-in-water (O/W) or water-in-oil (W/O) systems. For example, in an O/W fabrication, the primary constituent of the drug delivery vehicle and the payload are dissolved in an organic solvent. That organic solution is then poured into a larger volume of an aqueous solution and stirred rapidly. In order to improve the stability of the product, surfactants are typically also included into the mixture. In most cases, the dispersed phase solvent is then evaporated to solidify the micro/nanoparticle, a process referred to as the emulsion-evaporation method.

Another degree of complexity can be introduced to make a capsule using a process called double emulsification, particularly effective for encapsulating drugs that are soluble in the continuous phase. Briefly, in a W/O/W example (Figure 1.5), a water-soluble drug is dissolved in an aqueous phase with some surfactants. This solution is poured into a larger volume of an organic solvent in which the primary constituent of the delivery vehicle is dissolved. The two are vigorously mixed together, after which the product is transferred to a continuous aqueous phase containing another surfactant with an opposite HLB value and again emulsified. Evaporation of the organic solvent again solidifies the organic phase, in this case to create a solid capsule around an aqueous core instead of a solid nanoparticle[72].

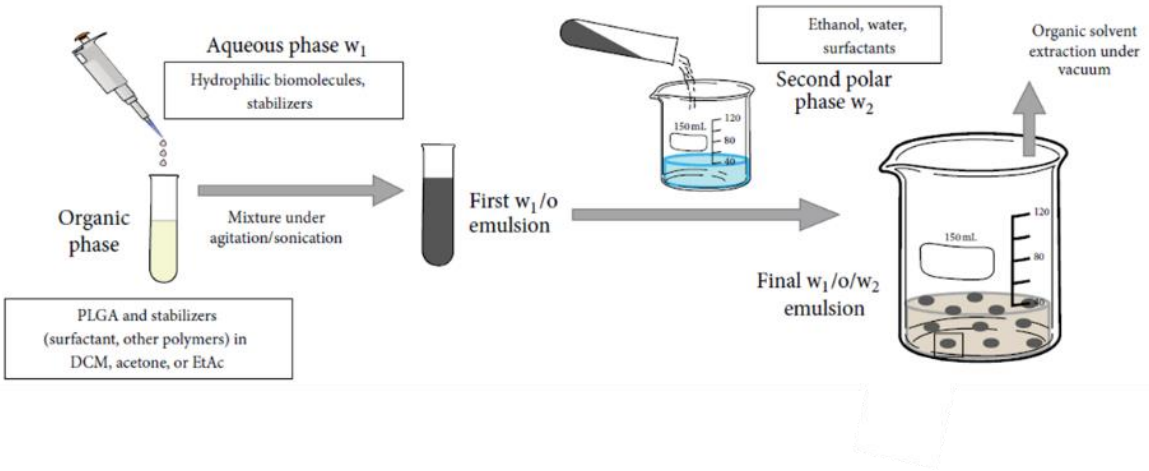

Figure 1.5: Example of a double emulsion fabrication process. Adapted from [72]

The process yields a large quantity of product, but lower encapsulation efficiencies are typically observed [34, 44]. Single emulsification processes, in which the drug is only soluble in the dispersed phase, typically lead to higher encapsulation efficiencies than

double emulsification processes, in which the drug is soluble in both the inner core phase and the continuous phase.

1.3.2 Controlled Flow Processes

The broad polydispersity and often variable encapsulation efficiency observed in normal shear-based emulsion and double emulsion fabrication is a result of the inconsistency of the shear field experienced by each particle[31]. This inconsistency can be addressed by making drug delivery vehicles one by one. Two common processes are microfluidics and electrohydrodynamics. Microfluidics provides control over the size, shape, and components of the vehicle by creating a chip with specially designed flow channels. By controlling the size and geometry of the channels and the flow rates of the solutions, precise control over the local shear field and thus the particle size and shape can be achieved for individual vehicles[34, 55, 93]. Complex and simple delivery vehicles can equally be made using this process. Figure 1.6 depicts some of the various delivery vehicle morphologies achievable using microfluidics.

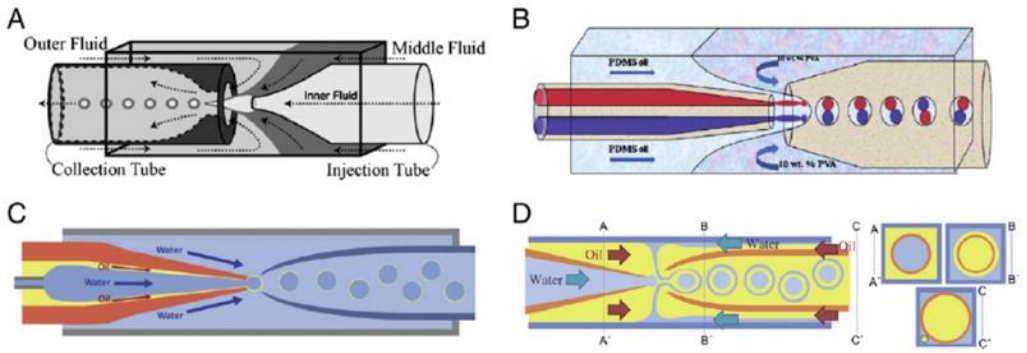

Figure 1.6: Microfluidic fabrication of drug delivery vehicles demonstrating the versatility of the fabrication process. Adapted from [55]

Electrohydrodynamic fabrication (also referred to as electrospraying or EHD) also uses controlled flow for fabrication. The only difference is that microfluidics requires a chip for fabrication while EHD requires a high voltage source attached to an electrically conductive extruder, like a needle [30, 48, 94]. The high voltage source induces shear forces on individual droplets, providing a higher degree of control on size and shape relative to traditional emulsification processes. EHD without any modifications would yield materials like a single emulsion, but advances in the field have introduced the use of coaxial and triaxial extruders to make multiphase drug delivery vehicles[43, 95, 96]; Figure 1.7 depicts an example of such a complex coaxial EHD fabrication process, the products of which are visualized using fluorescence. Although EHD provides good control over fabrication and can typically produce particles at a somewhat faster rate than microfluidics, more complex structures can be developed using microfluidics due to the more precise shear fields and regulated fluid interactions that can be achieved[48].

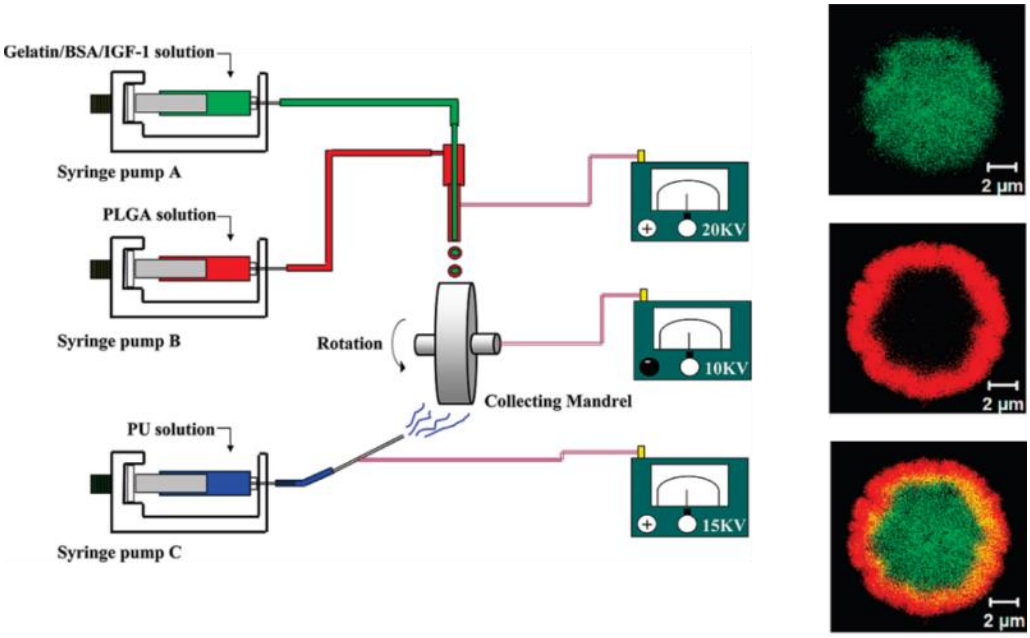

Figure 1.7: Coaxial electrohydrodynamic fabrication using fluorescent labels to show the cross section of the product. Adapted from [96]

While both microfluidics and EHD provide control over the delivery vehicle morphology and size, these processes have an innate limitation in terms of small batch sizes and slow throughput restrictions which inevitably lead to difficulties with scaleup[34, 55]. For example, electrospinning a heart valve can take as much as 10 hours[97].

1.3.3 Other Processes

There are also many other fabrication processes that can be applied to create particulate drug delivery systems. Gel fabrication is commonly achieved by the deposition of material into a mould, and allowing the components to cross-link, either with time, or by additional stimulus such as heat and UV curing[6, 20, 51, 56, 57, 98, 99]. Drug delivery vehicles may

also fabricated via spray drying, a process that produces a powder form of the delivery vehicles using heat to evaporate the solvent[92]. Other methods include complex coacervation[100, 101], and flash nanoprecipitation[102], to name a few.

1.4 Release Mechanisms

1.4.1 Release Mechanisms

Two primary mechanisms are typically used to govern controlled release – diffusion and degradation[103].

1.4.1.1 Diffusion-Based Systems

In diffusion-based systems, drug is loaded either directly into a polymer matrix (as a solid solution or a dispersion) or dissolved within a reservoir. The gradient in drug concentration inside and outside the delivery vehicle promotes drug release, with the affinity between the drug and the matrix in a matrix delivery system and the permeability and porosity of the reservoir membrane in the reservoir delivery system enabling tuning of release kinetics[103].

1.4.1.2 Degradation-Based Systems

Degradation-based systems rely on the material that is holding the drug to break down and thus free the previously entrapped contents[103]. Degradation can be localized at a surface or occur throughout the bulk, and the process can be initiated by friction, abrasion, fatigue due to cyclical loading, interactions with different physical states,

interaction with different microenvironments, and various chemical stimuli[103]. The degradation time can typically be controlled by using different polymers, polymers with different molecular weights, or modifying the polymer with additional materials[103].

1.4.2 Pharmacokinetics

The pharmacokinetics of a drug play an important role in determining how effective a treatment is. A therapeutic window of effective drug concentration is illustrated in Figure 1.8, [49, 103], above which the drug is toxic and below which the drug is therapeutically ineffective.

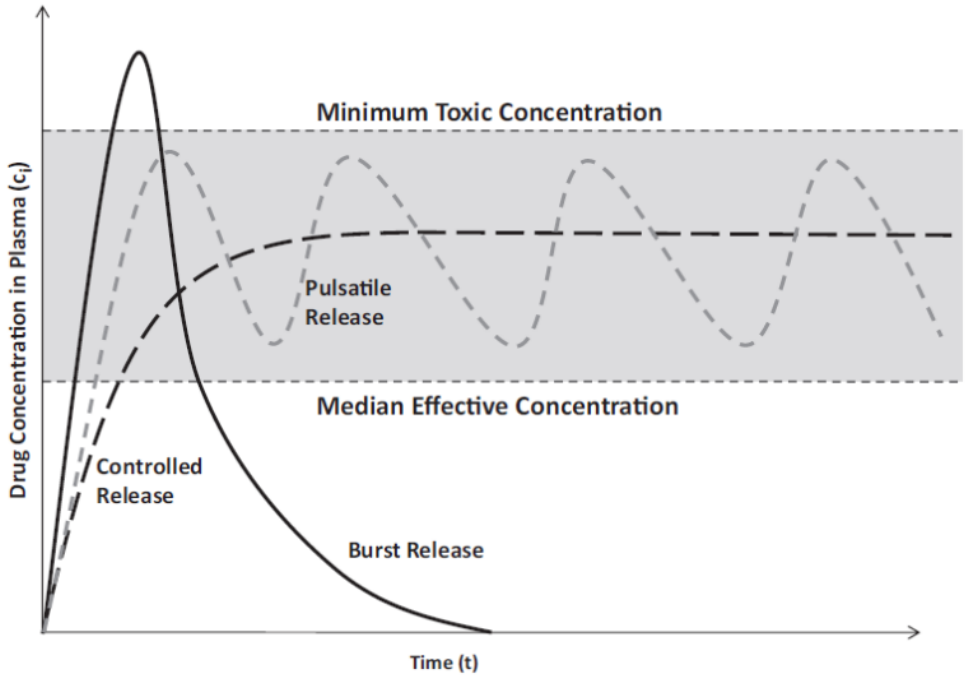

Figure 1.8: Therapeutic window associated with controlled drug release. Adapted from [49]

1.4.2.1 Release Kinetics

The rate of release of a drug is important to regulate in controlled and sustained release applications. In most applications, zero-order release (i.e. constant drug release rate over time) is sought due to its capacity to maintain a drug concentration at an exact level within the therapeutic window[103, 104]. Symmetric membrane-based reservoir devices typically exhibit this type of release profile, although fibrous delivery vehicles typically show zero-order release radially but not tangentially and more asymmetric vehicles will show less uniform release. In comparison, symmetric matrix delivery vehicles instead exhibit first-order release, in which a higher amount of drug is released early in the release process and release tapers off over time [103-105]. First-order release allows drug concentrations to reach the therapeutic window quickly, although remaining in the window is quite challenging and drug concentration is more likely to exceed the minimum toxic concentration threshold [104, 105].

Pulsatile release provides an opportunity to reversibly enter the therapeutic window "on demand", either in an on-off manner or in a manner in which the "on" switch can be timed followed by some sort of controlled release[49, 103-105]. For such a system to exist, there has to be some type of external activation, leading to extensive research in the field of controlled, targeted, and on-demand drug delivery. The thesis work attempts to achieve on-demand and pulsatile release so as to effectively maintain within the therapeutic window.

1.4.3 Endogenous Release

Endogenous release systems have the potential to deliver drugs where and when they are

needed by responding to the surrounding microenvironment of the patient. The three most common microenvironments considered in such designs are areas with varying pH, enzyme concentrations, and temperatures, although other types of endogeneous signals (e.g. glucose[106], inflammatory markers like H_2O_2 [63], DNA sequences [74], etc.) also exist.

1.4.3.1 pH Responsive Delivery Vehicles

In pH-based targeted drug delivery, vehicles could be designed to degrade or swell in a more acidic environment, characteristic of inflammation sites or rapidly metabolizing cancerous tissues[7, 9, 16] and/or the lysosome/endosome of cells once a drug is internalized[10]. Alternatively, pH-dependent materials have been reported that can selectively swell, compress, or break down in more basic microenvironments[7, 10], of potential use to protect drugs in the stomach but release them in the upper intestine. Figure 1.9 shows some of the more common ways in which pH can be applied to drive site-specific release. In any case, pH sensitive delivery vehicles must include ionizable chemical groups to initiate the conformation or degradation changes desired, most commonly carboxylic acids or amines [6, 7, 9, 16].

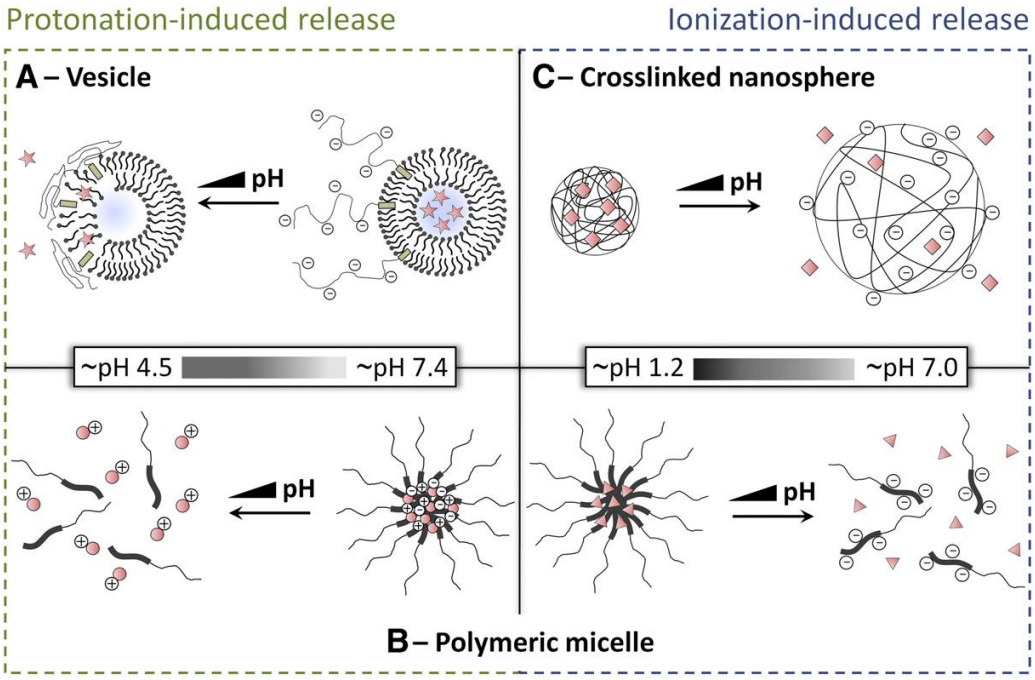

Figure 1.9: Mechanism of triggered drug release based on different types of pH-responsive drug delivery vehicles. Adapted from [9]

However, the selectivity of many pH-responsive release vehicles is in many applications minimal given the multiple types of pH gradients present *in vivo*. As such, more complex multi-component delivery vehicles are now being explored. For example, polydopamine has been used to coat microparticles and conjugate target ligands which will degrade in acidic environments in order to expose the protected payload[10, 41]. This type of additional modality is also becoming more common for other mechanisms of drug release in an effort to make "smart" materials that only release their contents when and where it is desired.

1.4.3.2 Enzyme Responsive Delivery Vehicles

Enzymatic response is attractive given that different enzymes at different concentrations are inherently present in different tissues or different disease states [5, 107]. Among such approaches, phosphorylation and dephosphorylation of materials is commonly pursued, as phosphates are easily cleavable by enzymes[5]. Another example is the glucose oxidase-mediated destruction of polymeric vesicles composed of block copolymers of PEG and poly(propylene sulfide) (PPS), the latter of which oxidizes in the presence of glucose and glucose oxidase to eliminate the amphiphilicity of the vehicle and thus drug release via vesicle disassembly[5, 108]; such systems containing insulin can meter insulin release in response to changes in glucose concentration[35, 109]. Degradation of hyaluronic acid-based delivery vehicles in the presence of hyaluronidase has also been widely used for controlled release, particularly within cancer cells in which hyaluronidase is often up-regulated[110].

The drawback of some of these systems is their relative lack of stability, as the body can naturally break down the delivery vehicle non-specifically in environments with lower enzyme concentrations. Control in this scenario requires an additional layer of complexity to ensure better mechanics and release dynamics[5, 35, 109, 111, 112]. In particular, pectin, chitin, and chitosan are polysaccharides that are commonly used for enzyme-controlled drug release as protective agents from stomach enzymes to slow down the degradation cycle of the delivery vehicle, allowing for better controlled release[5, 35, 92, 109]. Another difficult aspect of enzymatically controlled systems is their necessity to be fabricated and stored in controlled pH environments, particularly relative to the

conditions best suited for loading and stabilizing a particular drug [5, 35, 41, 92, 107, 109, 112].

1.4.3.3 Thermally Responsive Delivery Vehicles

Temperature controlled release allows the delivery vehicle to swell, contract, or evaporate upon changing temperatures[6, 18, 21, 113]. Most commonly this is manifested by materials like poly(N-isopropylacrylamide) (PNIPAM) and, more recently, poly(oligoethylene glycol methacrylate) (POEGMA), both of which exhibit a lower critical solution temperature (LCST) close to physiological temperature[8, 20, 110, 114]. As such, when these materials are heated, they contract to either precipitate the vehicle at a target site or convectively squeeze drug out of the hydrogel matrix to induce site-specific release[8, 12, 21, 110]. Other systems may use the temperature in conjunction with LCST polymers to open or close pores on membranes to facilitate diffusion through a more permeable membrane at higher temperatures. Figure 1.10 depicts the various scenarios around how drug release can be mediated in using LCST as a method of control. Alternately, other materials like N-perfluoropentane can vaporize in similar conditions and cause pressure-driven release via the bursting of capsules or microbubbles[113, 115, 116].

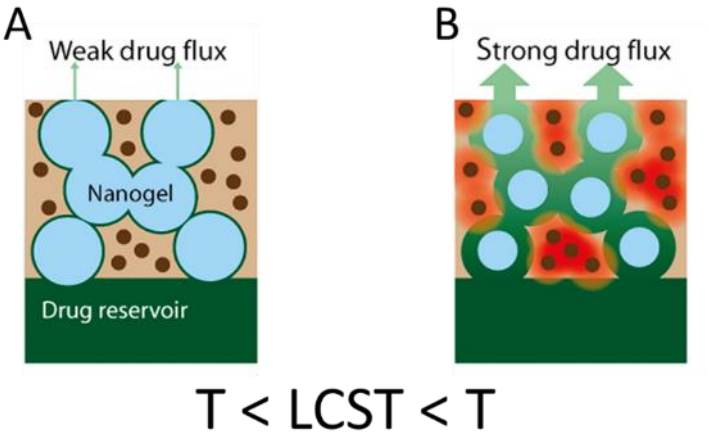

Figure 1.10: Thermally-responsive drug delivery mechanisms associated with lower critical solution temperature behaviour. (A) below the LCST, the hydrogels are swollen, minimizing drug flux, (B) above the LCST, the hydrogels are shrunken, increasing drug flux. Adapted from [117]

There are however some limitations around the use of temperature-responsive technologies. The high toxicity of the NIPAM monomer has been a barrier as to its approval by the U.S. Food and Drug Administration (FDA) for *in vivo* use, while the substantial pressure changes in the body from perfluorocarbon vaporization for release can sometimes be harmful[8, 113, 118]. Additionally, given that protein adsorption can significantly change the LCST values observed *in vivo* relative to *in vitro*, relying on LCST changes via endogenous signals offers challenges in terms of precisely engineering the correct vehicle composition to achieve the desired release location/rate. If one is to consider thermal triggered drug delivery as an external stimulus with endogenous control, it can also be noted that localized heating may be problematic for patients or cause some degree of discomfort[119]. Regulating the temperature of these delivery vehicles and thermal enablers (like heating pads) is important, as temperatures as low as 45°C will lead

to burns and/or cell killing, and the duration of exposure resulting in a burn decreases with increased temperature[120, 121].

1.4.3.4 Endogenous Release Summary

Overall, endogenous release provides the opportunity to use the body's natural triggers to release a payload in response to local changes in pH, enzyme concentrations, and temperatures. Such triggers can be useful for identifying cancers without the use of additional binding ligands or promoting release of insulin on demand for diabetics. However, the generalized drawback is that the systems lack specificity or sensitivity and therefore need to be made more complex either through the incorporation of an additional endogenous activation mechanism or through the co-integration of exogenous release mechanisms.

1.4.4 Exogenous Release

Exogenous release requires an external stimulus in order to initiate release, avoiding in large part the unintended release observed in many endogenous systems associated with the lack of precision over materials tuning to a particular pH/temperature or down-regulated enzyme concentrations in off-target tissues. While there are many modes by which exogenous delivery vehicles may deposit their payloads, we will focus on magnetic activation, radiation, and ultrasound ablation which are the most commonly researched and most likely to be translated into a clinical setting.

1.4.4.1 Magnetically Triggered Drug Release

Magnetic release can be achieved by fabricating delivery vehicles in whole or in part with ferromagnetic or superparamagnetic materials[12, 22, 24, 79, 122]. In the most common implementations of magnetically-triggered release, superparamagnetic iron oxide nanoparticles (SPIONs) are incorporated into a drug delivery vehicle to provide the potential for magnetic guidance to a specific site of action (static magnetic field) or hysteresis heating to generate a local temperature stimulus (alternating magnetic field) [12, 24, 39, 79, 122-124]. Magnetic fields can also be used to non-invasively align anisotropic materials (e.g. membranes doped with directionally porous materials can be aligned in a magnetic field to provide a clear path for drug diffusion[123-125]). Figure 1.11 demonstrates how diffusion of drug can be manipulated in a SPION-containing gel in the presence of a magnetic field[125]. In many cases, the rationale for using magnetic particles is their potential two-fold application as both potential stimuli for driving on-demand drug release coupled with their potential as imaging agents for magnetic resonance imaging (MRI) applications[4, 12, 22, 38, 126].

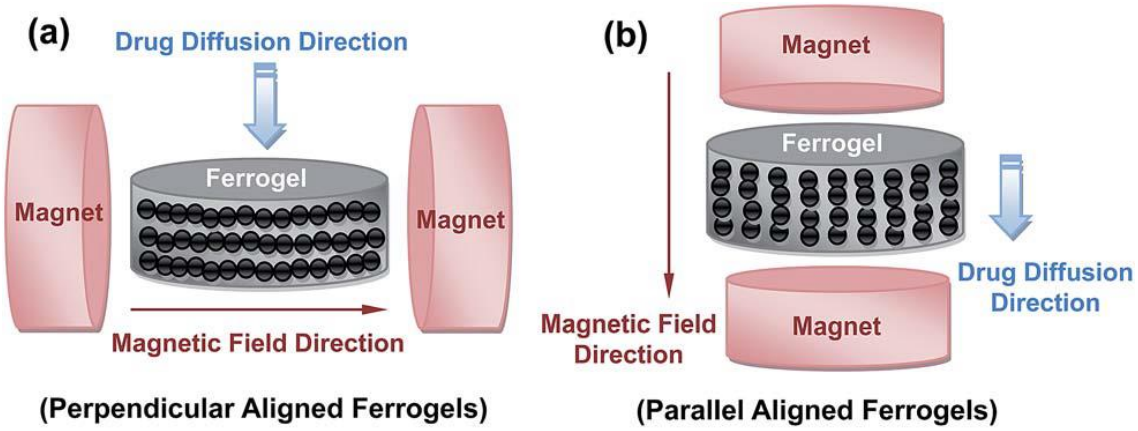

Figure 1.11: Magnetically triggered release mediated through the alignment of magnetic particles in a gel. Adapted from [125]

However, it should be noted that SPIONs have not been used as a standalone system for exogenously activated drug delivery, requiring their integration into the matrix of a membrane or a microcapsule/fibre for driving effective release and thus typically more complex fabrication procedures. In addition, a strong magnet (in particular a strong oscillating magnet) is not always readily available in all healthcare systems, making magnetic activation somewhat less broadly accessible in terms of impacting patients.

1.4.4.2 Radiation Triggered Drug Release

Radiation triggered drug release is a complex process that requires special materials but offers significant translational potential. Similar to magnetic release, such systems typically combine a conventional delivery vehicle with, in this case, a photosensitive material to actuate the application of a radiation source, which is commonly near-infrared radiation (NIR) or X-ray radiation[13, 40, 64, 127-129]. Commonly used photosensitizers

include metallic compounds such as gold nanoparticles (X-ray) or nanotubes/nanorods/nanosheets (NIR, X-ray), anisotropic carbon-based nanomaterials like nanorods or nanodots (NIR), thulium/ytterbium/bismuth compounds (X-ray), and others[13, 40, 127-129]. The mechanisms of activation in the presence of the photosensitive source depends on the delivery vehicle, which can include phospholipid degradation due to the formation of reactive oxygen species, energy transfer from the photosensitizer to a temperature-responsive material to actuate release, photolytic cleavage or crosslinking of a photolabile bond, and/or de-aggregation[13, 40, 64, 127-130].

Similarly, to magnetically triggered release, these delivery vehicles are material dependent, and rarely can operate as a standalone system. While the higher availability of X-rays and NIR sources in the healthcare system make them more likely to be readily integrated into clinical treatment, challenges around excessive exposure to ionizing X-ray irradiation and the frequent risk of skin burns and peripheral tissue damage associated with NIR irradiation limit the repeated practical use of these modalities.

1.4.4.3 Ultrasound Triggered Drug Release

Activation via ultrasound takes a somewhat different approach from the other exogenous and endogenous release mechanisms. Whereas the other delivery vehicles heavily rely on the chemical properties of the materials to drive a response specific to either the local microenvironment (pH, temperature, enzyme concentration) or to the applied exogenous source, ultrasound is considered a mechanically driven activation mechanism[4, 131-133].

Ultrasound triggered release primarily exploits the potential of acoustic waves to cause perturbations in the system, which in turn force the system to either break down, reconfigure, or become more permeable [88, 131, 134-139]. Unlike other exogenous signals, the response observed depends primarily on the mode of ultrasonic ablation rather than the inherent properties of the material (or at least release can be actuated using a range of different material types)[14, 37, 54, 88, 118, 131, 133, 137-139]. Below, the main mechanisms by which ultrasound is used in the context of controlled drug delivery are reviewed.

There are different ways in which ultrasound will actuate release from a specific drug delivery vehicle. Cavitation, whereby the ultrasound nucleates, grows and collapses a gas bubble, is one of the more common mechanisms[118]. Cavitation-based delivery vehicles expand and contract due to the creation and destruction of gas bubbles, which applies pressure on the capsules. This mode of activation is generally imparted by high intensity focused ultrasound (HIFU) signals that cause the capsules to burst altogether due to extremely high vapour pressured caused by cavitation, releasing their contents immediately[88, 118, 119, 140, 141]. The use of phase changing materials like perfluorocarbons that can vaporise easily under US ablation can assist in driving such cavitation-based ultrasound-mediated burst release[14, 37, 113, 119, 140, 141].

Ultrasound can also induce triggered release via mechanical disruption, particularly observed when low intensity and generally low frequency signals are used. Although ultrasound signals are less dependent on a material's chemical properties, the attenuation coefficients of the ultrasound within a particular material affect how the

ultrasound waves travel through the material[135, 138, 142]. Water has a very low attenuation coefficient, whereas air has a higher energy loss[135]. Because of the differences in attenuation and impedance, ultrasound waves travel at different speeds in different materials, causing mechanical disruptions particularly at the interfaces between those materials. The speed that the sonic wave travels directly relates to the energy imparted by the ultrasound, which can lead to the breaking of bonds and breaking down of polymer chains[131, 133]. In other cases where bonds are not broken, the mechanical disturbance increases the permeability of material by inducing a morphology change (most common in lipid or amphiphile-based self-assembly systems)[54, 139, 143] or by physically moving the matrix components (as often observed with polymer capsules), leading to an increased diffusion coefficient and enhanced release of drug from the vehicle[15, 109, 132, 144].

It should be noted that polymeric microcapsules behave like a hybrid of the two systems below in that they expand and contract similarly to lipid drug delivery vehicles but generally to a lesser extent[23, 115, 118, 132, 145]. Microcapsules with an aqueous reservoir typically undergo UTMD if the microcapsule is less elastic (e.g. most PLGA microcapsules)[4, 23, 82, 109, 146], while more elastomeric materials such as PDMS and gel based microcapsules tend to undergo polymorphism and increased diffusion[54, 131, 139, 144]. Altogether, although US does not rely on chemical properties to actuate release, the material does impact the modality of release observed.

Although ultrasound-based triggering systems show promise by being more material indiscriminate and being highly translatable for integration in healthcare systems, the implementation of release can be problematic depending on the application. If the delivery vehicle breaks down altogether, drug will be released with burst release kinetics, causing potential toxicity issues and/or enabling ultrasound to merely control the location or timing of release as opposed to drug dosing. In contrast, if one relies on the more tuneable release mediated by the material reconfiguration, constant ultrasonic application is required[15, 88, 118, 119, 132, 138-140, 147]. Thus, the development of an ultrasound-mediated vehicle that can release its payload in a controlled manner while minimizing the US exposure period would be attractive from a clinical standpoint.

1.4.4.4 Exogenous Release Summary

Endogenous release vehicles have useful pharmacokinetics at (sometimes) the expense of control of initiation of release, while exogenous release vehicles have the capability to withhold their contents until a very specific stimulus activates the release but often offer challenges around the resulting pharmacokinetics of release[5-7, 12, 13, 36]. Exogenous release systems are generally more complicated than endogenous systems, requiring specific materials for activation, and are commonly used in conjunction with endogenous delivery vehicles to address the difficulties of controlled release[4, 12, 22, 38, 39, 128, 129]. Ultrasound is one of the few activation mechanisms that does not rely primarily on a material's chemical properties for release, but has drawbacks associated with process controls upon activation.

1.5 Objectives

Many drug delivery vehicle morphologies, fabrication processes, and triggering mechanisms have been explored and reviewed above. Of note, the mechanical activation provided by ultrasound has clear potential for clinically-relevant release but with several key drawbacks associated with the burst release observed or the need for continuous ultrasound ablation to effect continuous release. Instead, developing a process by which permanent pores can be made in an injectable delivery vehicle on-demand using ultrasound as the stimulus would allow for increased control of release kinetics while eliminating the need of continuous ultrasound activation over the full release period.

In this thesis, a new ultrasound-activatable core-shell delivery vehicle is fabricated and demonstrated, as illustrated schematically in Figure 1.12. The shell is comprised of two phases – a primary constituent that forms a continuous microcapsule and an embedded phase that penetrates across the thickness of the shell. In the presence of ultrasound, the differences in mechanical indices of the continuous microcapsule and the embedded phase results in release of the embedded phase from the shell, akin to the popping of corks from a microcapsule to create pores. The number of pores created by ultrasound activation can then be related to the release rate of the drug from the core reservoir. While such a vehicle could be made using many fabrication processes, EHD fabrication is chosen to provide an additional degree of control over the size of the microcapsule.

Chapter 2 discusses the fabrication process by which these complex microcapsules are made. Briefly, corked microcapsules were made using electrospraying, with various

parameters of the process (e.g. voltage, polymer concentration, and extrusion speed) investigated to determine their impact on microcapsule properties [30]. Corked microcapsules were made using PLGA, and their fabrication parameters were studied for future modifications.

Chapter 3 discusses the release dynamics of the microcapsules fabricated in Chapter 2 as mediated using both sonication baths and focused ultrasound probes. Microcapsules with corks incorporated into the shell exhibit an increased rate of release upon US activation relative to uncorked microcapsules, which do not release even upon ultrasound exposure. This improves on the prior art by using PLGA based microcapsules to release their contents by diffusion through the shell without UTMD-based release.

Finally, Chapter 4 reviews the key conclusions of the work and proposes future work to improve the functionality of these cork-shell release vehicles across a broader range of potential applications.

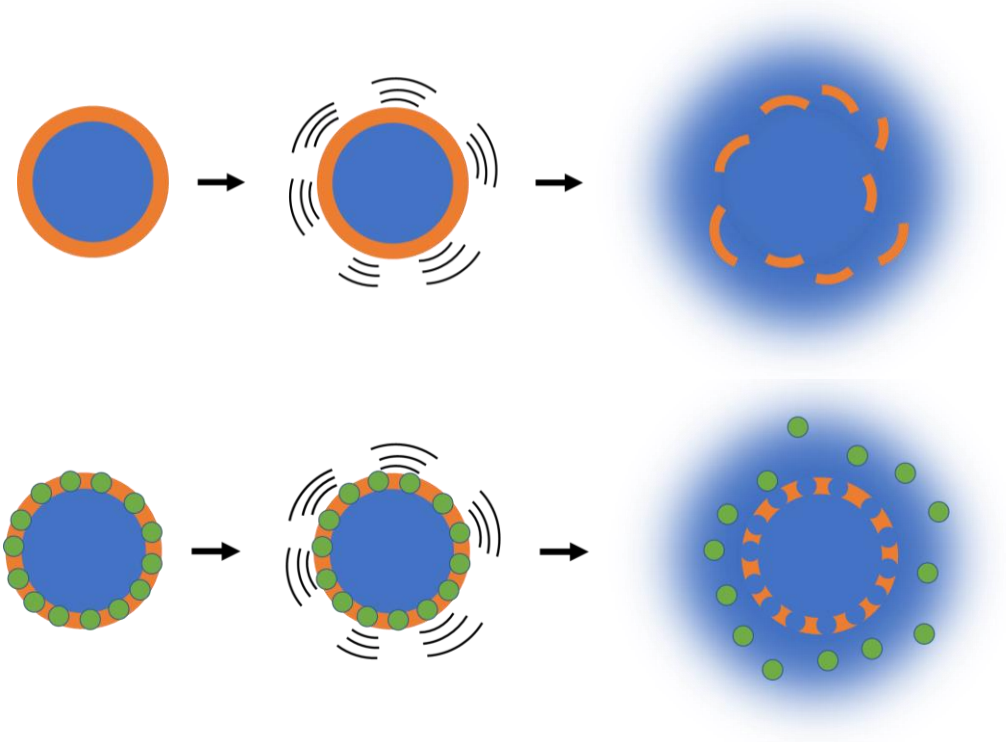

Figure 1.12: Ultrasound triggered drug delivery mechanisms. (Top) traditional ultrasound triggering resulting in microcapsule destruction. (Bottom) proposed delivery vehicle modified with corks in the shell that can be popped out to create pores without destroying the overall integrity of the microcapsule. Blue – aqueous phase with dissolved model drug; orange – PLGA shell; green – microcorks

1.6 References

1. Yun, Y.H., B.K. Lee, and K. Park, *Controlled Drug Delivery: Historical perspective for the next generation.* J Control Release, 2015. **219**: p. 2-7.
2. Hoffman, A.S., *The origins and evolution of "controlled" drug delivery systems.* J Control Release, 2008. **132**(3): p. 153-63.
3. *Controlled Release Drug Delivery Market Analysis Report*, in *Industry Report*. 2018, Grand View Research.
4. Zhang, Y., et al., *Mechanical Force-Triggered Drug Delivery.* Chem Rev, 2016. **116**(19): p. 12536-12563.

5. Hu, J., G. Zhang, and S. Liu, *Enzyme-responsive polymeric assemblies, nanoparticles and hydrogels.* Chem Soc Rev, 2012. **41**(18): p. 5933-49.
6. Hoare, T. and R. Pelton, *Highly pH and Temperature Responsive Microgels Functionalized with Vinylacetic Acid.* Macromolecules, 2004. **37**(7): p. 2544-2550.
7. Liu, J., et al., *pH-sensitive nano-systems for drug delivery in cancer therapy.* Biotechnol Adv, 2014. **32**(4): p. 693-710.
8. Simpson, M.J., et al., *Narrowly Dispersed, Degradable, and Scalable Poly(oligoethylene glycol methacrylate)-Based Nanogels via Thermal Self-Assembly.* Industrial & Engineering Chemistry Research, 2018. **57**(22): p. 7495-7506.
9. Felber, A.E., M.H. Dufresne, and J.C. Leroux, *pH-sensitive vesicles, polymeric micelles, and nanospheres prepared with polycarboxylates.* Adv Drug Deliv Rev, 2012. **64**(11): p. 979-92.
10. Cheng, W., et al., *pH-Sensitive Delivery Vehicle Based on Folic Acid-Conjugated Polydopamine-Modified Mesoporous Silica Nanoparticles for Targeted Cancer Therapy.* ACS Appl Mater Interfaces, 2017. **9**(22): p. 18462-18473.
11. Anderson, J.M., A. Rodriguez, and D.T. Chang, *Foreign body reaction to biomaterials.* Semin Immunol, 2008. **20**(2): p. 86-100.
12. Brazel, C.S., *Magnetothermally-responsive nanomaterials: combining magnetic nanostructures and thermally-sensitive polymers for triggered drug release.* Pharm Res, 2009. **26**(3): p. 644-56.
13. Volodkin, D.V., A.G. Skirtach, and H. Mohwald, *Near-IR remote release from assemblies of liposomes and nanoparticles.* Angew Chem Int Ed Engl, 2009. **48**(10): p. 1807-9.
14. Coussios, C.C. and R.A. Roy, *Applications of Acoustics and Cavitation to Noninvasive Therapy and Drug Delivery.* Annual Review of Fluid Mechanics, 2008. **40**(1): p. 395-420.
15. Schroeder, A., et al., *Controlling Liposomal Drug Release with Low Frequency Ultrasound: Mechanism and Feasibility.* Langmuir, 2007. **23**(7): p. 4019-4025.
16. Li, H.J., et al., *Smart Superstructures with Ultrahigh pH-Sensitivity for Targeting Acidic Tumor Microenvironment: Instantaneous Size Switching and Improved Tumor Penetration.* ACS Nano, 2016. **10**(7): p. 6753-61.

17. Yu, S., et al., *A novel pH-induced thermosensitive hydrogel composed of carboxymethyl chitosan and poloxamer cross-linked by glutaraldehyde for ophthalmic drug delivery.* Carbohydr Polym, 2017. 155: p. 208-217.
18. Choi, S.W., Y. Zhang, and Y. Xia, *A temperature-sensitive drug release system based on phase-change materials.* Angew Chem Int Ed Engl, 2010. 49(43): p. 7904-8.
19. Li, W., et al., *Gold nanocages covered with thermally-responsive polymers for controlled release by high-intensity focused ultrasound.* Nanoscale, 2011. 3(4): p. 1724-30.
20. Mueller, E., et al., *Dynamically Cross-Linked Self-Assembled Thermoresponsive Microgels with Homogeneous Internal Structures.* Langmuir, 2018. 34(4): p. 1601-1612.
21. Ta, T. and T.M. Porter, *Thermosensitive liposomes for localized delivery and triggered release of chemotherapy.* J Control Release, 2013. 169(1-2): p. 112-25.
22. Ulbrich, K., et al., *Targeted Drug Delivery with Polymers and Magnetic Nanoparticles: Covalent and Noncovalent Approaches, Release Control, and Clinical Studies.* Chem Rev, 2016. 116(9): p. 5338-431.
23. Zhang, H., et al., *High intensity focused ultrasound-responsive release behavior of PLA-b-PEG copolymer micelles.* J Control Release, 2009. 139(1): p. 31-9.
24. Hoare, T., et al., *Magnetically Triggered Composite Membrane for On-Demand Drug Delivery.* Nano Letters, 2009. 9(10): p. 3651-3657.
25. Gao, F., et al., *Preparation of aminated core-shell fluorescent nanoparticles and their application to the synchronous fluorescence determination of gamma-globulin.* Luminescence, 2008. 23(6): p. 392-6.
26. Mabrouk, M., et al., *The Influence of Lyophilized EmuGel Silica Microspheres on the Physicomechanical Properties, In Vitro Bioactivity and Biodegradation of a Novel Ciprofloxacin-Loaded PCL/PAA Scaffold.* Polymers, 2016. 8(6).
27. Nanaki, S., et al., *PLGA/SBA-15 mesoporous silica composite microparticles loaded with paclitaxel for local chemotherapy.* Eur J Pharm Sci, 2017. 99: p. 32-44.

28. Xu, W., et al., *A mesoporous silicon/poly-(DL-lactic-co-glycolic) acid microsphere for long time anti-tuberculosis drug delivery.* Int J Pharm, 2014. 476(1-2): p. 116-23.
29. Gao, Y., et al., *Optimising the shell thickness-to-radius ratio for the fabrication of oil-encapsulated polymeric microspheres.* Chemical Engineering Journal, 2016. 284: p. 963-971.
30. Li, Z. and C. Wang, *Effects of Working Parameters on Electrospinning*, in *One-Dimensional nanostructures*. 2013. p. 15-28.
31. Xu, Q., et al., *Coaxial electrohydrodynamic atomization process for production of polymeric composite microspheres.* Chem Eng Sci, 2013. 104.
32. Ito, F., H. Fujimori, and K. Makino, *Incorporation of water-soluble drugs in PLGA microspheres.* Colloids Surf B Biointerfaces, 2007. 54(2): p. 173-8.
33. Agrahari, V., *Novel drug delivery systems, devices, and fabrication methods.* Drug Deliv Transl Res, 2018. 8(2): p. 303-306.
34. Sanjay, S.T., et al., *Controlled Drug Delivery Using Microdevices.* Curr Pharm Biotechnology, 2016. 17(9): p. 772-787.
35. Muanprasat, C. and V. Chatsudthipong, *Chitosan oligosaccharide: Biological activities and potential therapeutic applications.* Pharmacol Ther, 2017. 170: p. 80-97.
36. Figueiredo, M. and R. Esenaliev, *PLGA Nanoparticles for Ultrasound-Mediated Gene Delivery to Solid Tumors.* J Drug Deliv, 2012. 2012: p. 767839.
37. Luan, Y., et al., *Lipid shedding from single oscillating microbubbles.* Ultrasound Med Biol, 2014. 40(8): p. 1834-46.
38. Mikhaylov, G., et al., *Ferri-liposomes as an MRI-visible drug-delivery system for targeting tumours and their microenvironment.* Nat Nanotechnol, 2011. 6(9): p. 594-602.
39. Campbell, S.B., M. Patenaude, and T. Hoare, *Injectable superparamagnets: highly elastic and degradable poly(N-isopropylacrylamide)-superparamagnetic iron oxide nanoparticle (SPION) composite hydrogels.* Biomacromolecules, 2013. 14(3): p. 644-53.
40. Deng, W., et al., *Controlled gene and drug release from a liposomal delivery platform triggered by X-ray radiation.* Nat Commun, 2018. 9(1): p. 2713.

41. Park, J., et al., *Polydopamine-Based Simple and Versatile Surface Modification of Polymeric Nano Drug Carriers.* ACS Nano, 2014. **8**(4): p. 3347-3356.
42. Lengert, E., et al., *Silver Alginate Hydrogel Micro- and Nanocontainers for Theranostics: Synthesis, Encapsulation, Remote Release, and Detection.* ACS Appl Mater Interfaces, 2017. **9**(26): p. 21949-21958.
43. Ahmad, Z., et al., *Generation of multilayered structures for biomedical applications using a novel tri-needle coaxial device and electrohydrodynamic flow.* J R Soc Interface, 2008. **5**(27): p. 1255-61.
44. Azizi, M., et al., *Fabrication of protein-loaded PLGA nanoparticles: effect of selected formulation variables on particle size and release profile.* Journal of Polymer Research, 2013. **20**(4).
45. Ishak, R.A.H., N.M. Mostafa, and A.O. Kamel, *Stealth lipid polymer hybrid nanoparticles loaded with rutin for effective brain delivery - comparative study with the gold standard (Tween 80): optimization, characterization and biodistribution.* Drug Deliv, 2017. **24**(1): p. 1874-1890.
46. Lussier, B. and A.A. Wilson, *Alpha-1 Antitrypsin: The Protein*, in *Alpha-1 Antitrypsin*. 2016. p. 17-30.
47. Kim, M.R., et al., *Golf ball-shaped PLGA microparticles with internal pores fabricated by simple O/W emulsion.* Chem Commun (Camb), 2010. **46**(39): p. 7433-5.
48. Cheng, J., et al., *Electrospinning versus microfluidic spinning of functional fibers for biomedical applications.* Biomaterials, 2017. **114**: p. 121-143.
49. Liechty, W.B., et al., *Polymers for drug delivery systems.* Annu Rev Chem Biomol Eng, 2010. **1**: p. 149-73.
50. Escoffre, J.M., et al., *Doxorubicin delivery into tumor cells with ultrasound and microbubbles.* Mol Pharm, 2011. **8**(3): p. 799-806.
51. Bakaic, E., N.M.B. Smeets, and T. Hoare, *Injectable hydrogels based on poly(ethylene glycol) and derivatives as functional biomaterials.* RSC Advances, 2015. **5**(45): p. 35469-35486.
52. Husseini, G.A., et al., *Investigating the acoustic release of doxorubicin from targeted micelles.* Colloids Surf B Biointerfaces, 2013. **101**: p. 153-5.

53. Husseini, G.A. and W.G. Pitt, *Micelles and nanoparticles for ultrasonic drug and gene delivery.* Adv Drug Deliv Rev, 2008. 60(10): p. 1137-52.
54. Fong, W.K., et al., *Responsive self-assembled nanostructured lipid systems for drug delivery and diagnostics.* J Colloid Interface Sci, 2016. 484: p. 320-339.
55. Zhao, C.X., *Multiphase flow microfluidics for the production of single or multiple emulsions for drug delivery.* Adv Drug Deliv Rev, 2013. 65(11-12): p. 1420-46.
56. Growney Kalaf, E.A., et al., *Characterization of slow-gelling alginate hydrogels for intervertebral disc tissue-engineering applications.* Mater Sci Eng C Mater Biol Appl, 2016. 63: p. 198-210.
57. Sivakumaran, D., E. Mueller, and T. Hoare, *Temperature-Induced Assembly of Monodisperse, Covalently Cross-Linked, and Degradable Poly(N-isopropylacrylamide) Microgels Based on Oligomeric Precursors.* Langmuir, 2015. 31(21): p. 5767-78.
58. Zhang, L., et al., *Co-delivery of hydrophobic and hydrophilic drugs from nanoparticle-aptamer bioconjugates.* ChemMedChem, 2007. 2(9): p. 1268-71.
59. Wang, H., et al., *Enhanced anti-tumor efficacy by co-delivery of doxorubicin and paclitaxel with amphiphilic methoxy PEG-PLGA copolymer nanoparticles.* Biomaterials, 2011. 32(32): p. 8281-90.
60. Zhang, X.J., et al., *Preparation of thermo/pH-sensitive reduced graphene oxide interpenetrating hydrogel nanocomposites for co-delivery of paclitaxel and epirubicin.* Materials Technology, 2018. 33(4): p. 245-252.
61. Kolesnichenko, I.V. and E.V. Anslyn, *Practical applications of supramolecular chemistry.* Chem Soc Rev, 2017. 46(9): p. 2385-2390.
62. Liu, R., et al., *Core-shell Fe3O4 polydopamine nanoparticles serve multipurpose as drug carrier, catalyst support and carbon adsorbent.* ACS Appl Mater Interfaces, 2013. 5(18): p. 9167-71.
63. de Gracia Lux, C., et al., *Biocompatible polymeric nanoparticles degrade and release cargo in response to biologically relevant levels of hydrogen peroxide.* J Am Chem Soc, 2012. 134(38): p. 15758-64.
64. Li, H., et al., *Near-infrared light-triggered drug release from a multiple lipid carrier complex using an all-in-one strategy.* J Control Release, 2017. 261: p. 126-137.

65. Griffin, W.C. and M.J. Lynch, *Surface Active Agents*, in *Handbook of Food Additives*, T. Furia, Editor. 1968.
66. Ltd., C.E., *Span and Tween*, C.E. Ltd., Editor. 2009: England.
67. Kanicky, J.R., et al., *Surface Chemistry in the Petroleum Industry*, in *Handbook of Applied Surface and Colloid Chemistry*, K. Holmberg, Editor. 2001, John Wiley & Sons, Ltd.
68. Salager, J.-L., *Surfactants - Types and Uses*, in *FIRP Booklet #E300-A*, FIRP, Editor. 2002: Venezuela.
69. Wang, F., et al., *Polyelectrolyte Complex Nanoparticles from Chitosan and Acylated Rapeseed Cruciferin Protein for Curcumin Delivery.* J Agric Food Chem, 2018. 66(11): p. 2685-2693.
70. Liu, Y., H. Miyoshi, and M. Nakamura, *Encapsulated ultrasound microbubbles: therapeutic application in drug/gene delivery.* J Control Release, 2006. 114(1): p. 89-99.
71. Makadia, H.K. and S.J. Siegel, *Poly Lactic-co-Glycolic Acid (PLGA) as Biodegradable Controlled Drug Delivery Carrier.* Polymers (Basel), 2011. 3(3): p. 1377-1397.
72. Ortega-Oller, I., et al., *Bone Regeneration from PLGA Micro-Nanoparticles.* Biomed Res Int, 2015. 2015: p. 415289.
73. Khvedelidze, M., et al., *Calorimetric and spectrophotometric investigation of PLGA nanoparticles and their complex with DNA*. Vol. 99. 2010. 337-348.
74. Mura, S., J. Nicolas, and P. Couvreur, *Stimuli-responsive nanocarriers for drug delivery.* Nat Mater, 2013. 12(11): p. 991-1003.
75. Li, Y. and T.M. Liu, *Discovering Macrophage Functions Using In Vivo Optical Imaging Techniques.* Front Immunol, 2018. 9: p. 502.
76. Ramsay, R.R., et al., *A perspective on multi-target drug discovery and design for complex diseases.* Clin Transl Med, 2018. 7(1): p. 3.
77. Wang, C., et al., *Predicting target-ligand interactions using protein ligand-binding site and ligand substructures.* BMC Systems Biology, 2015. 9(1): p. S2.
78. Matsumoto, A., et al., *Fabrication of Janus particles composed of poly (lactic-co-glycolic) acid and hard fat using a solvent evaporation method.* Drug Discov Ther, 2016. 10(6): p. 307-313.
79. Yang, X., et al., *Superparamagnetic graphene oxide–Fe3O4 nanoparticles hybrid for controlled targeted drug carriers.* Journal of Materials Chemistry, 2009. 19(18).

80. Chowdhuri, A.R., et al., *Carbon Dots Embedded Magnetic Nanoparticles @Chitosan @Metal Organic Framework as a Nanoprobe for pH Sensitive Targeted Anticancer Drug Delivery.* ACS Appl Mater Interfaces, 2016. **8**(26): p. 16573-83.
81. Yarin, A.L., et al., *Material encapsulation and transport in core–shell micro/nanofibers, polymer and carbon nanotubes and micro/nanochannels.* Journal of Materials Chemistry, 2007. **17**(25): p. 2585 - 2599.
82. Yang, Q., et al., *Facile Synthesis of Lipid-Perfluorocarbon Nanoemulsion Coated with Silica Shell as an Ultrasound Imaging Agent.* Adv Healthc Mater, 2018. **7**(4).
83. Li, J., et al., *Janus polymeric cages.* Polymer, 2012. **53**(17): p. 3712-3718.
84. Rao, K.J., et al., *A Force to Be Reckoned With: A Review of Synthetic Microswimmers Powered by Ultrasound.* Small, 2015. **11**(24): p. 2836-46.
85. Shemi, O. and M.J. Solomon, *Self-Propulsion and Active Motion of Janus Ellipsoids.* J Phys Chem B, 2018. **122**(44): p. 10247-10255.
86. Jiang, H.R., N. Yoshinaga, and M. Sano, *Active motion of a Janus particle by self-thermophoresis in a defocused laser beam.* Phys Rev Lett, 2010. **105**(26): p. 268302.
87. Moghaddam, M.K., S.M. Mortazavi, and T. Khaymian, *Micro/nano-encapsulation of a phase change material by coaxial electrospray method.* Iranian Polymer Journal, 2015. **24**(9): p. 759-774.
88. Hernot, S. and A.L. Klibanov, *Microbubbles in ultrasound-triggered drug and gene delivery.* Adv Drug Deliv Rev, 2008. **60**(10): p. 1153-66.
89. Mendelsohn, A.D., et al., *Patterning of mono- and multilayered pancreatic beta-cell clusters.* Langmuir, 2010. **26**(12): p. 9943-9.
90. Sadowski, L.P., et al., *Synthesis of Polyester Dendritic Scaffolds for Biomedical Applications.* Macromol Biosci, 2016. **16**(10): p. 1475-1484.
91. Pooja, D., et al., *Dendrimer-TPGS mixed micelles for enhanced solubility and cellular toxicity of taxanes.* Colloids Surf B Biointerfaces, 2014. **121**: p. 461-8.
92. Zhou, M., et al., *Low density lipoprotein/pectin complex nanogels as potential oral delivery vehicles for curcumin.* Food Hydrocolloids, 2016. **57**: p. 20-29.

93. Steinhilber, D., et al., *A microgel construction kit for bioorthogonal encapsulation and pH-controlled release of living cells.* Angew Chem Int Ed Engl, 2013. **52**(51): p. 13538-43.
94. Taylor, G., *Disintegration of Water Drops in an Electric Field.* Proceedings of the Royal Society of London. Series A, Mathematical and Physical Sciences, 1964. **280**(1382): p. 383-397.
95. Jaworek, A., *Electrospray droplet sources for thin film deposition.* Journal of Materials Science, 2006. **42**(1): p. 266-297.
96. Wang, F., et al., *Fabrication and Characterization of Prosurvival Growth Factor Releasing, Anisotropic scaffolds for Enhanced Mesenchymal Stem Cell Survival Growth and Orientation.* Biomacromolecules, 2009. **10**(9): p. 2609-2618.
97. D'Amore, A., et al., *Heart valve scaffold fabrication: Bioinspired control of macro-scale morphology, mechanics and micro-structure.* Biomaterials, 2018. **150**: p. 25-37.
98. Pena, B., et al., *Biomimetic Polymers for Cardiac Tissue Engineering.* Biomacromolecules, 2016. **17**(5): p. 1593-601.
99. Reuter, K.G., et al., *Targeted PRINT Hydrogels: The Role of Nanoparticle Size and Ligand Density on Cell Association, Biodistribution, and Tumor Accumulation.* Nano Lett, 2015. **15**(10): p. 6371-8.
100. Soukoulis, C. and T. Bohn, *A comprehensive overview on the micro- and nano-technological encapsulation advances for enhancing the chemical stability and bioavailability of carotenoids.* Crit Rev Food Sci Nutr, 2018. **58**(1): p. 1-36.
101. Yuan, Y., et al., *Complex coacervation of soy protein with chitosan: Constructing antioxidant microcapsule for algal oil delivery.* LWT - Food Science and Technology, 2017. **75**(Complete): p. 171 - 179.
102. Akbulut, M., et al., *Generic Method of Preparing Multifunctional Fluorescent Nanoparticles Using Flash NanoPrecipitation.* Advanced Functional Materials, 2009. **19**(5): p. 718-725.
103. Holowka, E.P. and S.K. Bhatia, *Controlled Release Systems*, in *Drug Delivery: Materials Design and Clinical Perspective*. 2014, Springer-Verlag: New York.
104. Fu, Y. and W.J. Kao, *Drug release kinetics and transport mechanisms of non-degradable and degradable polymeric delivery systems.* Expert opinion on drug delivery, 2010. **7**(4): p. 429-444.

105. Dash, S., et al., *KINETIC MODELING ON DRUG RELEASE FROM CONTROLLED DRUG DELIVERY SYSTEMS.* Acta Poloniae Pharmaceutica, 2010. **67**(3): p. 217-223.
106. Yu, J., et al., *Stimuli-Responsive Delivery of Therapeutics for Diabetes Treatment.* Bioeng Transl Med, 2016. **1**(3): p. 323-337.
107. Fischel-Ghodsian, F., et al., *Enzymatically controlled drug delivery.* Proceedings of the National Academy of Sciences, 1988. **85**(7): p. 2403-2406.
108. Napoli, A., et al., *Glucose-oxidase Based Self-Destructing Polymeric Vesicles.* Langmuir, 2004. **20**(9): p. 3487-3491.
109. Di, J., et al., *Ultrasound-triggered noninvasive regulation of blood glucose levels using microgels integrated with insulin nanocapsules.* Nano Research, 2017. **10**(4): p. 1393-1402.
110. Tan, H., et al., *Thermosensitive injectable hyaluronic acid hydrogel for adipose tissue engineering.* Biomaterials, 2009. **30**(36): p. 6844-53.
111. Li, L., et al., *Enzymatic Hydrolysis and Simultaneous Extraction for Preparation of Genipin from Bark of Eucommia ulmoides after Ultrasound, Microwave Pretreatment.* Molecules, 2015. **20**(10): p. 18717-31.
112. Li, Y., et al., *Enzyme-Responsive Polymeric Vesicles for Bacterial-Strain-Selective Delivery of Antimicrobial Agents.* Angew Chem Int Ed Engl, 2016. **55**(5): p. 1760-4.
113. Phillips, L.C., et al., *Phase-shift perfluorocarbon agents enhance high intensity focused ultrasound thermal delivery with reduced near-field heating.* J Acoust Soc Am, 2013. **134**(2): p. 1473-82.
114. Liu, H., et al., *Hydrophobic interaction-mediated capture and release of cancer cells on thermoresponsive nanostructured surfaces.* Adv Mater, 2013. **25**(6): p. 922-7.
115. Ferrara, K.W., *Driving delivery vehicles with ultrasound.* Adv Drug Deliv Rev, 2008. **60**(10): p. 1097-102.
116. Gao, Z., et al., *Drug-loaded nano/microbubbles for combining ultrasonography and targeted chemotherapy.* Ultrasonics, 2008. **48**(4): p. 260-70.
117. Hoare, T., et al., *Magnetically triggered nanocomposite membranes: a versatile platform for triggered drug release.* Nano Lett, 2011. **11**(3): p. 1395-400.

118. Lafond, M., et al., *Cavitation-threshold Determination and Rheological-parameters Estimation of Albumin-stabilized Nanobubbles.* Sci Rep, 2018. **8**(1): p. 7472.
119. Moyer, L.C., et al., *High-intensity focused ultrasound ablation enhancement in vivo via phase-shift nanodroplets compared to microbubbles.* J Ther Ultrasound, 2015. **3**: p. 7.
120. Suzuki, T., et al., *Experimental studies of moderate temperature burns.* Burns, 1991. **17**(6): p. 443-451.
121. Dai, T., et al., *Chitosan Acetate Bandage as a Topical Antimicrobial Dressing for Infected Burns.* Antimicrobial Agents and Chemotherapy, 2009. **53**(2): p. 393.
122. Laurent, S., et al., *Superparamagnetic iron oxide nanoparticles for delivery of therapeutic agents: opportunities and challenges.* Expert Opin Drug Deliv, 2014. **11**(9): p. 1449-70.
123. Vallooran, J.J., R. Negrini, and R. Mezzenga, *Controlling anisotropic drug diffusion in lipid-Fe3O4 nanoparticle hybrid mesophases by magnetic alignment.* Langmuir, 2013. **29**(4): p. 999-1004.
124. Shah, S.A., et al., *Mixed Brownian alignment and Neel rotations in superparamagnetic iron oxide nanoparticle suspensions driven by an ac field.* Phys Rev B Condens Matter Mater Phys, 2015. **92**(9).
125. Liu, T.-Y., et al., *Influence of magnetic nanoparticle arrangement in ferrogels for tunable biomolecule diffusion.* RSC Advances, 2015. **5**(109): p. 90098-90102.
126. Miao, X., et al., *Application of Dye-coated Ultrasmall Gadolinium Oxide Nanoparticles for Biomedical Dual Imaging.* Bulletin of the Korean Chemical Society, 2017. **38**(9): p. 1058-1068.
127. Fedoryshin, L.L., et al., *Near-infrared-triggered anticancer drug release from upconverting nanoparticles.* ACS Appl Mater Interfaces, 2014. **6**(16): p. 13600-6.
128. Goodman, A.M., et al., *Near-infrared remotely triggered drug-release strategies for cancer treatment.* Proc Natl Acad Sci U S A, 2017. **114**(47): p. 12419-12424.
129. Song, G., et al., *Perfluorocarbon-Loaded Hollow Bi2Se3 Nanoparticles for Timely Supply of Oxygen under Near-Infrared Light to Enhance the Radiotherapy of Cancer.* Adv Mater, 2016. **28**(14): p. 2716-23.
130. Farag, M.M., W.M. Abd-Allah, and A.M. Ibrahim, *Effect of gamma irradiation on drug releasing from nano-bioactive glass.* Drug Deliv Transl Res, 2015. **5**(1): p. 63-73.

131. Caruso, M.M., et al., *Mechanically-induced chemical changes in polymeric materials.* Chem Rev, 2009. 109(11): p. 5755-98.
132. Hu, Y., J.M. Wan, and A.C. Yu, *Cytomechanical perturbations during low-intensity ultrasound pulsing.* Ultrasound Med Biol, 2014. 40(7): p. 1587-98.
133. Li, J., C. Nagamani, and J.S. Moore, *Polymer mechanochemistry: from destructive to productive.* Acc Chem Res, 2015. 48(8): p. 2181-90.
134. Feigenbaum, H., W.F. Armstrong, and T. Ryan, *Feigenbaum's Echocardiography*. 2005: Lippincott Williams & Wilkins.
135. Prince, J.L. and J.M. Links, *Medical Imaging Signals and Systems*, in *Medical Imaging Signals and Systems*. 2006, Pearson Prentice Hall.
136. Sakai, S., *Chapter 2*.
137. Chen, X., et al., *Single-site sonoporation disrupts actin cytoskeleton organization.* J R Soc Interface, 2014. 11(95): p. 20140071.
138. D'Onofrio, M., et al., *Acoustic radiation force impulse of the liver.* World J Gastroenterol, 2013. 19(30): p. 4841-9.
139. Kang, M., G. Huang, and C. Leal, *Role of lipid polymorphism in acoustically sensitive liposomes.* Soft Matter, 2014. 10(44): p. 8846-54.
140. ter Haar, G. and C. Coussios, *High Intensity Focused Ultrasound: Past, present and future.* International Journal of Hyperthermia, 2009. 23(2): p. 85-87.
141. Kawabata, K.-i., et al., *Nanoparticles with Multiple Perfluorocarbons for Controllable Ultrasonically Induced Phase Shifting.* Japanese Journal of Applied Physics, 2005. 44(6B): p. 4548-4552.
142. Jablonowski, L.J., et al., *Shell effects on acoustic performance of a drug-delivery system activated by ultrasound.* J Biomed Mater Res A, 2017. 105(11): p. 3189-3196.
143. Li, G., et al., *Spatial and temporal control of shape memory polymers and simultaneous drug release using high intensity focused ultrasound.* Journal of Materials Chemistry, 2012. 22(16).
144. Tang, J., et al., *Controlled drug release from ultrasound-visualized elastic eccentric microcapsules using different resonant modes.* Journal of Materials Chemistry B, 2018. 6(13): p. 1920-1929.
145. Deckers, R., et al., *New insights into the HIFU-triggered release from polymeric micelles.* Langmuir, 2013. 29(30): p. 9483-90.

146. Arpicco, S., et al., *Recent studies on the delivery of hydrophilic drugs in nanoparticulate systems.* Journal of Drug Delivery Science and Technology, 2016. **32**: p. 298-312.
147. Seip, R., et al., *Targeted ultrasound-mediated delivery of nanoparticles: on the development of a new HIFU-based therapy and imaging device.* IEEE Trans Biomed Eng, 2010. **57**(1): p. 61-70.

Chapter 2 – Fabrication of Cork-Shell Microcapsules using Electrospray

2.1 Introduction

Capsular micro or nano-particles have been widely investigated for applications in drug delivery for cancer[36, 148], diabetes management [89, 106], and other diseases as well as medical imaging contrast agents [38, 113, 116, 118, 149]. A variety of fabrication methods can be used to produce such vehicles, including double emulsions[44, 150], microfluidics[144, 151], solvent evaporation[78], self-assembly [8, 20, 57, 139], and electrohydrodynamics[31, 43, 152-157], among others. All these processes have particular advantages and disadvantages, with the primary trade-offs being related to balancing the efficiency of drug encapsulation, the complexity/reproducibility of the methodology, and the throughput of capsule fabrication[4, 11, 109, 129, 158].

Among all the potential processes to choose from, electrohydrodynamic processing (EHD) offers an attractive mixture of control, throughput, and encapsulation efficiency. EHD processes use high voltage to manipulate liquids to behave in a particular manner. A liquid is fed through a conductive needle and, upon the application of a voltage, the applied electric field charges the liquid to induce shear stress that elongates the dimensions of the liquid stream[95, 154]. If the liquid is charged to at least above a critical proportion of the Rayleigh limit (i.e. the maximum charge a liquid droplet can carry)[94, 159], the shape of the meniscus will transform from spherical to conical in nature (i.e. a Taylor cone), at the tip of which the liquid is both highly charged and extremely small in dimensions. This

fine charged liquid stream is pulled towards an oppositely charged collector in order to complete an electric circuit[30, 94, 159, 160], creating a thin stream of liquid that, depending on process parameters, may either stay as a stream (electrospinning) or break up into droplets (electrospraying) as it travels towards the collector[31, 94, 154, 161]. Depending on the stability of the meniscus, the contents being electrosprayed, and charge imbalances, different EHD modes can be achieved. Figure 2.1 compares the conventional dripping of liquid from a needle (uncharged) with charged modes of EHD including unstable jetting mode, cone-jet mode, and multi-jet mode[29]. In dripping mode, the only way to control the size of the drop is by manipulating the surface tension between the air/liquid interface, which can only be controlled by the material itself instead of processing conditions[29, 31, 161, 162]. As such, stable jet mode is the optimal choice, as the Taylor cone is consistent and symmetric and results in uniform products, including in cases in which a coaxial needle (a smaller needle within a larger needle) is used[31, 161, 162]. Conversely, unstable cone and multijet modes result in intermittent changes in the Taylor cone that result in broad ranges of product size, and shell thicknesses that would be highly problematic for coaxial fabrications[29, 31, 161, 162].

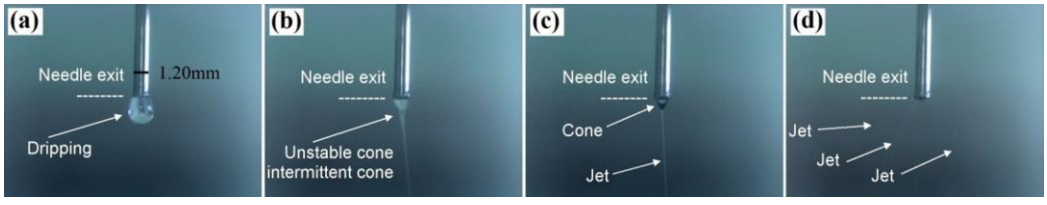

Figure 2.1: Different modes of EHD: (a) dripping mode, (b) unstable cone mode, (c) stable cone/jet mode, (d) multijet mode. Adapted from [162]

Electrospinning generally results when the liquid stream is highly viscous (associated with the use of higher molecular weight polymers and/or larger amounts of dissolved polymer) and is widely used to produce micro/nanofibres applied as scaffolds[97, 156], patches[163], and films[155] (Figure 2.2A); the fibres can also be selectively aligned[96] or unaligned[164] depending on the method by which the product is collected. Alternatively, electrospraying generally results when lower viscosity liquids without substantial intermolecular entanglements are processed, enabling the creation of droplets or capsules depending on the materials and flow regimes used (Figure 2.2B) [161, 165-167]. Of particular importance, the type of needle chosen can dictate the morphology of the particle or capsule formed. The use of a single needle will produce will produce particles with a single interface[155]; However, the use of a coaxial, triaxial, or any other number of concentric needles will result in multiple interfaces, allowing for the creation of (multi)-capsular vehicles[43, 161].

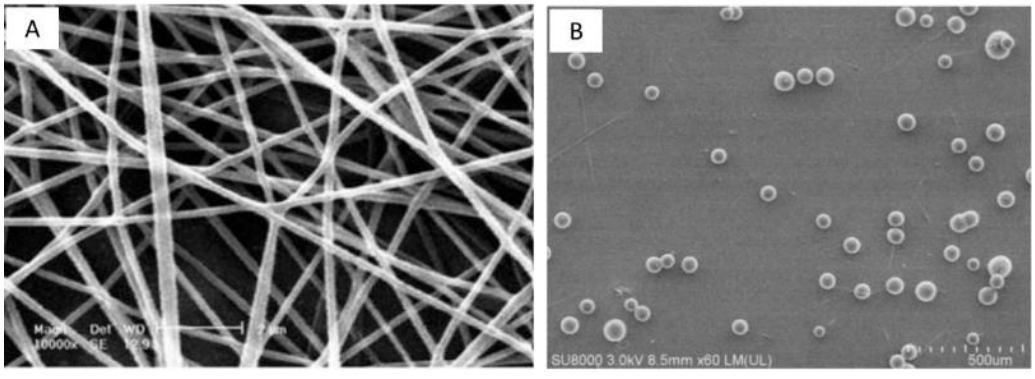

Figure 2.2: EHD fabrication products imaged using scanning electron microscopy (SEM): (A) electrospun fibres, (B) electrosprayed particles. Figure adapted from [29, 30].

2.1.1 Electrospraying Parameters

Extensive work has been done in modeling the effects of various parameters of EHD on the product properties[155]. While the mathematics associated with these effects are outside the scope of this thesis, the qualitative trends will be summarized below as categorized into four families: solution parameters, processing parameters, collector parameters, and ambient parameters[30, 87, 95, 153, 161, 165].

2.1.1.1 Solution Parameters

Solution parameters of relevance to EHD include the concentration of the material dissolved in solution, the viscosity of the solution, the conductivity of the solution, and the surface tension of the solution. For polymer processing, increasing the viscosity of the solution (which is intimately linked with the concentration and the molecular weight of the polymer used) increases the probability of electrospinning while reducing the viscosity results in electrospraying (lower viscosity creating smaller droplets). Increasing molecular weight or the flexibility of the polymer structure is particularly important if electrospinning is targeted, as the physical entanglements between the chains are essential to preserve the fibrous structure of the product. Electrospinning is also more likely if the surface tension of the solution with the receiving medium (typically air in dry EHD processes) is lower, resulting in less energy cost associated with creating the higher specific surface area associated with fibres rather than spheres. Higher solution

conductivities (i.e. processing in water) result in higher charging of the solution and thus higher pulling of the Taylor cone to form smaller fibres or droplets.

2.1.1.2 Processing Parameters

Of the processing parameters in EHD, voltage is likely the most impactful. Under a threshold voltage, a Taylor cone will not be formed, while beyond the threshold voltage some research shows no significant effect on feature size[29] or (more commonly) a decrease in size as voltage is increased[31, 154, 167, 168]. The increase in electric field theoretically imparts more electrostatic pull on the solution, causing smaller droplets/fibres to form. Flow rate is also important given that it affects the time available for the electric field to charge the liquid at the needle tip but also is the key factor affecting process productivity. Slower flow rates tend to yield more consistent products, as the liquid has more time to polarize[30]; however, lower process production rates are achieved [95, 154, 167]. In cases of coaxial or multiaxial electrospraying, the ratio of the inner and outer flow rates is also critical for determining both the overall size of the product as well as the thickness of the different shell(s) formed[29, 87, 154].

2.1.1.3 Collection Parameters

The collector parameters play an important role on the fabrication process. The most common collectors are solid grounded conductive plates[95] or solid grounded rotating mandrels, the latter of which are often used to collect aligned electrospun fibres[30, 96, 152, 156]. More complex collectors can also be fabricated with defined gaps between conductors to collect gradient fibrous structures[169]. For electrospray, wet EHD fabrication can also be used in which a solution mounted on top of a ground can be used

as a collector[43, 153, 154, 166, 167, 170]; in such a case, the surface tension between the jet and the collector solutions plays a key role in determining the product size/shape. The distance between the needle and the collector is also essential to control. Too long of a distance may eventually make it more difficult for the material to be pulled towards the collector with a given applied voltage, inducing the formation of larger size products; however, too short of a distance does not provide enough drying time for the solvent to evaporate, a particularly critical parameter when performing electrospinning[29, 30, 95, 152, 154, 156, 159].

2.1.1.4 Ambient Conditions

Finally, the ambient environment surrounding the EHD setup may impact the result of the fabrication. For example, an increase in humidity may increase the surface tension between the charged droplets, such that materials that would have been electrospun on a less humid day may be electrosprayed on a more humid day[171]. Also, an increase in the ambient temperature may decrease the viscosity of the solution, which may reduce the dimensions of the product[172].

2.2 Experimental – Objective

In this chapter, the use of electrospraying for creating complex capsules in which the shell contains multiple components is explored. The formation of such capsules with EHD has not been previously reported aside from [152], in which solvated electrospun fibres were bombarded with electrosprayed silica on a rotating mandrel to create “corked” microfibres whose corks could be removed by ultrasound activation. Herein, we aim to create a complex microcapsule in which the shell of the microcapsule (here, the slowly

degradable polymer poly(lactic-co-glycolic acid), or PLGA) is impregnated with a non-soluble phase (here, silica microparticles). The targeted morphology of the microcapsules is illustrated schematically in Figure 2.3, in which the blue phase represents the drug dissolved in an aqueous phase, the orange represents PLGA (the continuous component of the shell), and the green circles represent the silica particles incorporated into the shell phase. Upon ultrasound (as studied in Chapter 3), the silica particles or "corks" are anticipated to be popped out of the PLGA shell without otherwise fracturing the shell to create pores "on demand" and effect controlled triggered drug release. In this Chapter, the optimal conditions for making such microcapsules are investigated.

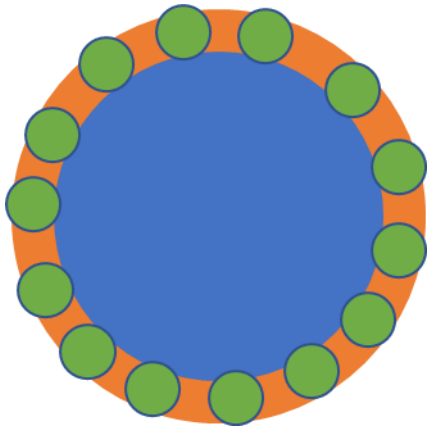

Figure 2.3: Proposed EHD-fabricated corked-shell microcapsule. Blue – aqueous phase with dissolved model drug; orange – PLGA shell; green – microcorks

2.3 Materials

Materials: Poly (D,L-lactide-co-glycolide) (PLGA) [85:15 lactide: glycolide ratio, M_w 50-75 kDa], bovine serum albumin (BSA), Span 80, Tween 80, porcine gelatin from pig skin,

fluorescein isothiocyanate (FITC), Rhodamine B, Rhodamine 123, Nile Blue, (3-aminopropyl) triethoxysilane (APTS), N-(3-dimethylaminopropyl)-N'-ethylcarbodiimide hydrochloride (EDC), 4-(dimethylamino) pyridine (DMAP), sodium bicarbonate, sodium carbonate decahydrate, and trypsin-EDTA were all purchased from Millipore Sigma (Oakville, ON or Milwaukee, WI) and used as received. Polyvinyl alcohol (PVA) [M_w 6 kDa, 80% hydrolyzed] was purchased from Polysciences Inc (Warrington, PA). Glass microbeads based on sodium silicate glass (3-10 μm diameter) were purchased from Corpuscular Inc (Cold Springs, NY). Mouse fibroblast cells (3T3) were purchased from Cedarlane Laboratories (Burlington, ON). Dulbecco's modified Eagle medium (DMEM, high glucose, pyruvate), bovine calf serum (BCS), and penicillin-streptomycin (PS, 10,000U/mL) were purchased from Thermo Fisher Scientific (Burlington, ON). MTS proliferation assay was procured from Abcam Inc (Toronto, ON). 1X phosphate buffered saline (PBS) was prepared with the standard composition (10 mM phosphate buffer, pH = 7.4). Chloroform (reagent grade), acetonitrile (reagent grade), dichloromethane (DCM) (reagent grade), acetone (reagent grade), ethanol (reagent grade), toluene (reagent grade), and N,N-dimethylformamide (DMF) (reagent grade) were purchased from Caledon Laboratory Chemicals (Georgetown, ON).

2.4 Material Preparation

2.4.1 Fluorescent Labeling of BSA

To functionalize BSA with a fluorescein fluorescent probe as per the instruction of [173, 174], controlled amounts of FITC and BSA were dissolved in pH 9.0 carbonate buffer (ionic strength 0.1 M) and stirred overnight at room temperature in the dark. After 24 h of stirring, the reaction solution was transferred to a 12.5 kDa dialysis tube and filtered 5 times to remove excess FITC, again kept in the dark. The conjugate solution was then frozen and lyophilized.

To functionalize BSA with Nile Blue as per the instruction of [175], 1.0g of BSA and 0.5g of EDC were dissolved in a 0.1M carbonate buffer (pH = 9.2). After stirring for 30 minutes, 25 mL of a stock solution consisting of 36 mg of Nile Blue dissolved in 50 mL of methanol was added and allowed to stir for 24 h in darkness. The reaction was then transferred to a 12.5 kDa dialysis tube and filtered 5 times to remove excess Nile Blue, methanol, and EDC, again under minimal lighting conditions. The conjugate solution was then frozen and lyophilized.

2.4.2 Microcork Functionalization

Microcorks were functionalized with PLGA using the method described in [176] in which the glass microbeads were first aminated followed by conjugation with the -COOH chain ends of PLGA. The reaction mechanism is depicted in Figure 2.4.

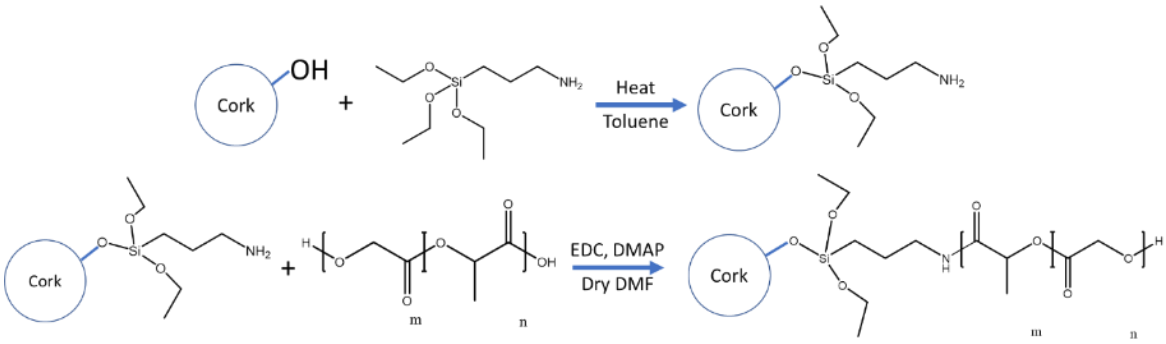

Figure 2.4: PLGA conjugation reaction scheme for preparing microcorks

2.4.2.1 Amination of Microbeads

4 g of glass microbeads were dispersed in 100 mL of toluene in a 500 mL Schlenk flask and sonicated under nitrogen. After 2 hours, a solution containing 50 mL of dry toluene and 10 mL of APTS was added dropwise for the first 30 mL, and then over 1 minute for the remaining volume to the Schlenk flask under continuing sonication and nitrogen and left to react under the same conditions for 2 hours. The solution was then removed from the sonicator and refluxed under nitrogen at 115°C for 3 hours, after which the product was cooled and filtered via vacuum filtration. The dried contents were transferred to the thimble of a Soxhlet extractor and washed in toluene at 130°C overnight to remove any residual APTS, after which the product aminated microbeads were dried in an oven for 24 h.

2.4.2.2 Grafting of PLGA to Aminated Microbeads

1 g of the product aminated microbeads from 2.4.2.1 was dispersed in 20 mL of a 0.52% DMAP in dry DMF solution in a 500 mL Schlenk flask under nitrogen and sonicated for 2 h. A 40 mL solution of dry DMF containing 615 mg of PLGA was then added slowly to the reaction chamber under nitrogen and sonication and left to react for 3 h. The product was then removed from the sonicator and allowed to reflux under nitrogen for 6 h at 160°C, after which the product was cooled to room temperature and stirred under nitrogen overnight. The contents were then centrifuged at 2200 RPM for 20 minutes, after which the supernatant was removed and the product was washed with DCM at least 3 times, or until the solvent was clear. The supernatant was then removed, and the product PLGA-functionalized microcorks (PLGA-corks) were placed in an oven to dry at 37°C for 3 hours.

2.4.2.3 Fluorescently Labeling PLGA-Conjugated Microcorks

To fluorescently label the microcorks to allow tracking of their location within the shell, a protocol described in [177] was used to graft FITC to residual amine groups on the microcorks. 2 mg of FITC was dissolved in 40 mL of ethanol in a round bottom flask in darkness. 1 g of the PLGA-conjugated microcorks were dispersed in the solution and allowed to stir overnight at room temperature. The contents of the round bottom flask were then transferred to a conical tube and centrifuged at 2200PRM for 20 mins. The supernatant was removed, and the washing protocol was repeated using ethanol as the washing solvent until the supernatant was clear.

2.4.3 Evaluation of Material Preparations

ATR-FTIR was performed after each of the microcork reaction steps (amination, PLGA grafting, fluorescent labeling) to track changes in particle composition, with each measurement consisting of 64 scans using a spectral resolution of 1 cm^{-1}. A microcork background was collected as the starting point, and the products of each reaction were compared to the initial background. The spectrum of the PLGA starting polymer was also collected separately with an air background and compared to the aminated microbeads and the PLGA-conjugated microbeads using the same analysis protocol.

2.5 Dry Single-Needle Electrospraying of Solid Microparticles

2.5.1 Equipment Setup

Figure 2.5 depicts the dry electrospraying setup used to create solid particles rather than microcapsules, an initial fabrication step intended to establish the key conditions for electrospraying that yield desirable particle size and size distributions. A KD Scientific Legato 200 syringe pump was loaded with a Cadence Science glass syringe attached to a stainless steel 18G needle. The needle was attached to the positive end of a Glassman high voltage generator (0-20 kV, 700 μA) using an alligator clip, with the corresponding negative ground connected to a metal disk covered in aluminum foil to act as the collector. The distance between the tip of the syringe needle and the collector plate could be adjusted by positioning the plate on a plastic slab with grooves separated by 1 cm. A modification to this setup included the use of aluminum 12.5 mm diameter scanning electron microscopy stubs as the grounding collector, allowing direct collection of particles for imaging during the process without requiring an additional transfer step.

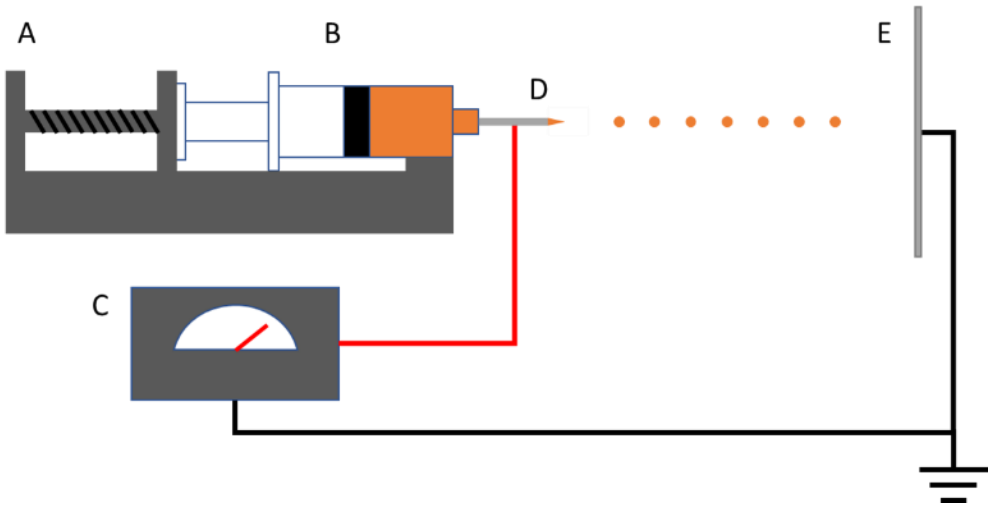

Figure 2.5: Dry electrospraying setup. (A) syringe pump, (B) syringe, (C) high voltage generator, (D) needle attached to positive end of high voltage leading to a Taylor cone, (E) grounded collection plate. Orange – PLGA dissolved in solvent

2.5.2 Fabrication Process

As a base case, 1 w/v% of PLGA was dissolved in chloroform and loaded into a glass syringe. An 18G needle was then attached to the syringe, and the positive end of the high voltage was clipped to the needle. The syringe was mounted on a syringe pump and primed. The metal disk that acts as a grounding plate was covered in aluminum foil and placed 10 cm away from the tip of the needle. The syringe pump was started at a flow rate of 1.5 mL/h, and a high voltage of 8 kV was applied. After 30 minutes, the high voltage was turned off (followed by the syringe pump), and the product deposited on the tin foil was removed and stored in a petri dish in the dark until needed.

2.5.3 Fabrication Parameters

The effects of the voltage, solvent type, concentration of PLGA, flow rate, and molecular weight of the polymer on particle size were studied to establish relevant conditions for more complex core-shell electrospraying reactions that will be addressed further in the thesis. Table 2.1 shows the full set of processing and solution parameters studied.

Table 2.1: Dry electrospraying variables. The total flow rate was kept constant at 1.5 mL/h

PLGA concentration	Solvent	Voltage
1 w/v%	acetonitrile	8 kV
1 w/v%	chloroform	8 kV
2 w/v%	chloroform	8 kV
3 w/v%	chloroform	8 kV
2 w/v%	chloroform	16 kV
2 w/v%	chloroform	19 kV

2.6 Coaxial Electrospray of Microcapsules with an Air Interface

2.6.1 Equipment Setup

Instead of using a generic blunt tipped stainless steel needle that could form only solid particles, a coaxial needle consisting of an inner 22G needle and an outer 18G needle (Ramé-Hart Instrument Co.) was used to form microcapsules. Figure 2.6 depicts the wet coaxial electrospraying apparatus used for these experiments. The inner phase (water, surfactant, and cargo) was loaded using a BD Plastipak syringe and connected to the inner bore of the concentric needle using Tygon tubing, while the outer phase (PLGA, DCM) was

loaded into a Cadence Science glass syringe and connected to the outer bore of the concentric needle using peroxide cured silicone tubing. Both syringes were loaded on KD Scientific Legato 200 syringe pumps, with the positive end of the Glassman high voltage device attached to the coaxial needle as described for dry electrospinning. In this case, to improve the efficiency of product collection, a beaker containing water and PVA (acting as an additional surface stabilizing agent) was placed on top of a metal plate connected to the ground of the high voltage to act as the collection bath and was continuously stirred during particle fabrication.

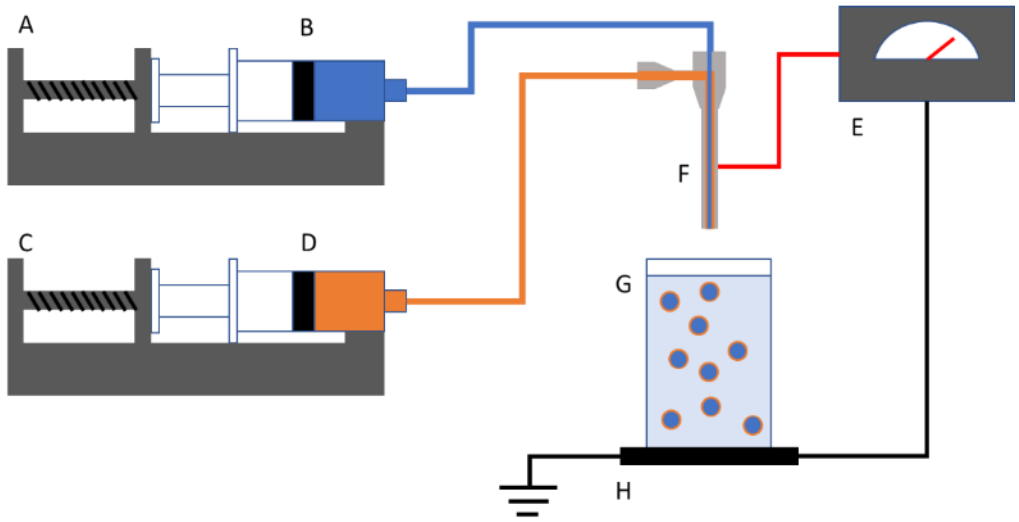

Figure 2.6: Wet coaxial electrospraying setup. (A) syringe pump 1, (B) syringe with inner core solution, (C) syringe pump 2, (D) syringe with shell phase solution, (E) high voltage generator, (F) coaxial needle connected to the positive end of the high voltage, (G) aqueous continuous phase collector, (H) grounded collection plate. Blue – aqueous phase with dissolved model drug; orange – PLGA dissolved in solvent (DCM); light blue – continuous aqueous phase with PVA acting as collector

2.6.2 Fabrication Process

As the base case, 1 w/v% of PLGA was dissolved in dichloromethane and loaded into the glass syringe (shell phase) while the 3 mL BD Plastipak™ syringe was loaded with 2.5 w/v% of BSA in MilliQ water (inner phase). The collector consisted of a 50 mL beaker filled with a 20 mg solution of PVA in 40 mL milliQ water, with the tip of the coaxial needle positioned 10 cm away from the surface of the aqueous collection bath. The shell phase syringe pump was set at 1mL/h while the inner phase syringe pump was set at 0.1 mL/h, with a voltage of 13 kV used for processing. After 30 minutes, the high voltage was turned off (followed by the syringe pumps), and the resulting microcapsules were collected via centrifugation.

Process modifications were implemented depending on the type of characterization experiment to be performed. For samples intended for SEM imaging, the liquid collector was replaced with aluminum foil. For samples intended to be imaged using fluorescence, Rhodamine B was added into the PLGA/DCM shell solution a concentration of 0.1% w/w relative to PLGA (for samples in which the shell is fluorescently labeled) and/or FITC was added to the inner phase solution at 0.5% w/w of BSA (for samples in which the inner core contents are fluorescently labeled).

2.6.3 Fabrication Parameters

With the addition of a coaxial needle and an aqueous collection bath, the number of variables that could affect the microcapsule properties significantly increases. Specifically, the total volume that pumped through the combination of the syringes, the

ratios of inner and outer flow rates, the materials used in each phase, and the concentration of PVA in the collection bath could all play a significant role in addition to the parameters studied in the dry electrospraying experiments. Table 2.2 shows the full scope of wet coaxial electrospraying parameters that were studied.

Table 2.2: Wet coaxial electrospraying variables. Constant variables are 1 w/v% PLGA in DCM, 1 mL/h outer flow rate, 13 kV applied voltage

Sample	BSA in Water (w/v %)	Inner Flow Rate (mL/h)	PVA in Collector Bath (w/v %)
1	5	0.05	0
2	2.5	0.1	0
3	1.25	0.2	0
4	2.5	0.1	0.05

2.7 Immersion Coaxial Electrospray

By submerging the exit terminal of the coaxial in the aqueous water bath (i.e. collecting the droplets using an aqueous collector and at an aqueous interface rather than the air interface used in the previous section, a process known as immersion electrospray), the surface tension can be used to create spherical structures and encapsulate the inner core in the shell phase [178, 179]. In accordance with Laplace's law, a sphere provides the minimal surface tension at the maximal volume due to a consistent radius of curvature as defined by the Young-Laplace equation (Equation 2.1), in which R_1 and R_2 are equal because spheres are one radius of curvature as opposed to ellipsoids that have two[180].

Equation 2.1

$$\Delta P = \gamma \left(\frac{1}{R_1} + \frac{1}{R_2} \right)$$

The submersion of the needle can also help to manipulate the surface tensions to ensure the complete encapsulation of one liquid phase in another liquid phase dispersed in a third phase, as required for formation of a coherent shell. As indicated in Equation 2.2[178-180], the optimal conditions for encapsulation are achieved when the wetting coefficients for the inner phase and the continuous phase are below 0 and the spreading coefficient for the shell phase is greater than 0, with the alternative (undesirable) scenarios in which various types of non-concentric phase separation occur when these conditions are not met shown schematically in Figure 2.7 [178]. By using water as the continuous phase, various surfactants or surface-active agents (e.g. PVA) can be used to modify the surface tensions as required, providing substantially more fabrication flexibility than provided using air as the droplet-forming medium.

Equation 2.2:

$$S_i = \gamma_{jk} - (\gamma_{ij} + \gamma_{ik})$$

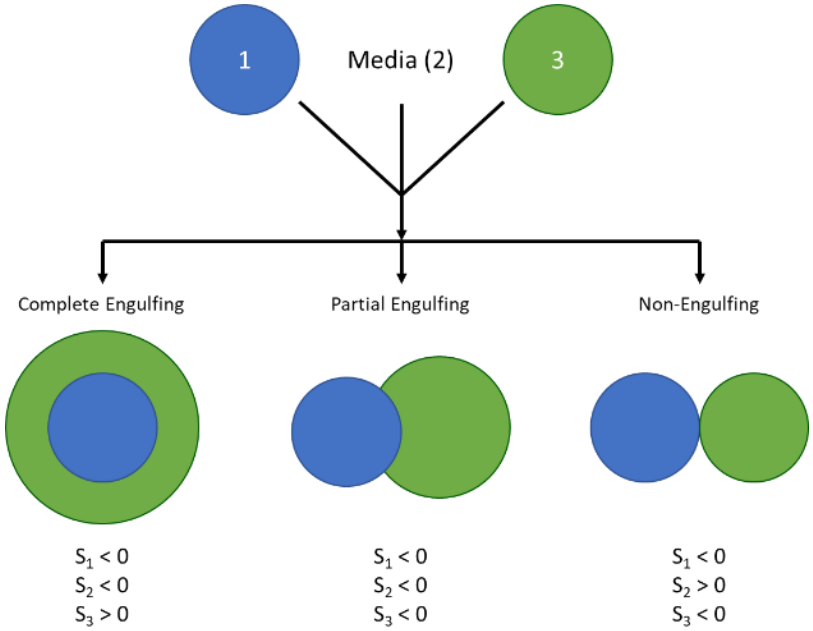

Figure 2.7: Three-phase interaction based on spreading coefficients. Adapted from [178]

2.7.1 Equipment Setup

Figure 2.8 depicts the immersion coaxial electrospraying apparatus used for these experiments. The assembly was identical to that described in section 2.6.1 , except the needle is submerged 2 cm into the collection bath instead of mounted 10 cm above the collection bath.

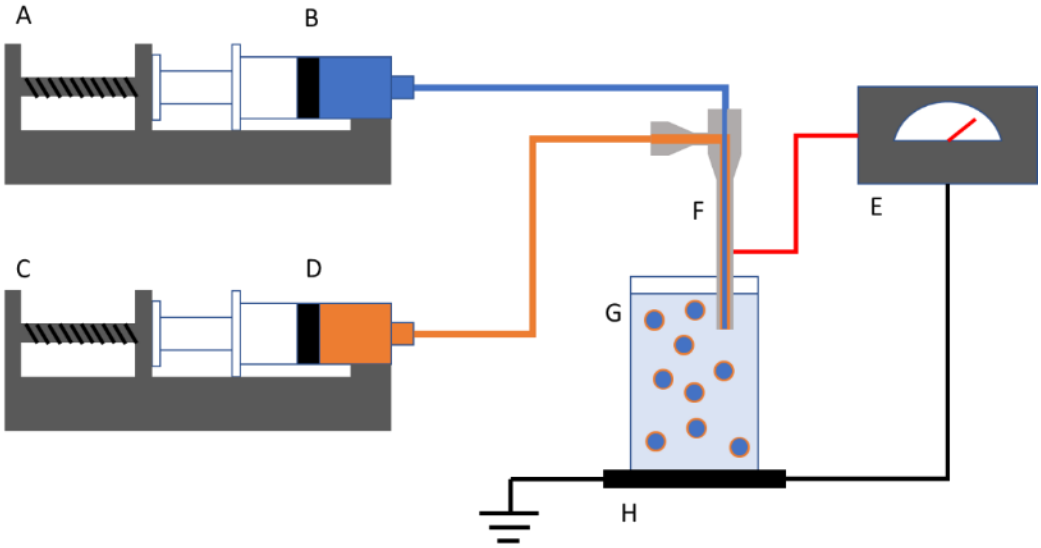

Figure 2.8: Immersion coaxial electrospraying setup. (A) syringe pump 1, (B) syringe with inner core solution, (C) syringe pump 2, (D) syringe with shell phase solution, (E) high voltage generator, (F) coaxial needle connected to the positive end of the high voltage and immersed in continuous phase, (G) aqueous continuous phase collector, (H) grounded collection plate. Blue – aqueous phase with dissolved model drug; orange – PLGA dissolved in solvent (DCM); light blue – continuous aqueous phase with PVA acting as collector

2.7.2 Fabrication Process

The same fabrication parameters were used as described in section 2.6.2 , except for the collector design and the duration of fabrication. For the collector, a metal disk (acting as a grounding plate) was placed under a 200 mL tall form beaker filled with 0.016 w/v% PVA in 185 mL milliQ water stirred at 300 RPM. The needle was submerged 2 cm below the surface of the water and halfway off-centre of the radius of the beaker. For duration, instead of electrospraying for 30 minutes, EHD was performed for 1 h.

2.7.3 Fabrication Parameters

The effect of a range of different parameters on the microcapsule properties formed following immersion wet electrospraying was investigated as per Table 2.3.

Table 2.3: Range of immersion coaxial electrospraying fabrication parameters screened

Parameter	Base Case	Changes
Inner Core Phase BSA Concentration (w/v%)	2.5%	2%, 5%, 10%
Shell Phase PLGA Concentration (w/v%)	1%	2%, 5%, 10%
PVA Concentration in Continuous Phase (w/v% in DIW)	0.016%	0%, 0.005%, 0.011%, 0.032%
Voltage (kV)	15	0, 10, 13, 18
Total Flow Rate (mL/h)	1.1	0.55, 2.2, 3.3, 5.5
Inner Core Surfactant	BSA	Span 80, Tween 80, Tergitol-NP4, Porcine gelatin from pig skin

2.7.4 Incorporation of Microcorks in Microcapsules

To mitigate the settling of the microcorks over time by gravitational sedimentation, the microcorks were dispersed in the DCM/PLGA solution by vortex and immediately loaded into the glass syringe and used for electrospraying. The base case fabrication settings were: 2.5 w/v% BSA in water as the inner phase, 5 w/v% PLGA (dissolved) and 1 w/v% of PLGA-corks (dispersed) in DCM as the shell phase, 0.016 w/v% PVA in 185 mL of water as the continuous phase, 18 kV as the applied voltage, and 3.3 mL/h as the total flow rate 0.3 mL/h for the inner core and 3 mL/h for the shell phase). After the electrospraying process, the continuous phase was stirred for at least 45 more minutes to allow the DCM to evaporate and the shell to solidify. The sample was then centrifuged for 2 minutes at 600 RPM to collect the microcapsules, with an aliquot of the supernatant collected in

some cases to assess encapsulation efficiency or residual unincorporated cork content. The samples were washed three times with water via centrifugation and stored in 10 mL of water in a refrigerator until needed.

2.7.5 Fluorescent Labeling of Microcapsule Components

Multiple fluorescent labels were used to enable visualization of different components of the microcapsules. To visualize the inner phase, water-soluble Rhodamine 123 or FITC was used, while visualization of the shell phase was enabled by doping with hydrophobic Rhodamine B. In cases where the fluorescein-labeled corks are used, Nile Blue was used to visualize the inner core.

2.8 Evaluation of Microcapsule Fabrication

2.8.1 Microcapsule Physical Properties

Controlling the overall size and shell thickness of the microcapsules is essential to regulate their performance playing a major role on their behaviour in a biological environment. The overall size of the microcapsule determines the tissue interaction with the microcapsule, with smaller particles (<5 µm) being more mobile in the body and are phagocytosed by macrophages and larger particles (>20 µm) being typically immobilized at the injection site and inducing the formation of foreign body giant cells[11]. Correspondingly, the thickness of the microcapsule primarily regulates the release kinetics from the microcapsule shell, with thicker microcapsules corresponding to slower release. The thickness of the shell is particularly important to control and characterize in

this research since the cork material needs to be on the same size scale as the thickness of the shell in order to create pores instead of just dimples once they are removed via ultrasound from the delivery vehicle.

2.8.1.1 Scanning Electron Microscopy (SEM)

For dry electrospinning, samples were either scraped off the tin foil on the collection plate and adhered to metal SEM stubs using carbon tape or electrosprayed directly on the metal SEM stubs as the collector. Following, the samples were sputtered with 24 nm of gold and imaged using a TESCAN VP SEM microscope using a 20 kV electron beam under high vacuum. For wet or immersion coaxial electrospraying, 100 µL of about 0.1 w/v% suspension of the microcapsules was pipetted onto a SEM stub covered in carbon tape and allowed to dry overnight. Following, the samples were gold sputtered at a thickness of 24 nm and imaged using the same microscope operating at 10 kV.

2.8.1.2 Bright Field Microscopy

The size of wet and immersion coaxial electrospraying samples were analyzed by bright field optical microscopy following the deposition and drying of the microcapsules on a microscope slide. Images were collected using a Zeiss Axiovert 200M microscope outfitted with a Zeiss Axiocam 200. At least 30 microcapsules were imaged in order to attain a relevant sample size to analyze the microcapsule properties.

The images of the microcapsules were post-processed on ImageJ to quantify the size of the microcapsules using the following steps:

1. The images were converted to an 8-bit type.
2. The image threshold was modified so that only the outlines of the microcapsules were visible
3. The microcapsules were filled using the paintbrush tool
4. The noise surrounding the microcapsules was removed
5. If multiple microcapsules were touching, their boundaries were distinguished using the watershed tool
6. The measure tool would then output a list of the number of microcapsules and their associated data, including area, Feret diameter and Feret angles, to enable the calculation of the average and standard deviation of microcapsule size.

2.8.1.3 Confocal Microscopy

Confocal microscopy (Nikon Eclipse ME600 in combination with a Nikon D-Eclipse C1) was used to provide 3D images of the microcapsules and confirm the core-shell structure of the materials. The excitation and emission wavelengths were 488 nm and 515 nm (for FITC detection) or 543 nm and 590 nm (for Rhodamine B detection). Sample preparation was carried out as described in section 2.8.1.2 , except that drying was performed in the dark to avoid potential photobleaching. The laser gains and offsets were optimized to match the fluorescence of the samples while minimizing noise outside of the microcapsules. The microcapsules were given a preliminary scan for depth at 256x256 pixel density (32 total scans). Once the scanning depth and fluorescent intensities were satisfactory, confocal images were taken at 1024x1024 pixel density for between 40-64 z-slices typically spaced 3-4 μm apart. The images were postprocessed using ImageJ. The

channels of each slice were split, and any unused channels were deleted. The colours were adjusted such that channel 1 (associated with FITC) was made green, and channel 2 (associated with Rhodamine B) was made magenta. The channels from each slice were overlaid upon one another, flattened, and saved for the 3D projection or compiled into a 3D image.

2.8.2 Other Microcapsule Properties

2.8.2.1 Encapsulation Efficiency

The encapsulation efficiency associated with microcapsule fabrication was estimated based on comparing the concentration of the fluorescent probe outside the microcapsules relative to a calibration curve prepared with known concentrations of the same probe at concentrations ranging from assuming all probe is encapsulated (i.e. the blank continuous phase) to assuming all probe is unencapsulated (all extruded probe is in the continuous phase). Fluorescence was measured using Perkin-Elmer Victor3V 1420 Multilabel Reader using the appropriate excitation/emission wavelengths as described in section 2.8.1.3.

2.8.2.2 Cell Viability

A (3-(4,5-dimethylthiazol-2-yl)-5-(3-carboxymethoxyphenyl)-2-(4-sulfophenyl)-2H-tetrazolium) (MTS) assay was used to assess the cytocompatibility of both the corked microcapsules and the individual components of the formulation. MTS is metabolized by active cells into formazan, which has a strong absorbance measurable at 490 nm. Higher

absorbances (i.e. higher formazan conversions) correspond to higher cell metabolic rate. 3T3 murine fibroblast cells were maintained in growth media containing high glucose, pyruvate DMEM, 10% BCS and 1% PS, with media changes every 3-4 days. Cells were passed at 80-90% confluency approximately once per week. The cells were delaminated from their growing flask using trypsin-EDTA and counted. Cells were then plated in 200 µL aliquots of concentration 25 cells/µL in a 96-well plate and incubated for 24 h at 37°C. For samples treated with microcapsules without corks, microcapsules with corks, the corks by themselves, and microcapsules with varying surfactants, 20 µL of a suspension of 5 mg/mL microcapsules or 0.1 mg/mL for corks in sterile water was added in place of 20 µL of media to the cell wells and incubated at 37°C for 24 h. The same protocol was followed for the cell-only controls, only 20 µL of sterile water was added. Following, the capsules were removed by aspiration and the wells were re-filled with 200 µL of media and 10 µL of MTS solution. The plates were incubated for 4 h at 37°C, after which the formazan concentration was read using a Infinite 200Pro multi-well plate reader by first shaking of the plate for 10 s at an amplitude of 1 mm, waiting 30 s before reading, and reading the absorbance at 490 nm at a bandwidth of 9 nm for 25 flashes.

2.9 Results

2.9.1 Material Preparation

2.9.1.1 Microcork Conjugation

Figure 2.9 depicts the stacked ATR-FTIR spectra associated with the various steps for conjugating PLGA to the microcorks. The stretching bands at 856 cm^{-1} and 1100 cm^{-1}

associated with Si-O-Si structure were omitted from the presented spectra to better discern the remaining features. Comparing the base microcorks with the aminated microcorks, a broad peak appears between 1600 cm^{-1} and 1900 cm^{-1} (NH_2 bending [177]), and two shallow peaks appear at 2825 cm^{-1} and 2875 cm^{-1} (CH bond vibration of APS). All these peaks are indicative of the successful introduction of APTS on the base microbeads. Comparing the aminated microcorks to the PLGA-conjugated microcorks, a sharp peak appears at 1650 cm^{-1} corresponding to the C=O stretch of the ester linkages in the polyester and a broad peak was observed between 2950 cm^{-1} and 3000 cm^{-1} corresponding to the CH_2 and CH_3 groups from PLGA, confirming successful PLGA grafting[176].

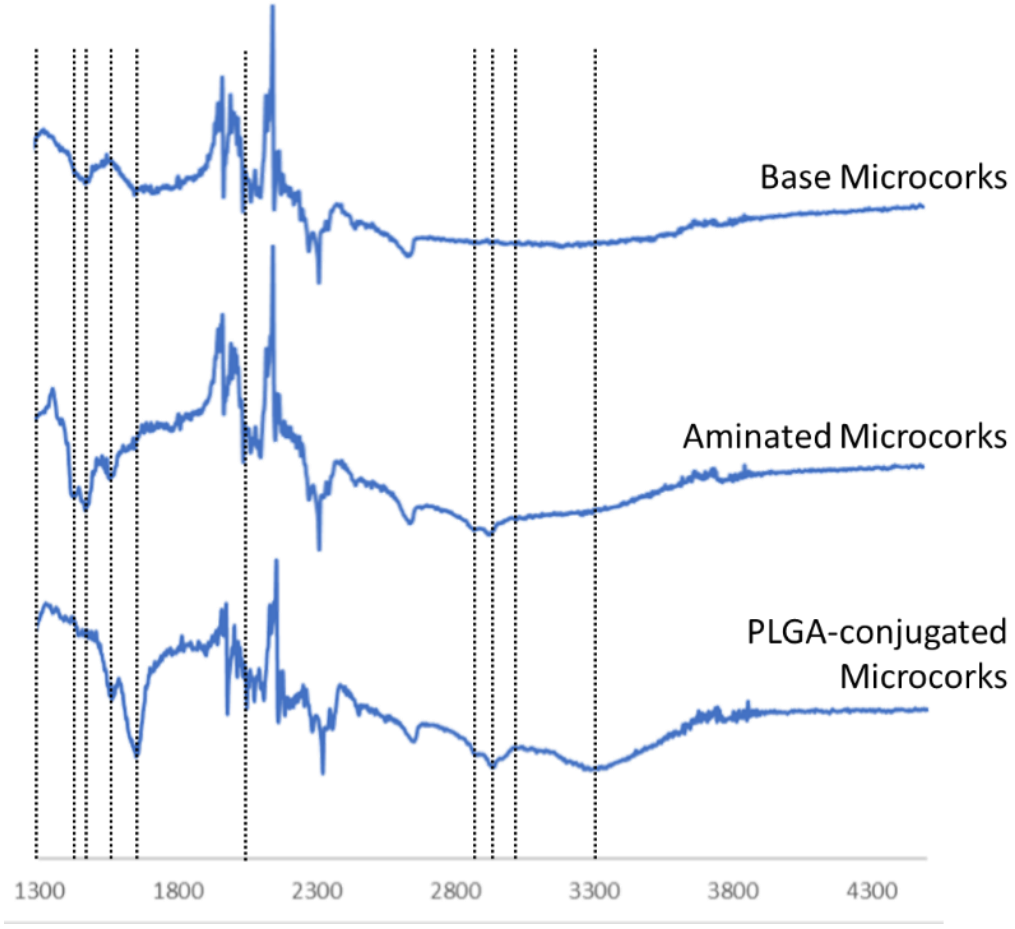

Figure 2.9: ATR-FTIR spectra for base corks (top), aminated corks (middle), and PLGA-conjugated corks (bottom)

2.9.2 Dry Electrospraying

The dry electrospraying setup was used to probe which solvent to use, what material concentrations were useful, and what voltages and flow rates would be relevant for particle formation. The SEM images in Figure 2.10 show the particles fabricated under various processing conditions.

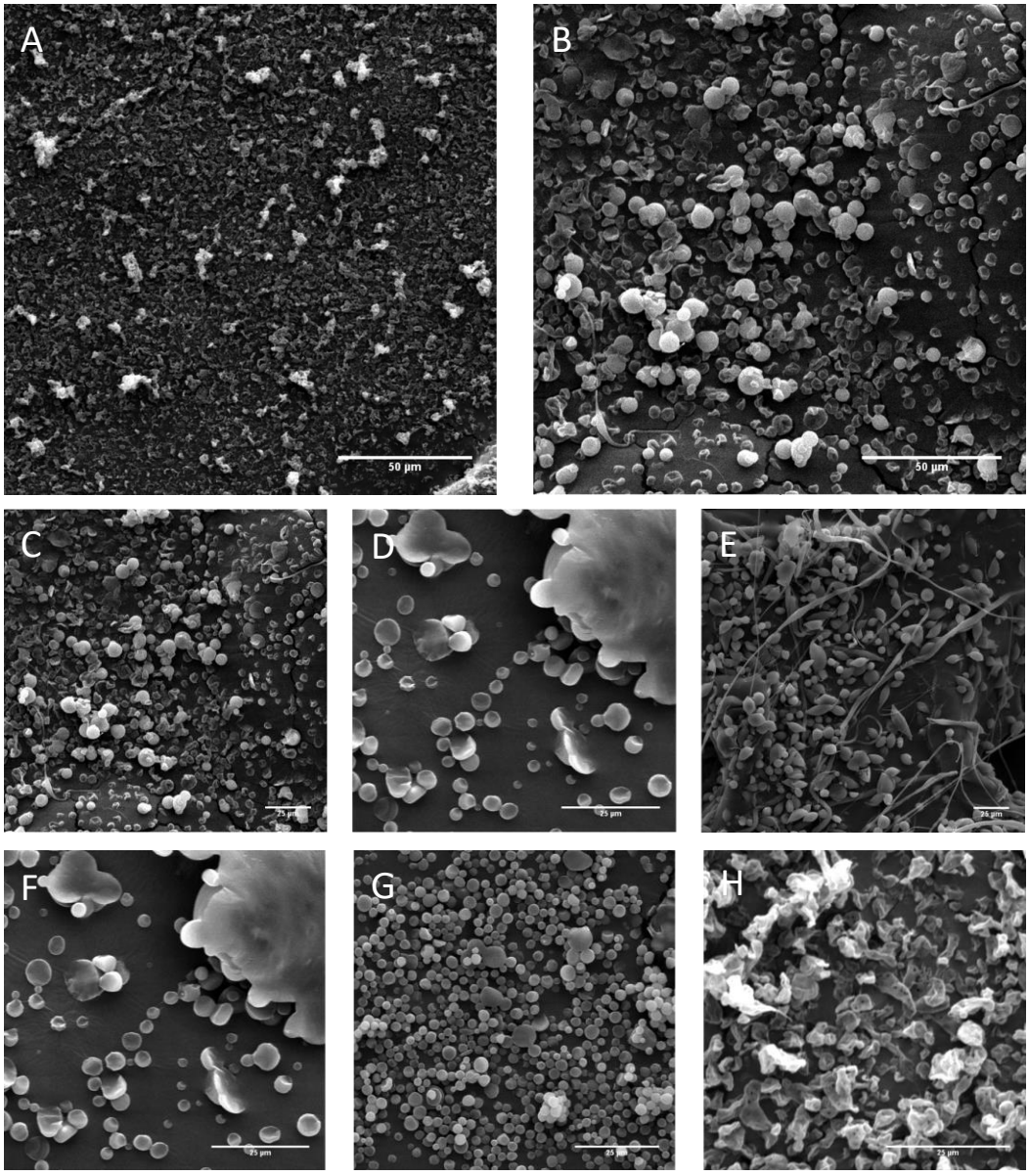

Figure 2.10: SEM images of EHD products of PLGA under different operational condition (base formulation = 1 w/v% PLGA in chloroform, extruded at 1.5 mL/h with 8 kV applied voltage. (A) using acetonitrile as the solvent for the shell phase, (B) using chloroform as the solvent for the shell phase, (C) using 1 w/v% PLGA in the shell phase, (D) using 2 w/v % PLGA in the shell phase, (E) 3 w/v% PLGA in the shell phase, (F) using 8 kV as the voltage, (G) using 16 kV as the voltage, (H) using 19 kV as the voltage

In terms of solvents, acetonitrile (dielectric constant = 37.5) [181] creates an irregular spray (Figure 2.10A) while chloroform (dielectric constant = 4.8) [181] facilitates the formation of significantly more spherical and consistent products (Figure 2.10B). This result is consistent with the higher dielectric solvent facilitating increased charging in the fluid and thus more aggressive expulsion of the fluid out of the Taylor cone under a given voltage. In terms of polymer concentrations, spherical particles can be fabricated using 1 w/v% (Figure 2.10C) and 2 w/v% (Figure 2.10D) solutions of PLGA in chloroform but 3 w/v% of PLGA starts to induce the formation of fibres and ellipsoids (Figure 2.10E). This result is consistent with the observed increased viscosity in the extruded phase at higher polymer concentrations, resulting in a switch from electrospray to electrospinning as predicted by theory [30, 43, 164]. In terms of voltage, increasing the voltage from 8 kV (Figure 2.10F) to 16 kV (Figure 2.10G) decreases the size of the microcapsules, again consistent with theory; however, at 19kV (Figure 2.10H), the increased surface tension caused by the potential difference coupled with the increased acceleration of the material toward the collector causes the product to lose its sphericity.

2.9.3 Wet Coaxial Electrospraying

The use of a coaxial needle and an aqueous collection medium significantly changed the dynamics of the fabrication process and thus the nature of the particles formed. Figure 2.11 shows the products of the fabrication process using bright field microscopy (Figure 2.11A) and conventional fluorescent microscopy (Figure 2.11B), with the colours

representing an overlay of the FITC labeled inner core (green) and the rhodamine B labeled shell (pink/red).

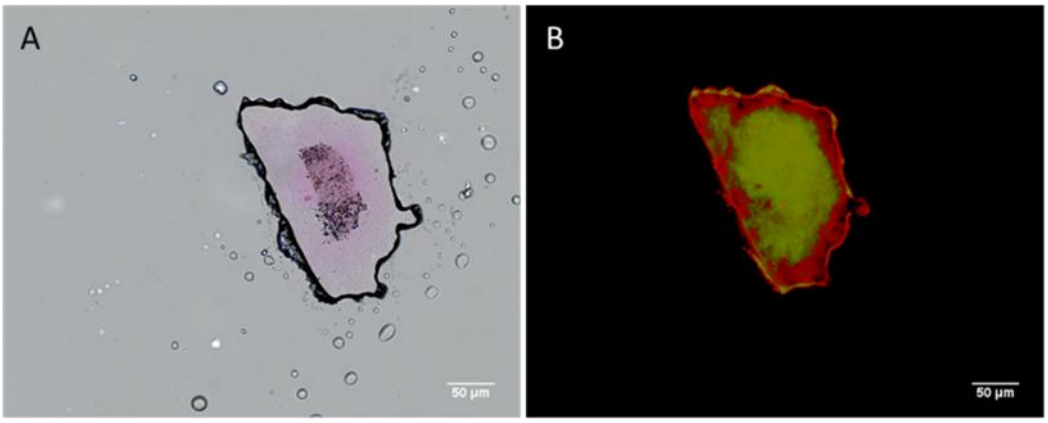

Figure 2.11:Irregular coaxial PLGA product under two different imaging modes. (A) bright field microscopy, (B) fluorescence microscopy. Green – rhodamine 123 in aqueous phase, red – rhodamine B in PLGA.

The most obvious difference between wet electrospraying (Figure 2.11) relative to dry electrospraying (Figure 2.10) is the unusual geometry of the wet electrospraying product, which was duplicated across the full sample population. This irregular shape is problematic for a capsular drug delivery vehicle, since inconsistent shell thicknesses would result in unpredictable or at least inconsistent release. However, significant other variability is also observed in this process. In many trials, the process would only yield a thin film on the surface of the water of the collection bath instead of particles, a result of the high surface tension between PLGA and water that favours trapping of the particles at the air-water interface [148].

2.9.4 Immersion Coaxial Electrospraying

To circumvent such problems, immersion coaxial electrospraying was attempted by submerging the tip of the coaxial needle in the collection bath to eliminate the air interface and, by using surfactants to engineer the interfacial tension, improve the likelihood of fabricating uniform spherical microcapsules. Figure 2.12 shows the effects of voltage (A), continuous phase surfactant concentration (B), total flow rate (C), and different inner phase surfactants at different concentrations (D) on the size of microcapsules produced using the immersion coaxial electrospray process.

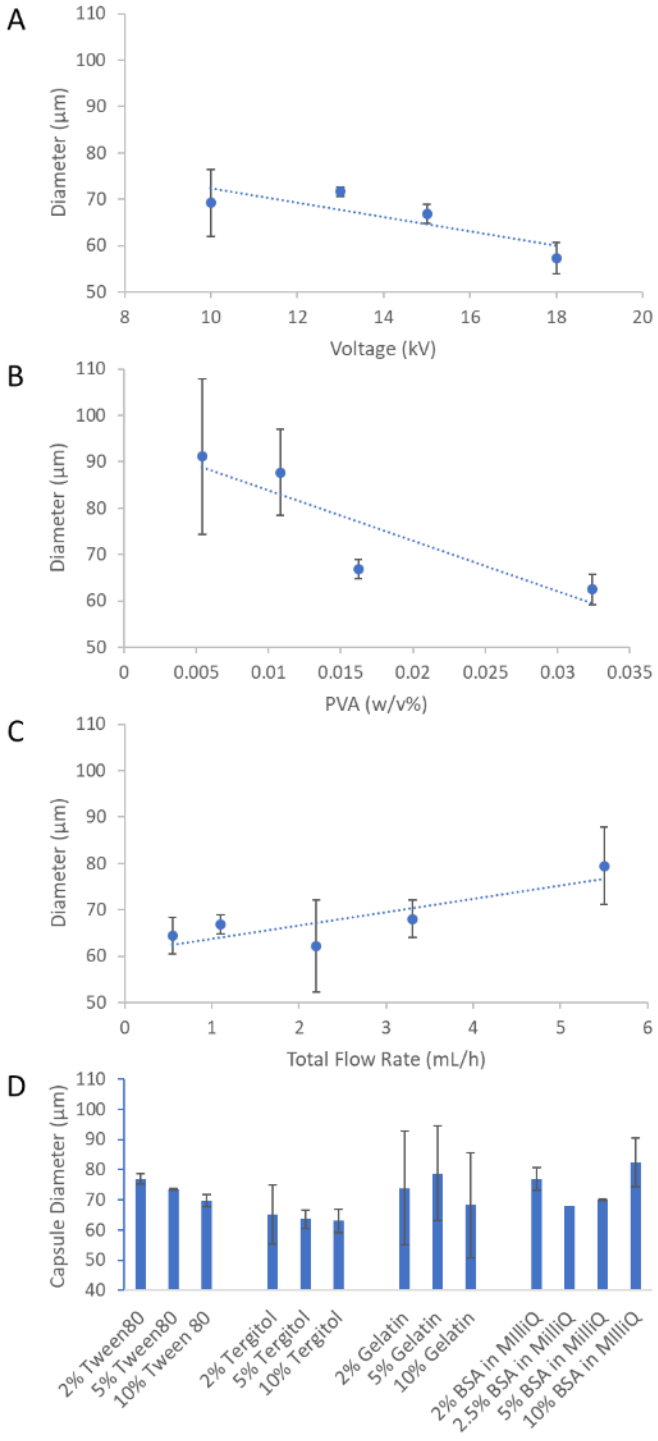

Figure 2.12: Effects of the working parameters of immersion coaxial electrospraying on PLGA microcapsule size: (A) voltage; (B) PVA concentration in the collector bath; (C) total flow rate; (D) type of surfactant used in the inner core phase

In comparison to the dry electrospraying experiments, the effects of voltage are slightly less noticeable, albeit with a significant decrease in microcapsule size at very high voltages (18 kV) (Figure 2.12A). In contrast, the amount of PVA in the continuous phase is highly influential (Figure 2.12B). In the absence of PVA, a film is formed around the needle and no microcapsules are produced. However, even upon a small amount of PVA addition, the formation of a broad dispersity microcapsule population is observed, with particle size decreasing as the PVA concentration was increased to 0.016 w/v%. Above this critical concentration, the particle size plateaus independent of the PVA concentration, with bright field microscopy images indicating the likely presence of residual PVA aggregates between the particles upon drying (Figure 2.13B). We hypothesize that PVA concentrations above 0.016 w/v% are beyond what is required to saturate the interface available in the system, making the addition of further PVA ineffective to further reduce interfacial tension and facilitate the fabrication of smaller microcapsules.

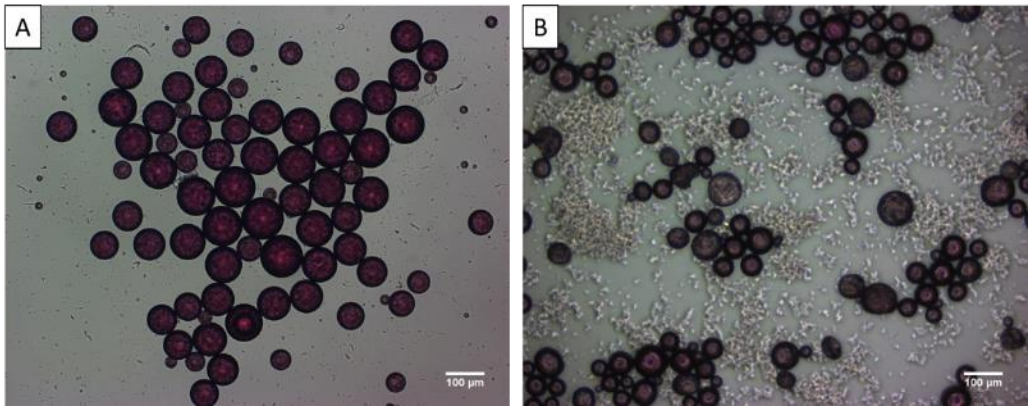

Figure 2.13: Bright field microscopy images of fabricated microcapsules prepared using different continuous phase PVA stabilizer concentrations. (A) 0.016 w/v%, (B) 0.032 w/v%

The total flow rate had only a minimal effect on particle size provided the relative core:shell flow rates were kept constant (Figure 2.12C), although a small increase in diameter is observed at very high flow rates which we relate to a decrease in the available charging time of the solution prior to expulsion from the needle. It seems that the relationship between microcapsule size, voltage, and flow rate follows Equation 2.3. Jaworek speaks about the size of the microcapsules being controlled by mutual coulombic repulsion[95], though the complex equation can be simplified conceptually to the following statement: the work applied to a singular microcapsule is the electric potential multiplied by the time of exposure to the electric potential at the tip of the needle. By increasing the flow rate, the amount of time for which a microcapsule is at the tip of the coaxial needle decreases, which gives less time for charging to occur as per prior literature[29-31, 43].

Equation 2.3

$$Size = a * \left(\frac{\#\ of\ capsules/s}{V}\right)$$

Finally, the type of surfactant used to stabilize the inner phase in the shell phase has a significant impact on the fabrication process (Figure 2.12D). Five different surface-active agents previously reported to stabilize interfaces in microcapsule formation processes - BSA, gelatin, Tergitol NP-4, Tween 80, and Span 80 – were screened to assess their potential for microcapsule fabrication. All the surfactants except Span 80 facilitated microcapsule formation. The HLB affects how the concentrations of each surfactant affect the microcapsule size. Surfactants with intermediate to higher HLB values (i.e. Tergitol NP-4 = 8.9[182] and Tween 80 = 15.0 [66]) facilitated the production of smaller

microcapsules, while low HLB surfactants (Span 80 = 4.3 [66]) could not make microcapsules. Surface stabilizers like BSA and gelatin, which both have capacity to interact with both water and oil phases at room temperature, give less systematic results in which BSA first decreases and then increases microcapsule size as its concentration is increased and gelatin giving no significant change in microcapsule size over the concentration range tested. For gelatin, this result is likely attributable to its extremely high viscosity at room temperature which may clog the needle; indeed, needle clogging was observed on the 5 w/v% sample. Effective use of gelatin would require pre-heating of the inner core to ensure the contents of the syringe are extruded, which raises problems around the volatile DCM matrix containing the PLGA. However, overall, provided the surfactant HLB was not too low to make microcapsules, collector bath surfactant effects were small relative to other parameters.

To assess the internal morphology and confirm the capsular structure of the produced particles, confocal microscopy was used. Figure 2.14 shows a confocal microscope cross-sectional image of a microcapsule prepared using the base immersion electrospray recipe in which the shell phase is labeled with Rhodamine B (hydrophobic) and the inner core is labeled with Rhodamine 123 (hydrophilic). The capsular structure is clearly visible, with a ~5 μm concentric shell within a ~40 μm total size microcapsule

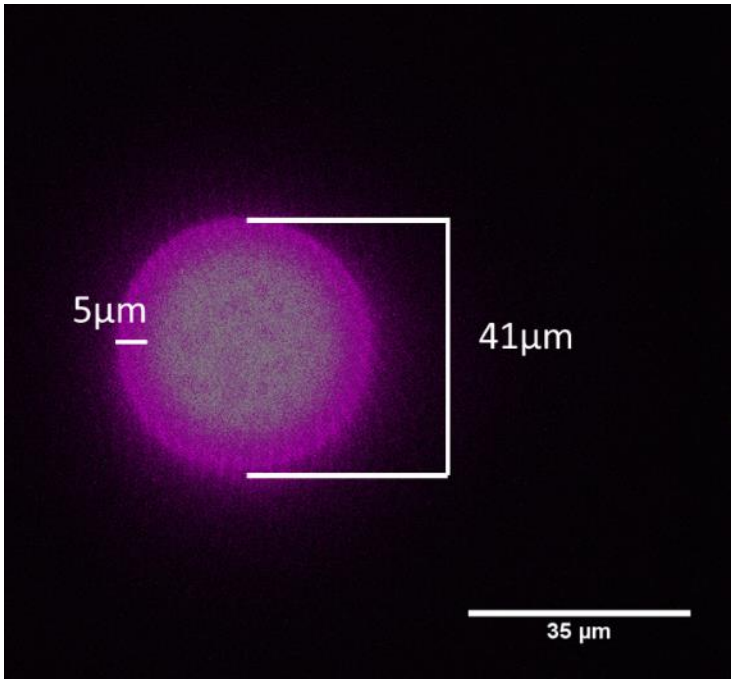

Figure 2.14: Confocal microscopy cross-section of a microcapsule whose inner aqueous BSA core is labeled with Rhodamine 123 (green) and PLGA shell phase is labeled with Rhodamine B (magenta)

2.9.5 Incorporation of Microcorks in the Microcapsules

When unmodified silica microcorks were dispersed at a concentration of 1 w/v% in a 1 w/v% PLGA/DCM solution, the microcorks sedimented almost immediately due to the low interfacial stabilization of the microcorks inside the DCM solution. To solve this problem, the surface of the microcorks was modified with PLGA (to match the chemistry of the polymer in the "dispersed" phase of the shell) and the concentration of PLGA in the DCM was increased (increasing the viscosity of the shell phase and thus reducing the rate of gravitational sedimentation independent of microcork surface properties). Using these

strategies, the microcorks remained much better suspended in the shell solution over the course of fabrication to enable the formation of corked microcapsules.

To assess the potential for cork entrapment in the shell, 1 w/v% FITC-conjugated microcorks were suspended in a 5 w/v% PLGA+Rhodamine B/DCM solution and electrosprayed at a total flow rate of 1.1 mL/h for 1 hour, with all other parameters corresponding to the base immersion electrospinning recipe. As can be seen in the confocal microscopy projection in Figure 2.15, corks were successfully embedded in the shell of the microcapsule. However, pumping problems associated with microcork settling were still observed after a process time of ~30 min, requiring the high voltage generator and syringe pumps be stopped and the syringe containing the microcorks and the PLGA agitated intensely to re-disperse the microcorks prior to resuming processing. Beyond this, further inspection of the microcapsules fabricated at a flow rate of 1.1 mL/h would be somewhat ellipsoidal instead of spherical, and the microcorks seemed to be embedded deep in the shell (i.e. closer to the inner core rather than balanced between the inside and the outside as required for forming a pore upon removal of the microcork). As such, the process of stopping and starting and staggering of the electrospraying fabrication was deemed ineffective. Increasing the total flow rate to 3.3 mL/h (reducing the time required to create the same yield of microcapsules from 1 h to 20 mins.) yields similar microcapsule diameters and spherical shapes (Figure 2.15C) to those achieved in the microcork-free formulations (Figure 2.15A, $p > 0.05$), although the voltage was increased to 18 kV to compensate for the higher viscosity of the shell phase in the corked samples. In addition, under this higher flow rate condition, the microcorks were more

evenly dispersed in the shell instead of being buried toward the interior of the microcapsule shell.

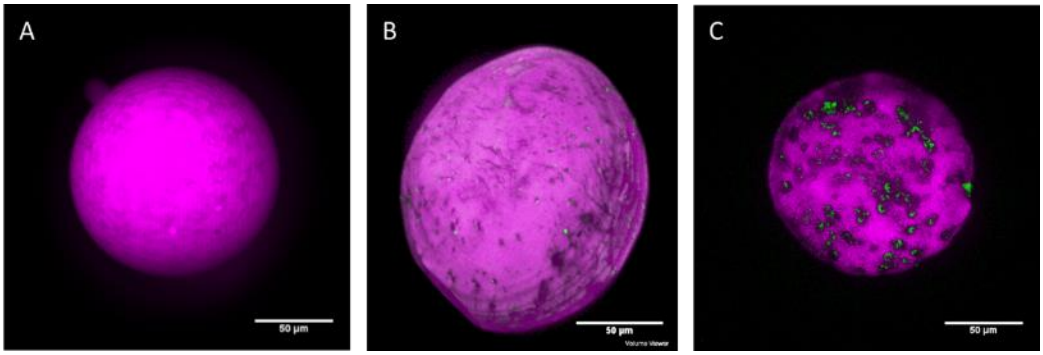

Figure 2.15: Fabrication of PLGA microcapsules. (A) without microcorks; (B) with PLGA microcorks embedded in the shell of a microcapsule fabricated using a total flow rate of 1.1 mL/h for 1 h; (C) with PLGA microcorks embedded in the shell of a microcapsule fabricated at a total flow rate of 3.3 mL/h for 20 mins. Magenta = Rhodamine B in PLGA shell; Green = FITC on microcorks

Even when the flow rate is increased, the corks suspended in the PLGA/DCM solution still sink in the syringe. Although this does not ultimately hinder the processability of the sample, Figure 2.16 shows that the settling process does introduce some variability to the number of corks embedded in each microcapsule at different time points during the EHD processing step. Figure 2.16 compares a "full-time" batch of microcapsules electrosprayed for 1 hour with a total flow rate of 1.1 mL/h to microcapsules that were sampled every 5 minutes over a 20 minute electrospraying process conducted at a total flow rate of 3.3 mL/h. The longer process shows considerable variability in the number of corks present per sample (Figure 2.16A), while the frequently collected samples in the 3.3 mL/h process show substantially higher densities of corks at the start of the process

(i.e. the 0-5 minute fraction, Figure 2.16B) relative to toward the end of the process (i.e. the 10-15 minute and 15-20 minute fractions, Figure 2.16D and E respectively). While this result suggests the potential for future process redesign to identify better ways of suspending the corks continuously within the syringe, this phenomenon also makes it possible to create diverse populations of cork-shell microcapsules in a single processing step, potentially useful for providing fine-tuned control over drug release as a function of time.

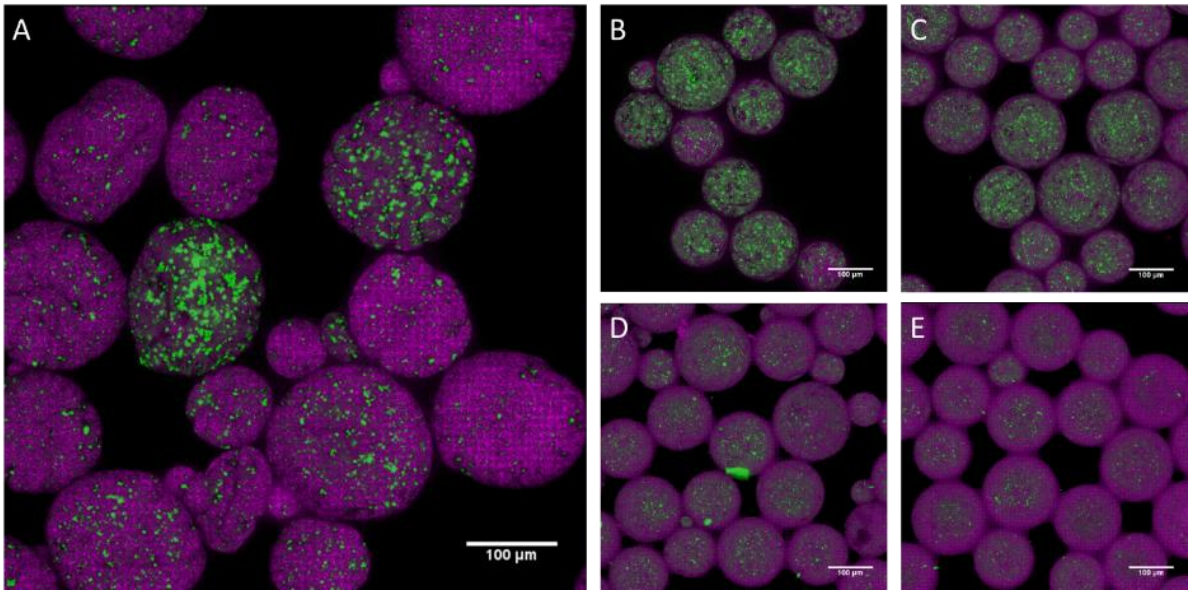

Figure 2.16: Study of the effect of processing time on microcork density within cork-shell microparticles: (A) Cumulatively collected microcapsules after 1 h of processing using a 1.1mL/hr total flow rate, (B) Microcapsules produced between 0-5 min processing times using a 3.3 mL/h total flow rate, (C) Microcapsules produced between 5-10 min processing times using a 3.3 mL/h total flow rate, (D) Microcapsules produced between 10-15 min processing times using a 3.3 mL/h total flow rate, (E) Microcapsules produced between 15-20 min processing times using a 3.3 mL/h total flow rate Magenta = PLGA shell, green = FITC in microcorks

2.9.6 Cell Viability

MTS assays were performed on the different variations of the microcapsules and their constituents to see the effects of the various compositions and microcapsule components on cell viability. Cork-free microcapsules were fabricated without any fluorescent labels using inner cores containing 2.5% w/v or v/v of Tween 80, Tergitol-NP4, or BSA; the PLGA-microcorks and BSA microcapsules with corks were also screened. A total mass of 0.1 mg of microcapsules or 0.02 mg of microcorks was introduced to the 3T3 fibroblasts (5000 cells/well), with the metabolic assay results shown in Figure 2.17. None of the formulations tested exhibited any significant toxicity to 3T3 mouse fibroblast cells relative to a cell-only (untreated) control, suggesting that the microcapsules, the corks, and the microcapsules with embedded corks are all non-cytotoxic and potentially useful for practical drug delivery applications.

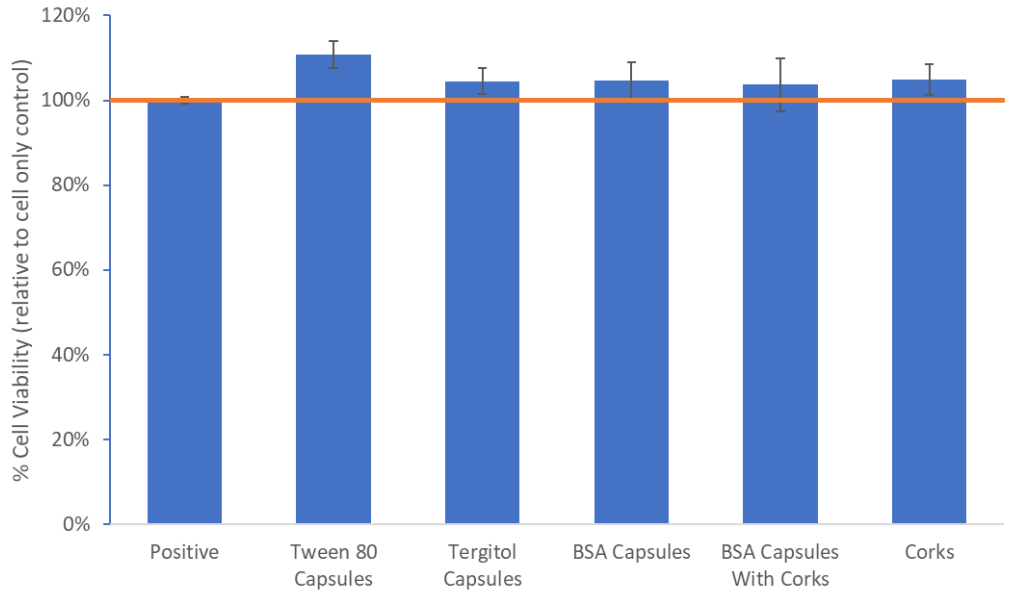

Figure 2.17: MTS proliferation assay on 3T3 mouse fibroblast cells treated with various components of the cork-shell microcapsule formulations developed

2.10 Discussion

The fabrication of PLGA microcapsules and microspheres was carried out using a variety of EHD fabrication processes, namely dry electrospraying, wet coaxial electrospraying, and the less-studied approach of immersion coaxial electrospraying. Increasing the PLGA concentration beyond 2% w/v in chloroform for dry electrospraying begins to form elongated microcapsules and fibres, identifying this concentration as the functional limit for PLGA to create spherical products (consistent with prior literature)[30, 96, 164, 181]; similarly consistent with prior works, using a solvent with a lower dielectric constant will more readily maintain and produce spheres[43, 162, 179] and increasing the voltage reduced the sphere size[29, 31].

Coaxial electrospraying introduced the variable of the inner core and the associated new interfaces created as a result of the two-phase input. In order to ensure the inner core was completely encapsulated by the PLGA shell, the surface tension of the inner aqueous phase needed to be modified[45, 148, 179], with BSA found to be effective for this purpose [51, 55, 162, 183]. However, when droplets were first formed in air, the geometry of the electrosprayed product was inconsistent; frequently, a film would form at the air/water interface, suggesting the surface tension between the PLGA and the continuous water bath was too high even with PVA added to the continuous phase[148]. Submersing the needle in the continuous bath removes the interface problem while still permitting electrospraying, enabling the generation of more reproducible spherical microcapsules. In addition, while 2 w/v% PLGA loading was the functional limit for electrospraying in the dry system, but the immersion technique allowed for a 2.5x increase in the PLGA concentration without negatively impacting the sphericity of the particles. Since the dielectric constant of the material affects the electrospraying result, it would be interesting to see how the effects of collector fluids with different dielectric constants would affect the fabrication process.

To incorporate microcorks into the shell, the combination of the higher PLGA content (i.e. higher shell phase viscosity) enabled with immersion electrospray and the surface functionalization of the microcorks with PLGA significantly slowed the sinking of the microcorks in the shell phase syringe to allow for the formation of corked microcapsules. This is a significant advancement given that, prior to this writing, the only such modification using EHD was an electrospinning process that required a rotating mandrel and 3 syringe pumps[152]. However, a clear decrease in cork density was observed as a

function of electrospraying time. Developing alternative ways to mix the shell solution prior to electrospinning and/or miniaturizing the microcapsules such that smaller corks with lower sedimentation velocities could be used could address this challenge, although the gradient of cork-shell microcapsules formed may in fact be beneficial in some drug delivery applications to tune release. MTS cytotoxicity assays indicated cell viabilities of ~100% relative to the cell-only control for both full cork-shell microcapsules as well as the individual components thereof, suggesting these components are non-cytotoxic and may be viable drug delivery vehicles.

2.11 Conclusions

A non-cytotoxic microcapsule was fabricated using a modified EHD process dubbed immersion coaxial electrospraying that can overcome the functional limitations of polymer concentration that typically transition electrospraying into electrospinning. The effects of common electrospraying parameters conformed with theoretical predictions with conventional EHD fabrication. Incorporation of PLGA-modified silica in the shell phase of the microcapsule resulted in the embedding of microcorks within the shell, although the microcork density in the microcapsules was dependent on the duration of the fabrication process.

Moving forward, several improvements could be made to this entire process. The first and most important is to better control the microcork density in the shell as a function of electrospray time. We expect this could be achieved by using a pneumatically controlled system capable of continuously stirring the solution/dispersion to maintain equal uniform

concentrations of microcorks throughout the delivery syringe over time. Another potential for future work would be to further study all of the working parameters of the immersion coaxial electrospraying process. Of note, it would be interesting to see how the dielectric constant of the continuous phase would affect the electrospraying process. By increasing the dielectric constant and decreasing the surface tension between PLGA and the continuous phase, significant miniaturization of the product may be achieved, of interest to (for example) create cork-shell microcapsules on the size scale that could circulate rather than simply be immobilized at the injection site. Additionally, it would be of interest to study the encapsulation efficiency of varying payloads. Finally, it would be of interest to see how different cork materials can be incorporated into the system as well as additional surface binding ligands, particularly with an eye toward *in vivo* translation in which eventual degradation of the corks is desirable.

2.12 References

1. Menon, J.U., et al., *Effects of surfactants on the properties of PLGA nanoparticles.* J Biomed Mater Res A, 2012. 100(8): p. 1998-2005.
2. Figueiredo, M. and R. Esenaliev, *PLGA Nanoparticles for Ultrasound-Mediated Gene Delivery to Solid Tumors.* J Drug Deliv, 2012. 2012: p. 767839.
3. Mendelsohn, A.D., et al., *Patterning of mono- and multilayered pancreatic beta-cell clusters.* Langmuir, 2010. 26(12): p. 9943-9.
4. Yu, J., et al., *Stimuli-Responsive Delivery of Therapeutics for Diabetes Treatment.* Bioeng Transl Med, 2016. 1(3): p. 323-337.
5. Lafond, M., et al., *Cavitation-threshold Determination and Rheological-parameters Estimation of Albumin-stabilized Nanobubbles.* Sci Rep, 2018. 8(1): p. 7472.
6. Gao, Z., et al., *Drug-loaded nano/microbubbles for combining ultrasonography and targeted chemotherapy.* Ultrasonics, 2008. 48(4): p. 260-70.

7. Mikhaylov, G., et al., *Ferri-liposomes as an MRI-visible drug-delivery system for targeting tumours and their microenvironment.* Nat Nanotechnol, 2011. 6(9): p. 594-602.
8. Fokong, S., et al., *Image-guided, targeted and triggered drug delivery to tumors using polymer-based microbubbles.* J Control Release, 2012. 163(1): p. 75-81.
9. Phillips, L.C., et al., *Phase-shift perfluorocarbon agents enhance high intensity focused ultrasound thermal delivery with reduced near-field heating.* J Acoust Soc Am, 2013. 134(2): p. 1473-82.
10. Azizi, M., et al., *Fabrication of protein-loaded PLGA nanoparticles: effect of selected formulation variables on particle size and release profile.* Journal of Polymer Research, 2013. 20(4).
11. Barz, M., et al., *P(HPMA)-block-P(LA) copolymers in paclitaxel formulations: polylactide stereochemistry controls micellization, cellular uptake kinetics, intracellular localization and drug efficiency.* J Control Release, 2012. 163(1): p. 63-74.
12. Tang, J., et al., *Controlled drug release from ultrasound-visualized elastic eccentric microcapsules using different resonant modes.* Journal of Materials Chemistry B, 2018. 6(13): p. 1920-1929.
13. Seo, M. and N. Matsuura, *Monodisperse, submicrometer droplets via condensation of microfluidic-generated gas bubbles.* Small, 2012. 8(17): p. 2704-14.
14. Matsumoto, A., et al., *Fabrication of Janus particles composed of poly (lactic-co-glycolic) acid and hard fat using a solvent evaporation method.* Drug Discov Ther, 2016. 10(6): p. 307-313.
15. Kang, M., G. Huang, and C. Leal, *Role of lipid polymorphism in acoustically sensitive liposomes.* Soft Matter, 2014. 10(44): p. 8846-54.
16. Mueller, E., et al., *Dynamically Cross-Linked Self-Assembled Thermoresponsive Microgels with Homogeneous Internal Structures.* Langmuir, 2018. 34(4): p. 1601-1612.
17. Simpson, M.J., et al., *Narrowly Dispersed, Degradable, and Scalable Poly(oligoethylene glycol methacrylate)-Based Nanogels via Thermal Self-Assembly.* Industrial & Engineering Chemistry Research, 2018. 57(22): p. 7495-7506.
18. Sivakumaran, D., E. Mueller, and T. Hoare, *Temperature-Induced Assembly of Monodisperse, Covalently Cross-Linked, and Degradable*

Poly(N-isopropylacrylamide) Microgels Based on Oligomeric Precursors. Langmuir, 2015. 31(21): p. 5767-78.
19. Ahmad, Z., et al., *Generation of multilayered structures for biomedical applications using a novel tri-needle coaxial device and electrohydrodynamic flow.* J R Soc Interface, 2008. 5(27): p. 1255-61.
20. Birajdar, M.S. and J. Lee, *Nanoscale Bumps and Dents on Nanofibers Enabling Sonication-Responsive Wetting and Improved Moisture Collection.* Macromolecular Materials and Engineering, 2015. 300(11): p. 1108-1115.
21. Gao, Y., et al., *Tuning Microparticle Porosity during Single Needle Electrospraying Synthesis via a Non-Solvent-Based Physicochemical Approach.* Polymers, 2015. 7(12): p. 2701-2710.
22. Ghayempour, S. and S.M. Mortazavi, *Fabrication of micro–nanocapsules by a new electrospraying method using coaxial jets and examination of effective parameters on their production.* Journal of Electrostatics, 2013. 71(4): p. 717-727.
23. Jaworek, A. and A.T. Sobczyk, *Electrospraying route to nanotechnology: An overview.* Journal of Electrostatics, 2008. 66(3-4): p. 197-219.
24. M, J.C., et al., *Mimicking Hierarchical Complexity of the Osteochondral Interface Using Electrospun Silk-Bioactive Glass Composites.* ACS Appl Mater Interfaces, 2017. 9(9): p. 8000-8013.
25. Xu, Q., et al., *Coaxial electrohydrodynamic atomization process for production of polymeric composite microspheres.* Chem Eng Sci, 2013. 104.
26. Xu, Y. and M.A. Hanna, *Electrospray encapsulation of water-soluble protein with polylactide. Effects of formulations on morphology, encapsulation efficiency and release profile of particles.* Int J Pharm, 2006. 320(1-2): p. 30-6.
27. Zhang, Y., et al., *Mechanical Force-Triggered Drug Delivery.* Chem Rev, 2016. 116(19): p. 12536-12563.
28. Song, G., et al., *Perfluorocarbon-Loaded Hollow Bi2Se3 Nanoparticles for Timely Supply of Oxygen under Near-Infrared Light to Enhance the Radiotherapy of Cancer.* Adv Mater, 2016. 28(14): p. 2716-23.
29. Di, J., et al., *Ultrasound-triggered noninvasive regulation of blood glucose levels using microgels integrated with insulin nanocapsules.* Nano Research, 2017. 10(4): p. 1393-1402.

30. Anderson, J.M., A. Rodriguez, and D.T. Chang, *Foreign body reaction to biomaterials.* Semin Immunol, 2008. **20**(2): p. 86-100.
31. Vasquez, K.O., C. Casavant, and J.D. Peterson, *Quantitative whole body biodistribution of fluorescent-labeled agents by non-invasive tomographic imaging.* PLoS One, 2011. **6**(6): p. e20594.
32. Jaworek, A., *Electrospray droplet sources for thin film deposition.* Journal of Materials Science, 2006. **42**(1): p. 266-297.
33. Latham, J. and I.W. Roxburgh, *Disintegration of Pairs of Water Drops in an Electric Field.* Proceedings of the Royal Society of London. Series A, Mathematical and Physical Sciences, 1966. **295**(1440): p. 84-97.
34. Taylor, G., *Disintegration of Water Drops in an Electric Field.* Proceedings of the Royal Society of London. Series A, Mathematical and Physical Sciences, 1964. **280**(1382): p. 383-397.
35. Li, Z. and C. Wang, *Effects of Working Parameters on Electrospinning*, in *One-Dimensional nanostructures*. 2013. p. 15-28.
36. Loeb, L.B., et al., *Pulses in Negative Point-to-Plane Corona.* Physical Review, 1941. **60**(10): p. 714-722.
37. Davoodi, P., et al., *Coaxial electrohydrodynamic atomization: microparticles for drug delivery applications.* J Control Release, 2015. **205**: p. 70-82.
38. Gao, Y., et al., *Optimising the shell thickness-to-radius ratio for the fabrication of oil-encapsulated polymeric microspheres.* Chemical Engineering Journal, 2016. **284**: p. 963-971.
39. Zhang, L., et al., *Coaxial electrospray of microparticles and nanoparticles for biomedical applications.* Expert Rev Med Devices, 2012. **9**(6): p. 595-612.
40. D'Amore, A., et al., *Heart valve scaffold fabrication: Bioinspired control of macro-scale morphology, mechanics and micro-structure.* Biomaterials, 2018. **150**: p. 25-37.
41. Fujimoto, K.L., et al., *An elastic, biodegradable cardiac patch induces contractile smooth muscle and improves cardiac remodeling and function in subacute myocardial infarction.* J Am Coll Cardiol, 2007. **49**(23): p. 2292-300.
42. Wang, F., et al., *Fabrication and Characterization of Prosurvival Growth Factor Releasing, Anisotropic scaffolds for Enhanced Mesenchymal Stem Cell Survival Growth and Orientation.* Biomacromolecules, 2009. **10**(9): p. 2609-2618.

43. Li, M., et al., *Culturing primary human osteoblasts on electrospun poly(lactic-co-glycolic acid) and poly(lactic-co-glycolic acid)/nanohydroxyapatite scaffolds for bone tissue engineering.* ACS Appl Mater Interfaces, 2013. **5**(13): p. 5921-6.
44. Jaworek, A., *Micro- and nanoparticle production by electrospraying.* Powder Technology, 2007. **176**(1): p. 18-35.
45. Lee, Y.H., et al., *Release profile characteristics of biodegradable-polymer-coated drug particles fabricated by dual-capillary electrospray.* J Control Release, 2010. **145**(1): p. 58-65.
46. Rasekh, M., et al., *Hollow-layered nanoparticles for therapeutic delivery of peptide prepared using electrospraying.* J Mater Sci Mater Med, 2015. **26**(11): p. 256.
47. Moghaddam, M.K., S.M. Mortazavi, and T. Khaymian, *Micro/nano-encapsulation of a phase change material by coaxial electrospray method.* Iranian Polymer Journal, 2015. **24**(9): p. 759-774.
48. Xie, J. and C.H. Wang, *Electrospray in the dripping mode for cell microencapsulation.* J Colloid Interface Sci, 2007. **312**(2): p. 247-55.
49. Kishan, A.P. and E.M. Cosgriff-Hernandez, *Recent advancements in electrospinning design for tissue engineering applications: A review.* J Biomed Mater Res A, 2017. **105**(10): p. 2892-2905.
50. Wu, Y. and R.L. Clark, *Controllable porous polymer particles generated by electrospraying.* J Colloid Interface Sci, 2007. **310**(2): p. 529-35.
51. Casper, C.L., et al., *Controlling Surface Morphology of Electrospun Polystyrene Fibers: Effect of Humidity and Molecular Weight in the Electrospinning Process.* Macromolecules, 2004. **37**(2): p. 573-578.
52. Mit-uppatham, C., M. Nithitanakul, and P. Supaphol, *Ultrafine Electrospun Polyamide-6 Fibers: Effect of Solution Conditions on Morphology and Average Fiber Diameter.* Macromolecular Chemistry and Physics, 2004. **205**(17): p. 2327-2338.
53. McDonagh, P.F. and S.K. Williams, *The Preparation and Use of FluorescentProtein Conjugates for Microvascular Research.* Microvascular Research, 1984. **27**(1): p. 14-27.
54. Wischke, C. and H.-H. Borchert, *Fluorescein isothiocyanate labelled bovine serum albumin (FITC-BSA) as a model protein drug: opportunities and drawbacks.* Pharmazie, 2005. **61**(9): p. 770-774.

55. Salomi, B.S.B., C.K. Mitra, and L. Gorton, *Electrochemical and spectrophotometric studies on dyes and proteins labelled with dyes.* Synthetic Metals, 2005. **155**(2): p. 426-429.
56. Wu, F., et al., *Grafting polymerization of polylactic acid on the surface of nano-SiO2and properties of PLA/PLA-grafted-SiO2nanocomposites.* Journal of Applied Polymer Science, 2013. **129**(5): p. 3019-3027.
57. Lee, Y.-C., et al., *Optical Properties of Fluorescein labeled Organoclay.* Photochemistry and Photobiology, 2010. **86**(3): p. 520-527.
58. Mei, F. and D.R. Chen, *Operational modes of dual-capillary electrospraying and the formation of the stable compound cone-jet mod.* Aerosol and Air Quality Research, 2008. **8**(2): p. 218-232.
59. Torza, S. and S.G. Mason, *Three-phase interactions in shear and electrical fields.* Journal of Colloid and Interface Science, 1970. **33**(1): p. 67-83.
60. Gennes, P.-G.d., F. Brochard-Wyart, and D. Quere, *Drops, Bubbles, Pearls, Waves*, in *Capillarity and Wetting Phenomena*. 2004, Springer-Verlag New York.
61. Smallwood, I.M., *Handbook of Organic Solvent Properties*. 1996, New York: Halsted Press.
62. Company, D.C., *Tergitol NP-4 Surfactant*, D.C. Company, Editor.
63. Ltd., C.E., *Span and Tween*, C.E. Ltd., Editor. 2009: England.
64. Ishak, R.A.H., N.M. Mostafa, and A.O. Kamel, *Stealth lipid polymer hybrid nanoparticles loaded with rutin for effective brain delivery - comparative study with the gold standard (Tween 80): optimization, characterization and biodistribution.* Drug Deliv, 2017. **24**(1): p. 1874-1890.
65. Chitkara, D. and N. Kumar, *BSA-PLGA-based core-shell nanoparticles as carrier system for water-soluble drugs.* Pharm Res, 2013. **30**(9): p. 2396-409.
66. Zhao, C.X., *Multiphase flow microfluidics for the production of single or multiple emulsions for drug delivery.* Adv Drug Deliv Rev, 2013. **65**(11-12): p. 1420-46.
67. Bakaic, E., N.M.B. Smeets, and T. Hoare, *Injectable hydrogels based on poly(ethylene glycol) and derivatives as functional biomaterials.* RSC Advances, 2015. **5**(45): p. 35469-35486.

Chapter 3 - Ultrasound-Triggered Release from Cork-Shell Microcapsules

On-demand drug delivery can be induced by a range of stimuli including pH, enzymatic degradation, magnetic field manipulations, radiative stimulus, and ultrasound ablation[4-6, 8, 12, 13, 16, 21, 22, 24, 35, 54, 110, 129, 184]. All but the last of these can be classified as chemically-dependent activation since specific material(s) are required in order to drive the response. In contrast, ultrasound ablation can be designed to constitute a more mechanical triggering technique that does not rely specifically on the chemical properties of the material [4, 131-133, 145]. Herein, the mechanisms of ultrasound ablation and their potential uses in drug delivery will be discussed.

3.1 Background

Ultrasound is a subset of acoustic waves with frequencies >20 kHz[135]. In biomedical applications, it is widely used for imaging purposes as well as an increasing number of therapeutic purposes, although it can also be used diagnostically in a range of other applications (e.g. crack detection in civil engineering [185, 186] or to improve the efficiency of food processing [187]). When the ultrasound waves travel through a material, they induce perturbations that form longitudinal waves and selectively induce shear waves on materials with different mechanical indices[14, 88, 131, 138]. Figure 3.1 shows the translation of an energy wave through a material and the image window for diagnostic ultrasound resulting from this propagative transfer. Waves propagate through

different materials at different speeds through compression and expansion, leading to a change in wavelength, uptake of ultrasound energy, and a usable signal for imaging[134, 135, 138]. Longitudinal waves are primarily used in ultrasonography to perform imaging, while shear waves moving perpendicular to the longitudinal waves are used for applications in drug delivery and stiffness measurements [37, 88, 118, 132-134, 138, 188].

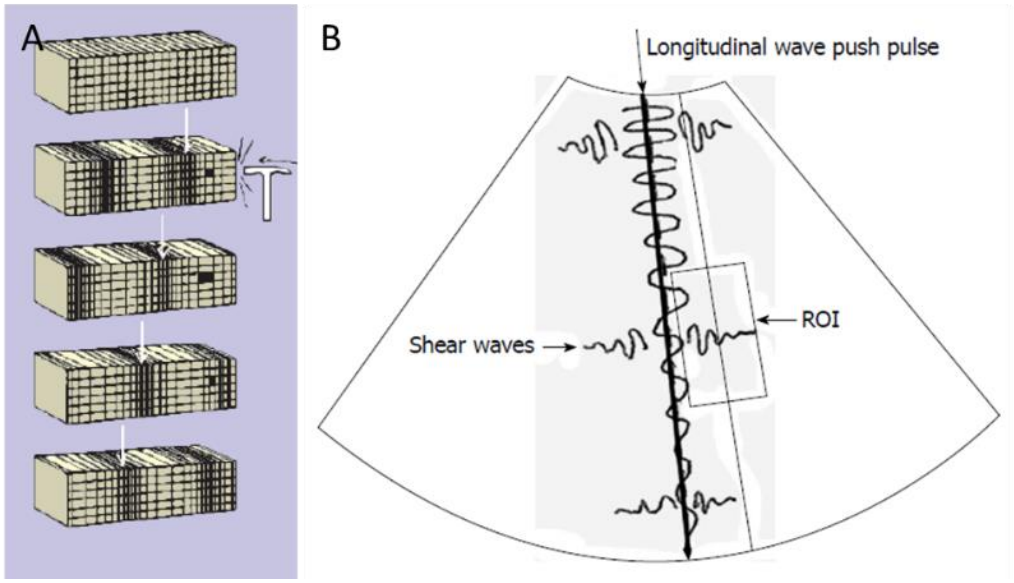

Figure 3.1: Propagation of acoustic waves through media. (A) demonstrates a longitudinal wave traveling through a block after being hit with a hammer. (B) provides an example of an ultrasound window with both longitudinal waves and shear waves. Adapted from [135, 138]

There are two key measurement units for ultrasound signals – acoustic pressure and ultrasound intensity[136]. Acoustic pressure (in units of Pa) is the difference between ambient pressure in the absence of any sound waves and the pressure in the presence of ultrasound. Acoustic pressure is measurable using a hydrophone[50, 131, 132, 139, 141],

which reads the peak negative pressure of a sinusoidal acoustic wave that accounts for expansion of the material. Acoustic intensity (in units of $W \cdot m^{-2}$) is the product of the acoustic pressure and the particle's velocity[135]. Since sound waves require a medium in which to travel, their propagation is dependent on the compressibility (κ, the reciprocal of the material's bulk modulus) and density (ρ) of that medium as per Equation 3.1. Based on this relationship, whereas sound travels at 330m/s in air, it travels at a rate of 1540 m/s in tissue and 1480 m/s in water[14, 134, 135].

Equation 3.1

$$c = \sqrt{\frac{1}{\kappa\rho}}$$

The acoustic intensity *I* is defined as the ratio between the square of the acoustic pressure *p* and the characteristic impedance of a material *Z*, defined as the product of material density and the speed of sound (Equation 3.2). Given the density dependence of the impedance, the intensity is dependent on the compressibility of materials[14].

Equation 3.2

$$I = \left(\frac{p^2}{Z}\right) = \left(\frac{p^2}{\rho c}\right)$$

In tissue, acoustic waves travel longitudinally since tissue has a similar characteristic impedance to water; however, with the introduction of harder materials, shear waves are

also induced[140, 189]. These shear waves, whose presence exerts shear stress and tension on the material, are the basis of ultrasound triggered drug delivery.

The mechanical stress induced by ultrasound will have at least one of several potential effects. Polymers may bend, stretch, rotate, break, slip, realign, or crumble[131, 133, 143]. Lipid systems may disassemble or perturbate in some manner that changes the material conformation[15, 37, 54, 139]. Other solid materials may vibrate. Cavitation, which refers to the nucleation, growth, and collapse of gas bubbles, is also commonly observed in ultrasound fields[113, 145, 190]. All these effects can have some potential benefits for regulating controlled drug delivery.

The effect of ultrasound on a material depends on how the ultrasound is administered, with continuous vs. pulsed waves, focused vs. unfocused, and varying frequencies and intensities all yielding different effects[14, 50, 54, 88, 131, 137, 191]. Their effects are further differentiated by the material upon which the ultrasound ablation is occurring. As such, it is important to know and understand the benefits and drawbacks of using each mode.

Continuous vs. pulsed ultrasound - Continuous ultrasound refers to ultrasonic waves applied without interruption, while pulsed wave mode refers to the repetitive activation and stoppage of a signal akin to a square wave [14, 50, 191]. Continuous waves have been linked to localized heating, which can be especially useful for drug delivery of thermally sensitive vehicles[113, 145, 147]. However, the continuous waves can also excessively heat healthy tissue, including a risk of thermal injury[119, 192]. Pulsed ultrasound more readily induces cavitation, causing the target to contract and expand at the pulse

repetition frequency (PRF). The delivery vehicle can contract and expand until it becomes unstable, leading to the release of its contents. In the event that the drug delivery vehicle bursts altogether, this phenomenon is called ultrasound triggered microparticle destruction (UTMD)[42, 115, 118, 149, 193].

Focused vs. unfocused ultrasound - Focused ultrasound can be achieved through the use of special focus ultrasound transducers whose focal point is determined by the manufacturer. Non-focused ultrasound propagates more radially, allowing for the spreading of the waves; in contrast, focused ultrasound increases the ultrasound intensity at a specific point (Figure 3.2)[134]. If one wants to target a specific site of interest for the release of a therapeutic, focused ultrasound systems offer significant benefits to minimize the exposure of the non-target tissue to ultrasound (particularly for heating applications) [14, 37, 109, 143, 188].

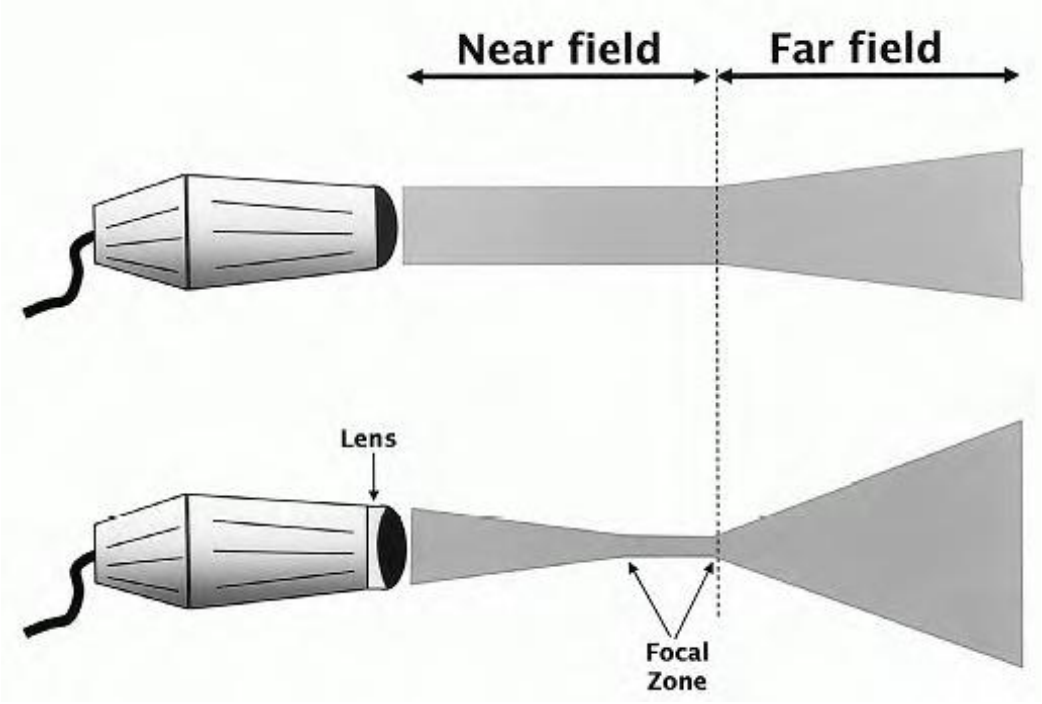

Figure 3.2: Propagation of acoustic waves in unfocused and focused ultrasound transducers. Adapted from [134]

Frequency effects - The frequency of ultrasound can determine (1) the rate at which cavitation will occur, which is dependent on the number of times that gas bubbles will nucleate, grow, and collapse; and (2) the type of ultrasound-induced perturbations achievable in different types of materials[15, 37, 50, 54, 82, 139, 145]. For example, low frequency ultrasound is more useful for temporarily manipulating structures like manipulating the morphology of lipids, enhancing the perforation of cell walls, and increasing the diffusive permeability of polymers[15, 37, 50, 54, 82, 139, 145].

Intensity effects - High intensity focused ultrasound (HIFU) directs ultrasound waves to a site-specific target. The higher energy associated with HIFU leads to high degrees of cavitation and more efficacious UTMD, even though the risk of damaging cells is higher[14, 194, 195]. Low intensity ultrasound, on the other hand can reversibly perturb the structure of living cells, with a notable ability to locally disrupt the endothelial layer in cranial blood vessels to overcome the blood brain barrier[132, 149, 196, 197]. In the case of drug delivery, the intensity will mediate how the system will respond. Figure 3.3 summarizes the comparative effects of ultrasound intensities on lipid and polymeric delivery vehicles[88].

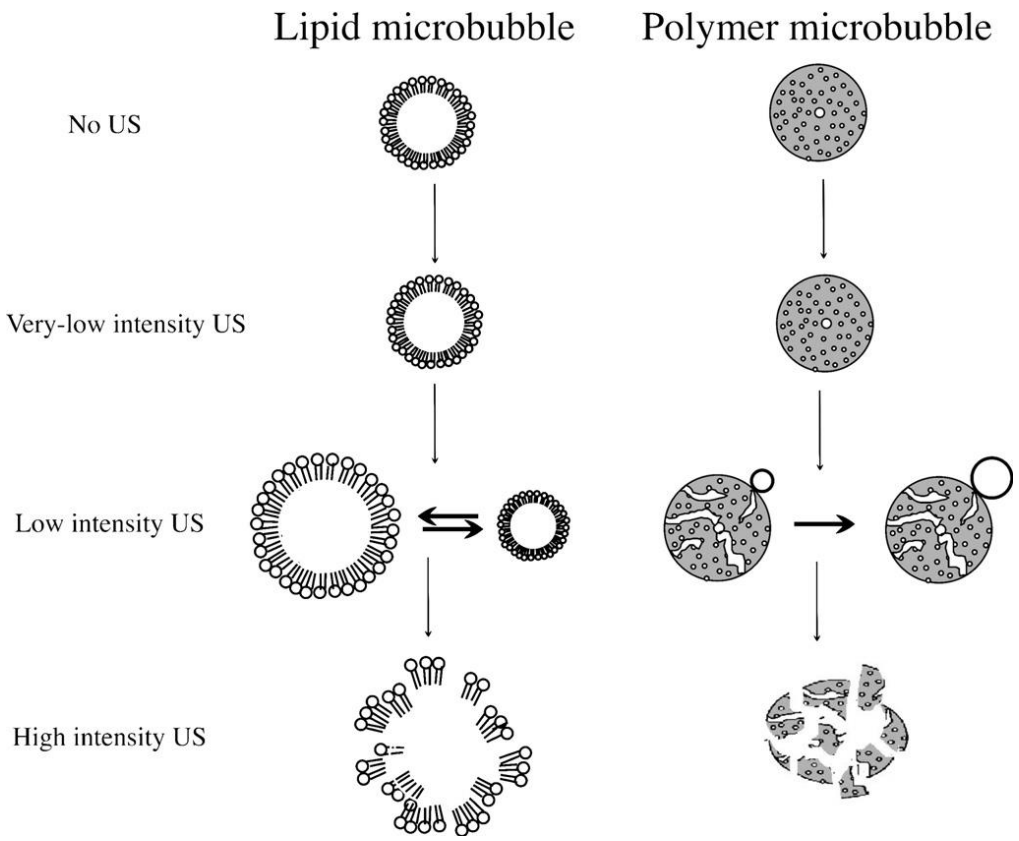

Figure 3.3: Drug delivery vehicle responses to the presence of varying ultrasound intensities. Adapted from [88]

Each mode of ultrasound delivery has both benefits and drawbacks. In continuous wave modes, the localized heating may cause problems with local tissue damage. Pulsatile delivery (HIFU included) can burst drug delivery vehicles and sometimes the surrounding cells as well. Also, continuous low frequency ultrasound used to induce changes to lipids and cells requires constant application to be effective.

In this Chapter, the effect of ultrasound on the cork-shell microcapsules described in Chapter 2 is investigated to mediate drug release. It is hypothesized that the corks will be displaced from the microcapsules (either transiently via *in situ* vibrations or irreversibly

to create a permanently porous shell structure by the microcorks popping out of the shell) without fracturing the shell by using low intensity ultrasound and the corresponding mechanical stimulation. The encapsulated payload would then be released from the delivery vehicle at a rate associated to the size and number of pores generated.

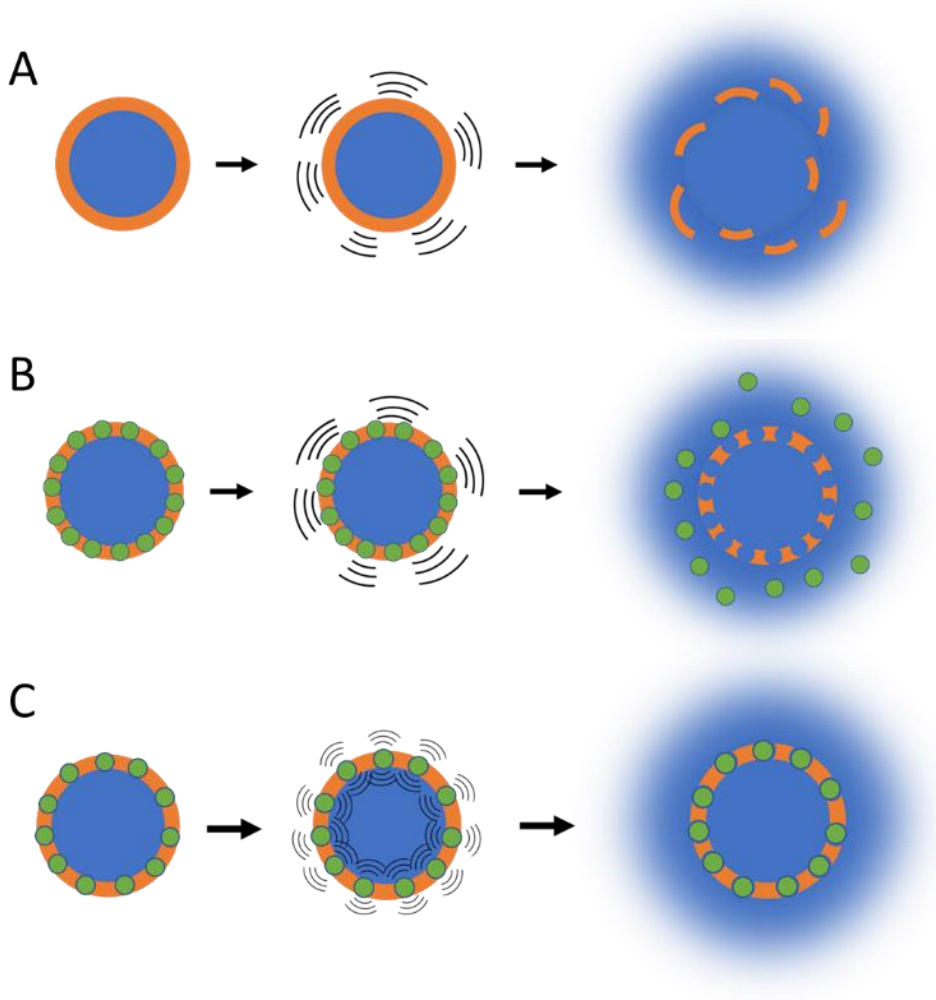

Figure 3.4: Comparison of ultrasound triggered release mechanisms. (A) conventional ultrasound triggered microbubble destruction compared to (B) proposed corked-shell microcapsule irreversible release mechanism (C) proposed corked-shell microcapsule transient release mechanism. Blue – aqueous phase with dissolved model drug; orange – PLGA shell; green – microcorks

3.2 Experimental

3.2.1 Materials and Equipment

Cork-shell microcapsules were fabricated using the same materials and methods as described in Chapter 2.

3.2.2 Analysis methods

3.2.2.1 Quantitative Release via Change in Fluorescence of Solution

To assess the amount of released payload, the microcapsules were exposed to ultrasound under a defined geometry and over a defined time inside various carriers: (1) 1 mL Float-a-Lyzer membranes (Spectrum, molecular weight cut-off = 100 kDa), for which solutions on both the inside and outside of the membrane were collected; (2) a 2 mL Eppendorf tube, from which the supernatant solution following microcapsule settling was collected; or (3) a latex sheath, from which only the solution inside the holder was collected. The release solutions were transferred into a 96 well-plate and triplicate samples of volume 200 µL were analyzed at an excitation wavelength of 485 nm and an emission wavelength of 535 nm (relevant for both FITC and Rhodamine 123). The fluorescence values were compared to a baseline of the fluorescence of the solutions before the sonication was initiated, with results expressed as a change in fluorescence units upon ultrasound treatment.

3.2.2.2 Qualitative Analysis of Fluorescence release.

After a predetermined duration of sonication, microcapsules were collected from the bottom of their respective sample holders by gravity and dispensed onto a microscope slide. Microcapsules used for the qualitative studies used a shell phase that also contained Rhodamine B, allowing confirmation via fluorescence analysis that the integrity of the microcapsules was maintained following ultrasound.

The microcapsules were dried on the microscope slide and subsequently analyzed using confocal or dark-field fluorescence microscopy. For dark-field microscopy, a Zeiss Axiocam 200 was attached to a Zeiss Axiovert 200M microscope equipped with fluorescence lasers and filters. The microcapsules were first identified using bright-field microscopy, after which the mode was changed to fluorescence. The shell integrity before and after ultrasonication was analyzed using a Rexas Red filter, while the contents of the core could be observed using the GFP filter. For confocal microscopy, dried samples were placed under a Nikon Eclipse M600 in combination with a Nikon D-Eclipse C1 confocal setup. Microcapsule shells (Rhodamine B labeled) were imaged using a 543 nm laser and a 590 nm detector, while the BSA loaded in the core (Rhodamine 123 or FITC labeled) was imaged using a 488 nm laser and a 515 nm detector. The laser gains and offsets were optimized to match the fluorescence of the samples while minimizing noise outside of the microcapsules. The microcapsules were exposed to a 32 preliminary scans at a 256x256 pixel density to confirm the laser intensities, after which confocal images were taken at 1024x1024 pixel density for between 40 and 64 z-positions (<4 μm spacing between z-stacks). Subsequently, images were postprocessed on ImageJ by splitting the channels of

each slice, deleting any unused channels, adjusting the colours such that channel 1 (FITC) was assigned green and channel 2 (Rhodamine B) was assigned magenta, overlaying the channels from each slice upon one another, and placing the slices in a stack to create a 3D volume projection.

3.2.3 Sonicator Bath Studies

Microcapsules were fabricated using the immersion coaxial electrospraying process described in section 2.7.4 , using BSA and Rhodamine 123 or FITC in water as the inner core phase, and PLGA and PLGA-conjugated microcorks in DCM as the shell phase. After fabrication, the microcapsules in the continuous phase were concentrated to a volume of 10 mL and then shaken lightly to redisperse. While dispersed, a controlled volume of microcapsules in solution were transferred to a Eppendorf tube (2 mL) or a Float-a-lyzer with an inner volume of 1 mL and outer volume of 5 mL. The sample holders were then placed in a Branson 3510 sonicator bath and sonicated at 4 kHz for up to 6 hours.

3.2.4 Focused Ultrasound Studies

Once proof-of-concept was established using the sonicating bath, a focused ultrasound experiment was conducted that offered more precise control over the nature of the ultrasound (i.e. varying ultrasound powers and pulse frequencies) and applied as well as a more clinically-relevant application strategy. An Olympus 3.5 MHz immersion ultrasound probe focused at 2.95 inches was connected to an Olympus 5077PR pulse generator.

3.2.4.1 Focused Ultrasound Calibration

In order to maximize the effectiveness of the focused ultrasound probe, a "heat map" of the ultrasound signal was first established. Although this calibration is generally done with a hydrophone that measures acoustic pressure[132], using another ultrasound prove as the receiver should yield a map with the same relative intensities but with different units. To do this, the focused ultrasound probe was connected to the Olympus pulse generator, set at 400V, 5000PRF, and 3.5MHz, submerged in a continuous water bath (1ftx1ftx3ft), and fixed in position. A point ultrasound probe was placed facing the face of the Olympus probe to act as a receiver, and their centres were aligned and brought to be nearly touching one another. The receiver probe was fixed to a user operated robotic arm and attached to a pre-amplifier to help improve the quality of the signal collection. The receiving probe was connected to a computer, with the intensity data collected using a MatLAB code developed by Mandakani Jain of the Farncombe lab. A raster scan was performed to gather data over a frame of 5 cm in the radial plane and 10 cm in the tangential plane. Subsequently, a waveguide (described in section 3.2.4.2) was attached to the Olympus ultrasound probe and the raster scan was repeated using a point of origin at the end of the waveguide and a 5 cm x 5 cm inspection area.

3.2.4.2 Waveguided Studies

Following the calibration of the ultrasound probe, a waveguide was fabricated from acrylic plastic to control the distance between the face of the ultrasound probe and the sample holder. In order to ensure that the signal travels unperturbed through the

waveguide, it was closed at one side by a latex sheet and filled with water, with a water overflow chamber/air escape chimney also incorporated to ensure that minimal air bubbles were present in the aqueous phase of the waveguide. Figure 3.5 shows the schematic of the waveguide as well as an AutoCAD image of the sonicator probe sitting in the waveguide. The length of the waveguide could be changed depending on the experimental setup; specifically, it could be adjusted to be slightly shorter than the focal length of the ultrasound probe or to the local maxima of the signal intensity (which was not at the focal point).

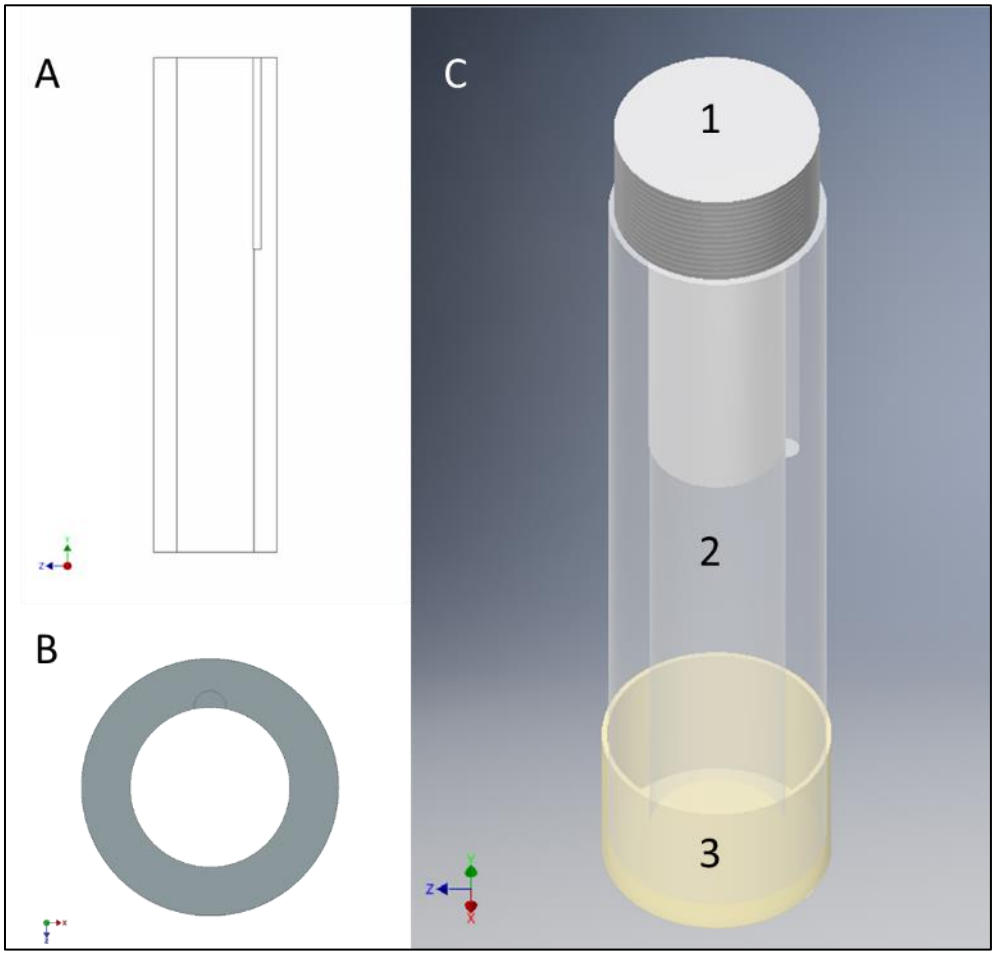

Figure 3.5: Cylindrical waveguide designed for the Olympus immersion ultrasound transducer. (A) side view of the waveguide, (B) view from the top of the waveguide, (C) the waveguide (2) attached to the US probe (1) and closed with a latex sheet (3).

The sample holders used for the waveguide experiments were developed to be many shapes and sizes. Figure 3.6 below depicts all the sample holders tested.

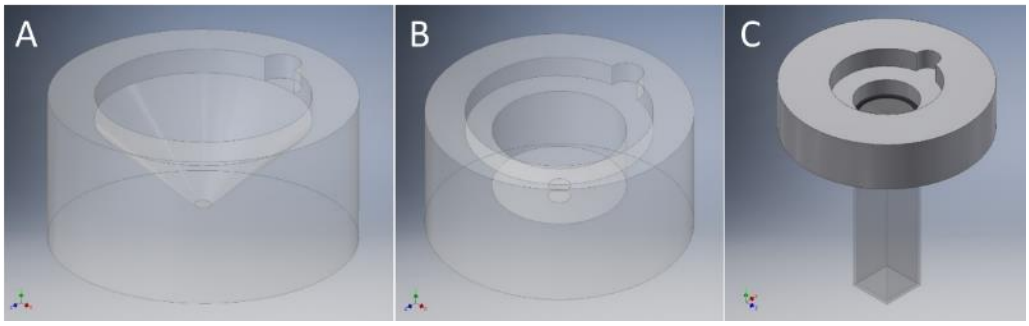

Figure 3.6: Waveguide experiment sample holders. (A) conical sample holder, (B) cylindrical sample holder, (C) cuvette sample holder

Figure 3.6A shows the schematic of a conical sample holder that allows all the microcapsules to sink to the bottom of the cone. This sample holder in combination with the waveguide sums to a total length of 2.95 inches between the face of the ultrasound probe and the smallest part of the cone. This ensures that only the microcapsules are exposed to the focal energy of the ultrasound probe. The rest of the conical sample holder was filled with water to allow the ultrasound signal to transmit and maintain a consistent volume between experiments. To perform the release experiments, the ultrasound probe was placed in the water-filled waveguide, and the waveguide was placed in the sample holder, and the ultrasound would be turned on for a controlled period. The change of fluorescence of the liquid in the sample holder would then be analyzed.

Figure 3.6B shows the schematic of a cylindrical sample holder comprised of consecutive cylinders of smaller diameters, with microcapsules intended to be deposited in the smallest of the cylinders. Similar to the conical sample holder, the combination of the cylindrical sample holder and the waveguide sums to a total length of 2.95 inches between the face of the ultrasound probe and the smallest cylinder. The size of the focal

point of the ultrasound probe was matched to the size of the smallest cylinder in which the microcapsules were dispensed. The rest of the sample holder was filled with water in attempt to control the total volume. The experiment was conducted as described for the conical sample holder.

Figure 3.6C shows a schematic of a cuvette sample holder fabricated to study the real time colorimetric change of the solution *in situ* using a UV-vis spectrophotometer. In contrast to the conical and cylindrical sample holders, in which the solution would need to be replaced each time of sampling, a hole was drilled completely through the cuvette sample holder and a 25 µm pore size metal mesh secured in the sample holder to support the microcapsules; note that all microcapsules tested were greater than 25 µm in diameter such that they would not fall through the pores but the solution could still pass through the membrane. A polystyrene cuvette used for DLS and UV-vis measurements was fitted to the bottom of the sample holder. Once the microcapsules were dispensed, the liquid would seep through and fill the cuvette. The remaining volume of the sample holder was filled with water to minimize air bubbles in the path of the ultrasound waves, after which the cuvette was inserted as normal in a Cary 100 UV-vis spectrophotometer and the waveguide was fitted on top. Kinetic sampling software was set to track the absorption of FITC in the cuvette, which would correspond to the release of FITC from the microcapsule for the duration of the experiment. The pulse generator was turned on, and the colorimetric tracking was initiated. This setup ensured a controlled volume throughout the experiment given the fixed volume of the cuvette used.

3.2.4.3 Latex Sample Holder/Infinite Bath Study

To better mimic release from within a water-rich tissue sample, the microcapsules were loaded into a latex sheath that is commonly used as vaginal and rectal ultrasound covers. Figure 3.7 shows the setup used for these ultrasound experiments. The latex sample holder could be unrolled to the desired size, and microcapsules can be injected to the bottom of the latex holder. The rest of the space was filled with water, and the latex sheath was fitted to a PVC cylinder that was holed out in the centre to fit the ultrasound probe to maintain the relative geometry between the probe to the microcapsules throughout the experiment. The commercial latex sheaths (sheathes.com) were too rigid, causing them to break too frequently; instead, ultrathin condoms (Trojan) were used following the washing out of all the water-based lubricant with soap and hot water. When lubricant was present in water, the water was a milky colour. The complete removal of the lubricant was confirmed by fresh water remaining clear.

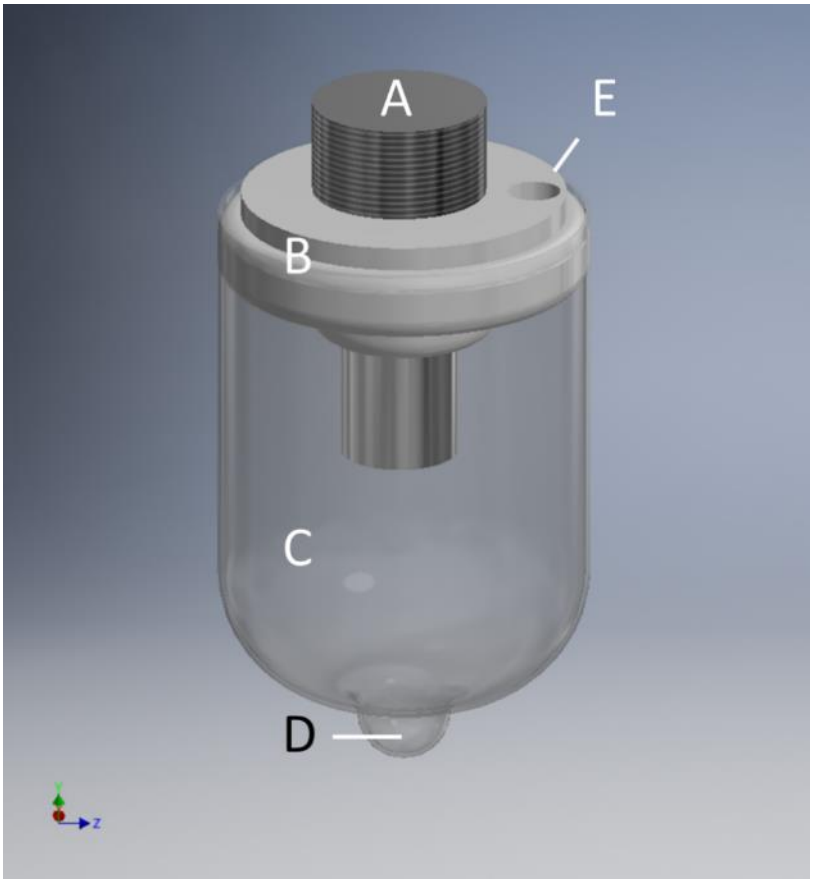

Figure 3.7: Ultrasound release setup with latex sample holder. (A) US probe, (B) PVC holder, (C) latex holder, (D) tip of latex holder where samples are dispensed, (E) sampling hole/air escape

The ultrasound probe was turned on, and aliquots of the solution in the latex holder were collected at 15 minutes, 30 minutes, 45 minutes, 1 hour, 2 hours, and 24 hours after the first the ultrasound probe was switched on. The probe was turned on for varying periods of time in order to ensure study the effects of different durations of ultrasound on the microcapsules. The aliquots were transferred in triplicate (200 µL volumes) to a 96-well plate and analyzed as described in section 3.2.2.1 .

3.3 Results

3.3.1 Sonicator Bath Studies

Microcapsules with and without impregnated corks were transferred to the sonicator bath after fabrication, exposed to the ultrasound bath for pre-determined periods of time, and imaged to assess the ultrasound-induced changes in microcapsule properties. Figure 3.8 shows the morphology of the corked microcapsules after 24 hours of incubation in the absence of sonication, after 2 hours of sonication followed by simple incubation for 22 hours, and after 6 hours of sonication followed by simple incubation for an additional 18 hours; note that each time was chosen so that each incubated sample (with or without sonication) was exposed to a continuous water phase for 24 hours total.

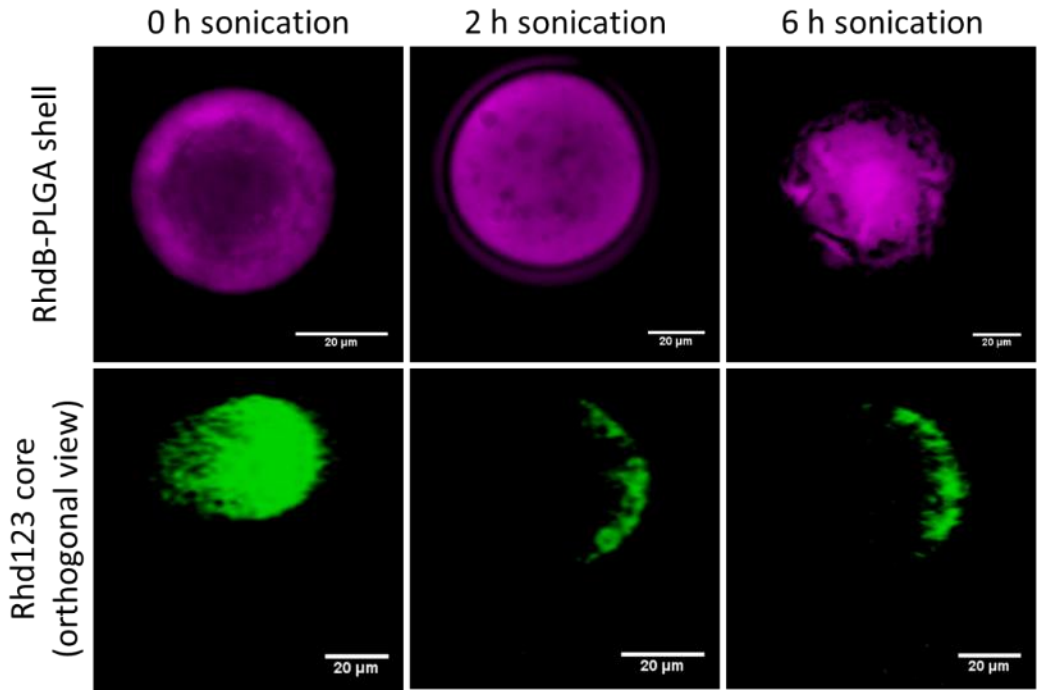

Figure 3.8: Qualitative depiction of sonicator bath release study on cork-shell microcapsules: (top) dark field fluorescence microscopy of microcapsules (magenta = Rhodamine B in shell) and (bottom) confocal microscopy of microcapsules (green = Rhd123 in core)

The microcapsule shell remains intact upon extended incubation in water without sonication, with no obvious pores present in the shell (top image) and the contents of the core all remaining localized as a sphere inside the microcapsule (bottom image). After 2 hours of sonication, the shell remains qualitatively intact but the contents of the core appear to be significantly lower in intensity and localized in a crescent-like shape, suggesting emptying of at least a significant percentage of the core contents. After 6 hours of sonication, the core is similarly emptied but the microcapsule appears clearly perturbed and irregular, suggesting rupture of the shell.

A quantitative analysis of the same study is seen in Figure 3.9. In the absence of ultrasound ablation, the microcapsules with corks do not release their contents even after 24 hours in 37°C; in contrast, the introduction of ultrasound induces release, with more release observed as the sonication time was increased. Given this clear time dependence on release, this result suggests that it is possible to drive release from the microcapsules without causing macroscopic fracturing of the shell, consistent with the corks being popped from the shell. In addition, this result suggests that the chosen shell thickness is too large for leaking of contents prior to ultrasound activation, as is often observed in thin-shell capsular ultrasound release vehicles[104, 183].

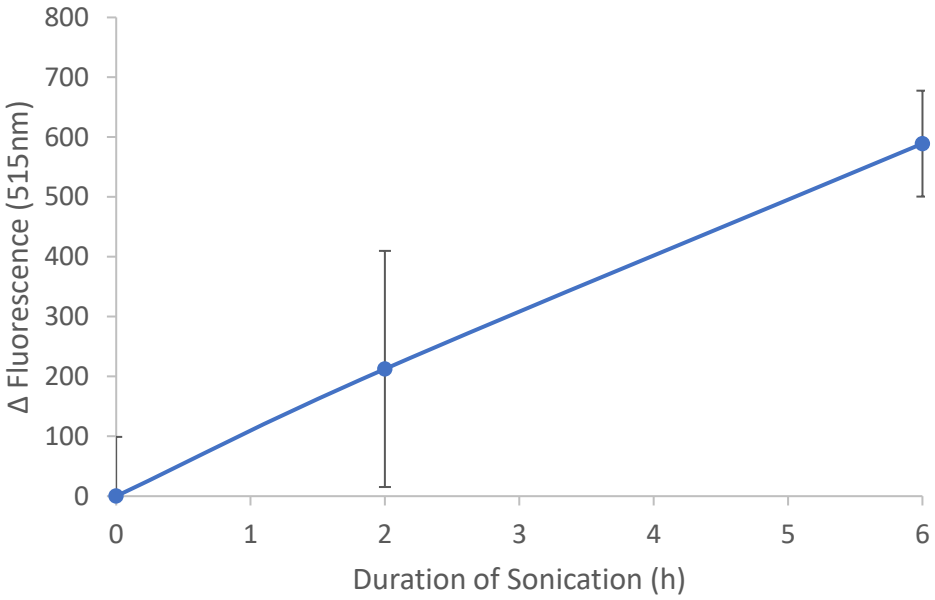

Figure 3.9: Qualitative analysis of sonicator bath release study

To assess if the thickness of the shell does indeed play a role in minimizing leaking of the microcapsules, corked and uncorked microcapsules with different shell thicknesses were

fabricated. Thick shells were created using a 5x flow rate of the shell phase (0.5 mL/h) compared to the inner phase (0.1 mL/h), while thin microcapsules shells were created using a 3x flow rate of the shell phase (0.15 mL/h) in comparison to the inner phase (0.45 mL/h); the full description of the technique in section 2.7.4 , The microcapsules were placed in the sonicator bath for 6 hours and release was tracked. However, there are several reasons as to why such a system is ineffective to study the release of model drug from the PLGA microcapsules. First, given that the sonicator bath reaches ~50°C over the 6-hour sonication period and the specific heat capacities of PLGA and silica are 1.98 J/gK and 0.84 J/gK respectively, local heating from the sonicator bath will affect these materials differently[73, 198]. In particular, the glass transition temperature of the PLGA used to form the shell is ~41°C [199], suggesting that the microcapsule may become rubbery in the bath with accompanied by significant increases in capsular content release via diffusion[39, 200, 201]. Second, the silica beads may help to mechanically reinforce the PLGA shell to reduce the potential for macroscopic fracture in the shell upon ultrasound exposure, consistent with the corked thin shell samples releasing less contents than the uncorked thin shell samples.

Further, the sonicator bath setup is highly imperfect for such studies since there are consistently areas in the bath where there is more ultrasound exposure than others, ranging from hot points to dead zones. As such, there is no consistent control over the actual ultrasound power experienced by each microcapsule, making the experiment inherently poorly reproducible. In addition, the significant heating observed makes the sonicator bath study more accurately an ultrasound-triggered, thermally assisted release study. As such, an improved test method was required.

3.3.2 Focused Ultrasound Probe Calibration

Instead of an ultrasound bath, a focused ultrasound probe was next used that was attached to a function generator that allowed for precise tuning of the ultrasound power and waveform applied to the sample. To use this probe practically for experiments, a heat map of the positions of highest ultrasound intensity must be first generated by raster scanning the probe output in space. Figure 3.10 shows this heat map of ultrasound intensity over a 10 cm x 5 cm area (note that the point of origin of the ultrasound is at (0 mm, 25 mm) in this diagram), first without the use of a waveguide.

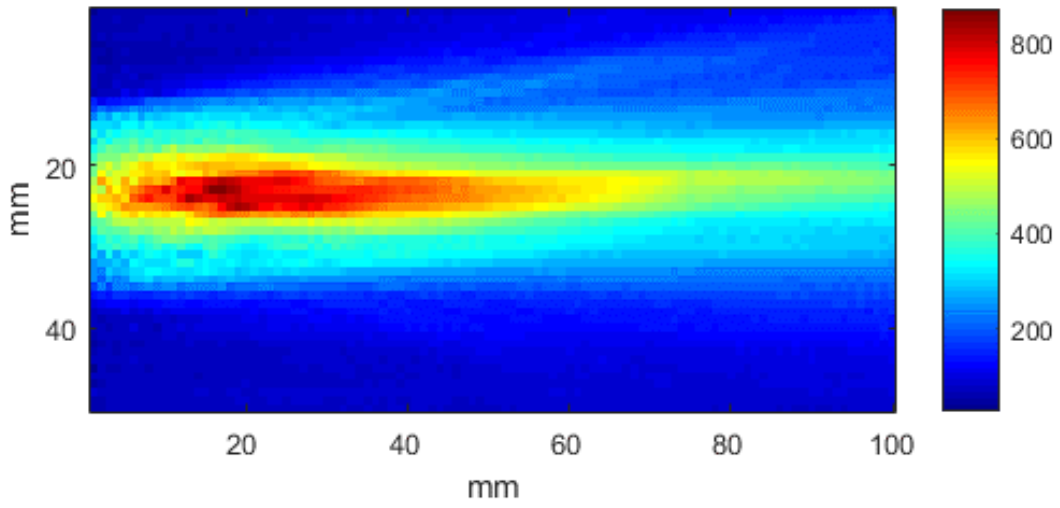

Figure 3.10: Ultrasound intensity heat map as measured in a continuous water bath without a waveguide. The transmitter is an Olympus transducer focused at 2.95 inches, while the receiver is a point ultrasound transducer connected to an amplifier.

The probe focal point (end of the yellow) is at ~75 mm, is consistent with the product specifications of a focus at 2.95 inches. However, the high intensity of the ultrasound (orange to red) terminates closer to 60mm, and the most intense overlap of energy occurs before 20mm and right in front of the transducer. This information is useful as it provides a more complete understanding of the transducer's profile and where the most ultrasound shear stress would be felt.

Next, the heat map associated with the same ultrasound probe when the ultrasound signal propagated through a waveguide was assessed, as this information is clinically relevant for superficial treatments. An acrylic waveguide fabricated as described in section 3.2.4.2 , and an ultrasound signal map was acquired using the same experimental protocol but setting the origin point of the raster scan to be at the end of the waveguide. Figure 3.11 shows the resulting heat map collected.

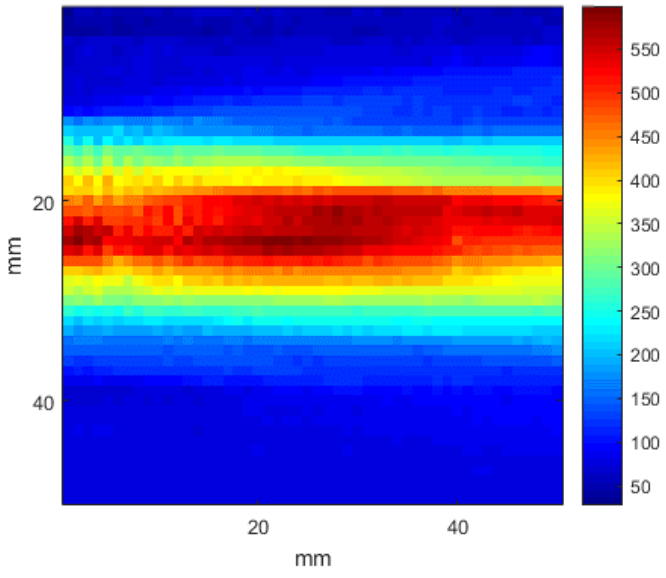

Figure 3.11: Ultrasound intensity heat map as measured in a continuous water using a 2.5" waveguide. The transmitter is an Olympus transducer focused at 2.95 inches, while the receiver is a point ultrasound transducer connected to an amplifier.

The ultrasound signal after the waveguide is much less tapered than the signal without the waveguide. The line of intensity holds a more consistent width, suggesting that the signal is becoming aligned. The focal point of the ultrasound probe (by the product specifications) is central in the graph around the coordinates (25 mm, 25 mm), where the darkest red datapoints are seen. However, further inspection of these dark red hotspots shows that their intensity (~600 V) is lesser than that of the non-waveguided hotspots (~900 V). As such, the waveguide provides a larger planar area that can be addressed but at the cost of reducing maximum ultrasound intensity that can be delivered by the probe.

3.3.3 Waveguide Studies

To assess the ultrasound-driven release of the microcapsules under more controlled conditions, the waveguide was closed off with a sheet of latex to enable filling of the waveguide with water (to allow the propagation of the signal) while also allowing the ultrasound waves to seamlessly pass through with minimal effect. Sample holders were made in different geometries in order to load the microcapsules and subsequently track their release. The following section describes the different types of sample holders produced and the corresponding results (or lack thereof) from release studies using these holders.

3.3.3.1 Conical Sample Holder

Microcapsules were dispensed in the conical sample holder, with the remainder of the volume filled with water. The microcapsules were allowed to settle down to the bottom of the holder due to their density, after which the waveguide was fitted onto the sample holder. After 3 hours of ultrasound stimulation using the focused probe, no significant release was observed. We attribute this result to the shape of the sample holder. The conical shape has a tangential angle around 45° which may start to redirect and reflect the incoming waveguided ultrasound signal, as illustrated schematically in Figure 3.12. As such, the distortions may cause the signal intensity to not be enough to drive uncorking and ultimate release.

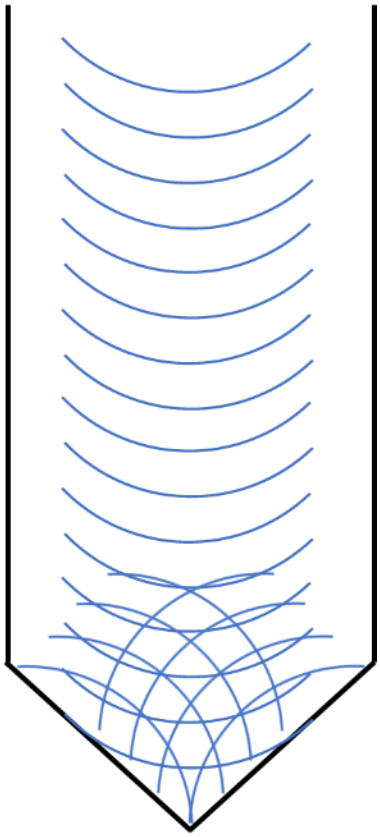

Figure 3.12: Schematic diagram of the propagation of ultrasound waves through the waveguide and conical sample holder

3.3.3.2 Cylindrical Sample Holder

Microcapsules were dispensed in the smallest trough of the cylindrical sample holder. The filling of this sample holder was more difficult, as the addition of the continuous phase to the sample holder may cause the microcapsules to rise out of the smallest cylinder. As such, the microcapsules were given more time to settle in addition to being pulled into the smallest hole using a spatula. Figure 3.13 shows the resulting fluorescence spectra of

the release medium at 15, 35, 50, and 65 minutes (left) and the corresponding released amount as a function of time (right).

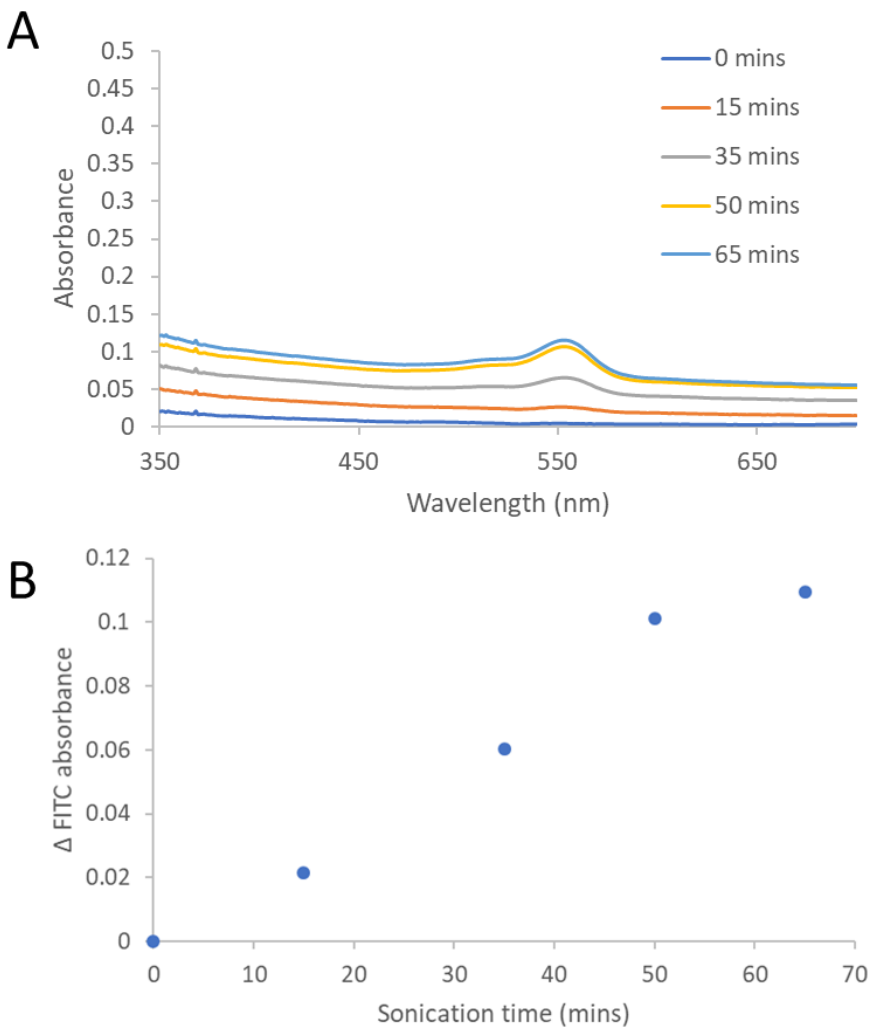

Figure 3.13: Release of FITC from corked microcapsules as stimulated by a waveguided focused ultrasound probe using a cylindrical sample holder. (A) absorbance spectrum of FITC as a function of different stimulation times; (B) change in FITC absorption in continuous phase as a function of sonication time

In this case, clear evidence of release as a function of ultrasonication time is presented, with an increase in FITC released observed upon longer sampling times. The change in geometry of the sample holder changes the propagation of ultrasound waves through the entire setup, as shown schematically in Figure 3.14, to apply functionally much higher ultrasound intensities to the microcapsules during the experiment.

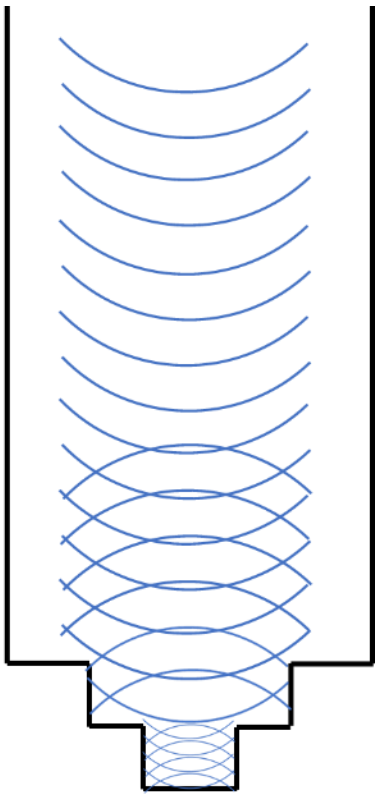

Figure 3.14: Propagation of ultrasound waves through the waveguide and cylindrical sample holder

Although the cylindrical holder overcame the geometric issues associated with the conical sample holder, it was much more difficult to use. When the waveguide was fitted onto

the sample holders (both conical and cylindrical), some liquid was displaced due to overflow and volume displacement. As such, volume control in this sample holder is challenging, which by extension makes it difficult to control the concentrations of released material.

3.3.3.3 UV-vis Spectrophotometer Sample Holder

Next, a sample holder system was developed to study the real time release dynamics using a UV-vis spectrophotometer. A cuvette was fitted to the bottom of the sample holder, with the microcapsules dispensed on a membrane through which the continuous phase liquid can pass. If the microcapsules release upon ultrasound activation, the microcapsules will remain on the membrane but the (soluble) core contents will seep through. This setup overcomes the issue of inconsistent volumes, as the only volume being analyzed is the constant volume inside the cuvette. The cuvette was zeroed at the start of the ultrasonication, and a scan between 400-600 nm was gathered every 30 seconds for the duration of the ultrasound.

Unfortunately, while the sample holder fixed the volume control issue, no useful data was collected from this assembly. The metal mesh may have been blocked by microparticle aggregation; alternately, the tight fitting of the cuvette to the bottom of the sample holder may create an extremely high capillary pressure, as suggested by the difficulty in filling the entire cell with continuous phase liquid. This high capillary pressure would make

the transfer of the fluorescent material from the samples sitting on the membrane to the cuvette challenging. Due to these issues, another type of sample holder needed to be developed.

3.3.4 Latex Sample Holder Studies

The latex sample holder enabled ready transmission of ultrasound through the container while still fixing the geometry between the probe and the microcapsules and enabling testing within a continuous water bath maintained at 37°C. Microcapsules were dispensed at the bottom of the latex sample holder, with the remaining volume filled with water at 37°C.

3.3.4.1 1 Hour Ultrasound Ablation

Corked and uncorked microcapsules suspended in 5 mL of continuous phase were deposited in the latex sample holders 2 inches away from the face of the ultrasound probe, with the remaining space then filled to a total volume of 40 mL. The samples were then exposed to ultrasound for a total of 1 hour, after which the ultrasound was turned off and the microcapsules were incubated for another hour. Figure 3.15 shows the change in fluorescence at 535 nm associated with the release of FITC.

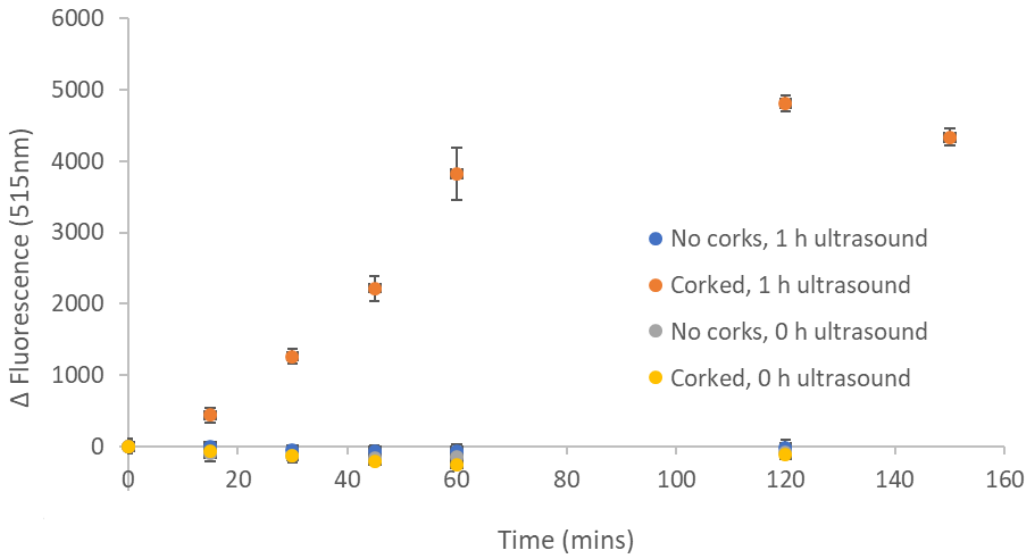

Figure 3.15: Latex holder ultrasound study for corked and uncorked samples

Figure 3.15 suggests that release is occurring only in the corked microcapsules, whereas the uncorked microcapsules do not release whether or not ultrasound is applied to the sample. This data clearly suggests that the release is related directly to the presence of corks embedded in the microcapsules. A zero-order release kinetic is achieved during the time period the ultrasound is left on (0-60 mins); however, after the ultrasound is switched off, the release is significantly lower until reaching an apparent plateau. If the corks were ejected from the microcapsule to create pores, it is unlikely that such a plateau would be observed, although the release rate may somewhat decrease due to the lower diffusion coefficients observed in the absence of ultrasound. As such, it is more likely that the different mechanical indices of the silica corks and the PLGA shell are inducing vibrations at the cork-shell interface that transiently open pores to facilitate release, although the popping mechanism cannot be completely dismissed (as will be considered

later). As such, while this data clearly shows that corked microcapsules activated by ultrasound can mediate on-demand release.

To confirm the release, confocal microscopy was carried out on the microcapsules before and after the ultrasonic activation. Only the inner core was labeled for these studies, as the addition of a fluorescent label for the shell introduces potential absorption/emission spectral overlap which would convolute the release data. Figure 3.16 compares the orthogonal view of microcapsules with and without corks before and after ultrasound activation. As with Figure 3.8, the circular shape of the fluorescence of the microcapsules indicates that they are full of the FITC payload. After fluorescence, the circular shape of the payload inside the microcapsules without corks is maintained, but the crescent shape of the microcapsules with corks suggests that they release at least a portion of their contents.

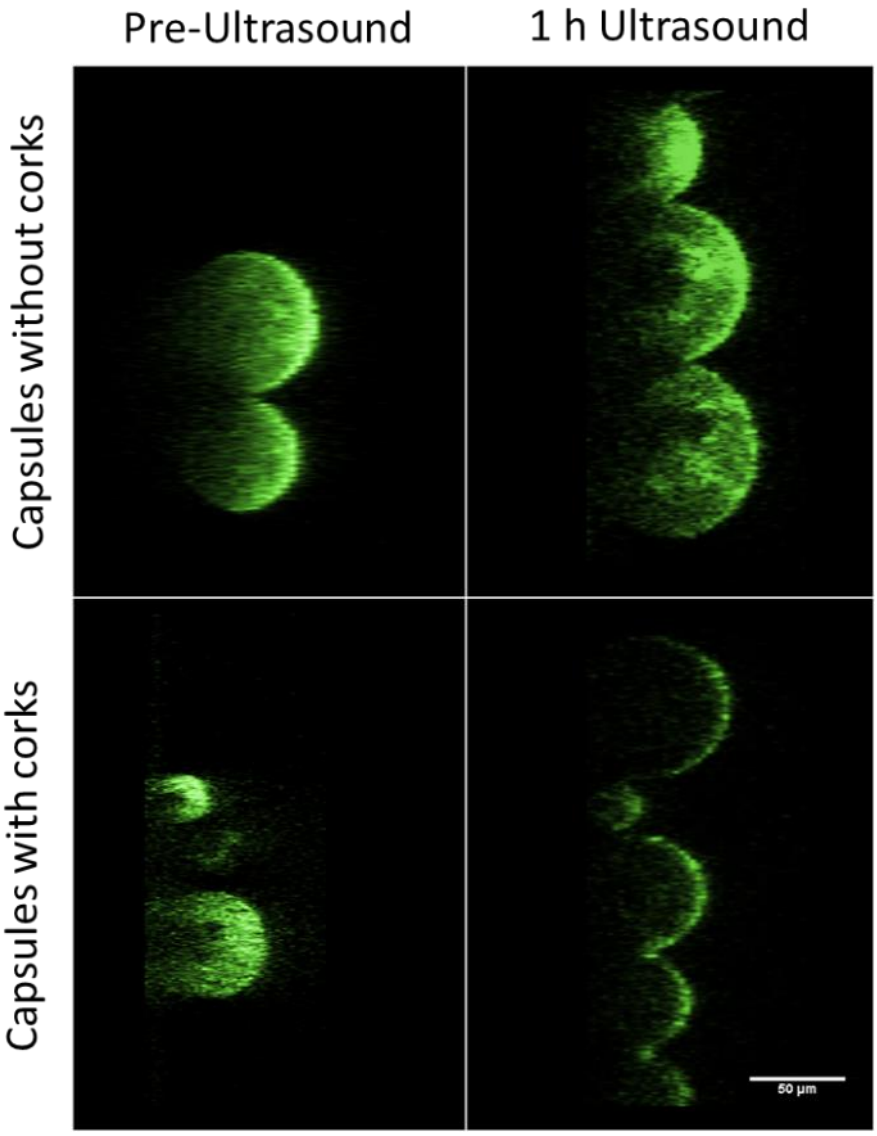

Figure 3.16: Orthogonal view of microcapsules prepared without corks (top) and with corks (bottom) before (left) and after (right) ultrasound activation. Green – FITC Isomer 1 dissolved in core aqueous phase

3.3.4.2 Drug Release in Relation to Different Durations of Ultrasound Ablation

To assess the effect of the duration of ultrasound on the release observed, shorter ultrasound durations of 1 minute, 5 minutes, and 10 minutes were applied, after which the ultrasound was shut off and the microcapsules were given the remainder of 2 hours to continue their release. Figure 3.17 shows the resulting release kinetics of the microcapsules at different durations of ultrasound.

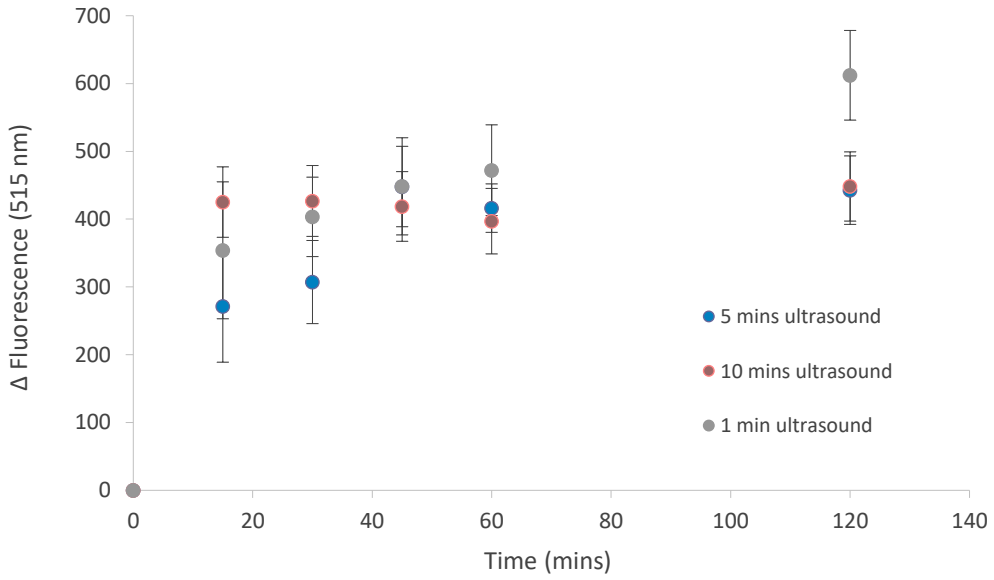

Figure 3.17: Release of FITC from corked microcapsules from different durations of ultrasound ablation

As can be seen, the release rates after 1 minute of ultrasound, 5 minutes of ultrasound, and 10 minutes of ultrasound are all within experimental error, with a larger initial release (during the early time periods when the ultrasound is switched on) and a significantly slower (but not zero) release after the ultrasound is turned off. This result again suggests

that a combination of mechanisms may be at play in terms of regulating release. The result that the first minute of ultrasound activation has the most significant impact on regulating the release supports the potential popping out of corks from the microcapsules upon ultrasound activation, with temporary pore formation due to the vibration of other corks also potentially supporting release; when the ultrasound is turned off, the vibration stimulus would stop but any corks popped out to make pores would still enable slow release from the microcapsules, as observed. Thus, depending on how the corks are embedded in the shell, we hypothesize that they may respond differently to ultrasound to provide fine-tuned release over the on and off state release profiles.

3.3.4.3 Drug Release in Relation to Cork Density

As shown in Figure 2.16, the number of corks entrapped in the microcapsule shell varies as a function of the fabrication time period as corks settle. Usefully, this allows fractions of microcapsules with different cork fractions to be fabricated in a single process, enabling the investigation of the effect of cork density on release rate. Microcapsules were fractionated into 4 consecutive 5-minute intervals of fabrication as described in section 2.9.5 , and triplicate samples from each fraction were placed in latex holders and exposed to 30 minutes of ultrasound; the microcapsules where then allowed to continue releasing their contents without ultrasound stimulation for another 1.5 hours. The results for this experiment are shown in Figure 3.18.

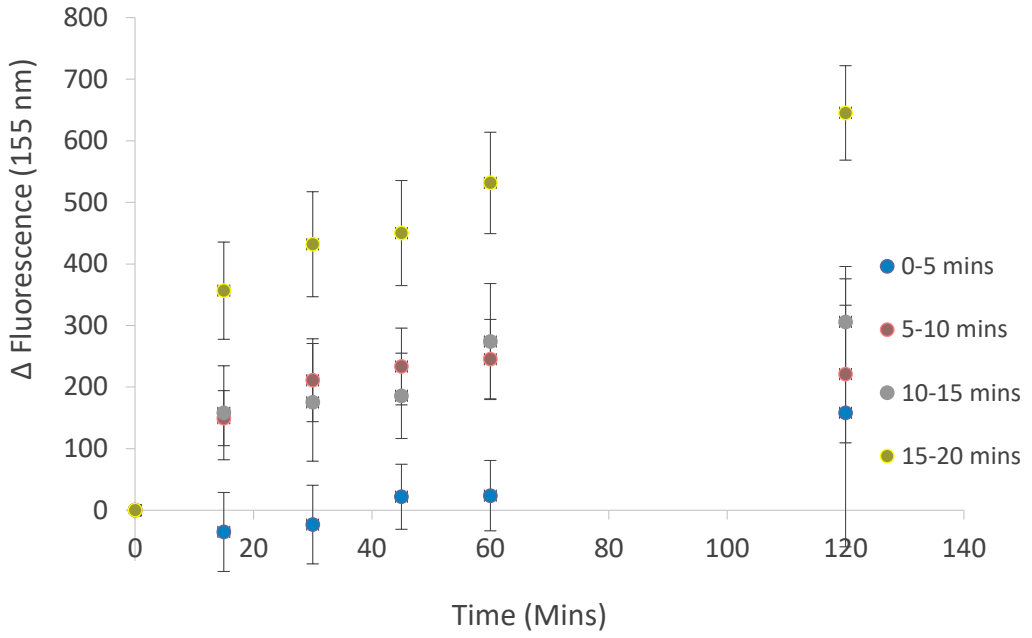

Figure 3.18: FITC release from microcapsules prepared with different cork densities (represented by the different collection times in the legend, where longer times correspond to lower cork densities; see Figure 2.16 for reference) under ultrasound activation using the latex sample holder

Since the number of possible pores generated is related to total number of corks embedded in the shell (whether they are popped out or vibrated upon ultrasound), it stands to reason that the corks made at different times of the fabrication process will behave differently in the presence of ultrasound. While a clear trend was observed, the result was non-intuitive. Longer processing times result in lower cork densities (Figure 2.16E) but also released significantly more FITC than samples prepared with shorter processing times that have larger cork densities (Figure 2.16B). This result can be rationalized in terms of the nature of mechanical perturbations in the shell upon ultrasound exposure. The PLGA in the shell material vibrates, contracts, and expands under ultrasonic signals at 3.5 MHz; previous literature has shown that similar (cork-free)

PLA microcapsules have a maximum attenuation between 3 and 5 MHz[142] and enable successful release of drugs from PLGA microcapsules between 1 MHz and 5 MHz[36, 109, 197, 202]. However, the silica microcorks likely do not, as the displacement of microcorks from the analogous similar fibrous system occurred at 40 kHz [152]. In the presence of too many corks in the microcapsule shell, this vibration could be further attenuated such that the corks do not release to the same degree from the microcapsules. However, it must again be emphasized that microcapsules with no corks do not release their contents to any significant degree (Fig. 3.16). As such, putting these results together suggests that there is an optimal loading of corks in the microcapsules to enable the most control over release.

3.4 Discussion

The microcapsules fabricated in Chapter 2 were studied for their capacity to release their payload in the presence of ultrasound signals in a variety of different sample holders/release geometries. Initial results in a sonicator bath confirmed that on-demand release of hydrophilic model drugs like FITC or rhodamine 123 was possible, consistent with fluorescent microscopy results whereby the microcapsule began to visibly deteriorate after 6 hours in the sonicator bath. However, inconsistent ultrasound power within the bath and the heating observed in the sonicator bath (up to 48°C) both proved to be problematic, the latter in particular with our microcapsule design given that the glass transition temperature of the PLGA used is 41°C. Indeed, prior literature has shown that there is a drastic change in the release kinetics of PLGA-based delivery systems between 37°C and the 45°C, suggesting that any release observed may be substantially

thermally assisted[200]. While the focused ultrasound used subsequently for release testing may mitigate the importance of this effect, varying the grade of PLGA used to make the shell may be of interest for future studies. All microcapsules used herein are fabricated using PLGA with a 65:35 LA:GA ratio and molecular weight of 40-75kDa; using shorter PLGA will decrease the glass transition temperature and thus increase microcapsule permeability at higher temperatures [200].

The majority of the release studies reported were conducted using a focused ultrasound probe whose beam had a focal point at 2.95 inches but a maximal intensity 2 cm away from the probe and maintained high intensities up to 6 cm away from the probe, as per the intensity map shown in Figure 3.10 Using an acrylic waveguide to control the positioning of the ultrasound wave focal point, three different sample holders were fabricated. The conical sample holder had no detectable release, while a sample holder consisting of tiered cylinders showed clear evidence of ultrasound-induced release. However, the methodology used to study these releases was deemed inconsistent, as the continuous phase volume was difficult to keep constant during the sampling process. While a real-time detection system was attempted to be developed in which a UV cuvette is incorporated directly into the release cell, the capillary pressure between the sample holder and the UV-vis cuvette made the use of this cuvette problematic in practical application.

To address these problems, a final release setup consisting of a de-lubricated latex condom and a PVC puck was developed that overcame all issues related with uncontrolled volumes, interference-plagued wave propagation geometries, and issues associated with

the transport of the studied active agent. Latex is often used by radiologists as an ultrasound-transparent protector and is thus a relevant material in this context. Corked microcapsules released their payload in the presence of US while uncorked microcapsules did not; neither types of microcapsules released any of their contents over the same time period in the absence of ultrasound. These results confirm that the presence of corks is essential to drive release from the drug delivery vehicles and that the microcapsule shell is thick enough to prevent passive diffusion or rupture under an ultrasound stimulus.

Further, it was noticed that the release rate was constant over the hour during which sonication was applied from the first point analyzed (15 minutes post-sonication) but significantly reduced (although not completely shut off) during the hour of post-sonication incubation. Subsequent studies of release kinetics due to different durations of ultrasound ablation (i.e. 1 minute, 5 minutes, and 10 minutes showed) also showed similar total releases over the full 2-hour duration of the test, with an apparent fast release facilitated by even a short ultrasound application followed by a reduced (but non-zero) release rate when the ultrasound was shut off. We tentatively attribute this result to some corks being popped from the shell (creating permanent pores that maintain slow release even in the absence of ultrasound) while other corks are vibrated (creating transient pores that are only open during ultrasound application). Due to the lower heat capacities of the PLGA and microcorks, friction between the differently vibrating microcork and the PLGA is anticipated to result in localized heating at the microcork-PLGA interface, potentially above the glass transition temperature of the PLGA. If this occurs, the resulting “rubbery” behaviour may lead to healing of in particular the transient pores developed if the microcorks are not popped from the shell, essential for achieving the

plateau “off”-state release desired in the absence of ultrasound stimulation.On this basis, we anticipate that changing the relative thickness of the shell to the diameter of the cork may enable shifting of this balance to pop more or fewer pores and thus change the relative release rates achieved in the on and off states, a subject for future investigation. In addition, the diffusion coefficient of the fluorescent probe should be measured with and without ultrasound to confirm that the significantly higher release rate observed under ultrasound is attributable to the shell properties and not just enhanced diffusion under sonic energy. Multiple triggering experiments in which the microcapsules are triggered the next day or the next week should be performed to confirm that re-application of ultrasound will again provide a significantly enhanced release rate. Such a profile would be of significant interest for treating chronic diseases like arthritis in which intermittent local delivery of a drug (i.e. an anti-inflammatory or an anesthetic) is desirable. Finally, release of other payloads (e.g. proteins or nanoparticles) will be probed to further discriminate the mechanism of release (i.e. popped corks should facilitate nanoparticle release up to a particular size cut-off while vibrated corks likely would not) as well as assess the potential scope of this technology for delivering different payloads at different release rates.

An investigation of the effect of cork density on release indicated that the release kinetics increase with decreasing cork density. This, coupled with the previous data that confirms that the corks are necessary to facilitate release in this microcapsule system, suggests that there is an optimal number of corks that should be incorporated into the shell for release. Although the mechanism again requires further study, literature has shown that PLGA resonates at 3.5 MHz [36, 109, 197, 202] while the microcorks likely require a lower

frequency to resonante[152]. As a result, too high of a cork density in the microcapsule would attenuate effective vibration of the whole shell and thus suppress release. Another potential explanation for this observation, given the polymer mass concentration of the shell phase is constant as the cork density is increased, the increased mechanics (higher filler content) coupled with the increased thickness of the shell as more corks are added (increased total mass concentration in the shell phase) may both reduce the effectiveness of cork popping to generate permanent pores as well as increase the tortuous path for release around vibrating corks, in either case reducing the observed release rate. In the absence of corks, it is possible that the uniform material composition of the microcapsules increases the overall integrity of the shell.

3.5 Conclusions

The ultrasound triggered release kinetics of corked, and uncorked PLGA microcapsules were studied. The microcapsules were fabricated as per the methods indicated in Chapter 2. Ultrasound-triggered release was observed in a sonication bath but was attributed at least in part to heating in the sonicator bath exceeding the glass transition temperature of the PLGA. Instead, a focused ultrasound probe was used with a latex sample holder to induce ultrasound-triggered release in a more reproducible manner. The corked microcapsules showed release in the presence of ultrasound while uncorked microcapsules did not, confirming that the corks were responsible for facilitating release; neither the corked or uncorked microcapsules demonstrated any release in the absence of ultrasound. Subsequent investigations on the effect of ultrasound time indicated no

observable difference in release between 1 and 10 minutes of sonication times. Collectively, these results suggest that release is mediated by a combination of popping of some corks from the shell upon ultrasound exposure (creating permanent pores in the microcapsule that can mediated slow release in the absence of ultrasound) and vibration of corks within the shell upon ultrasound exposure (creating transient pores that accelerate release during the ultrasound period). Finally, a high cork density was observed to reduce the payload release while a lower cork presence increased the release, a result attributed to the differences in resonance frequencies between the PLGA shell and the silica corks and/or changing mechanics and thicknesses of the microcapsule as more corks are added.

Relative to previous ultrasound-induced release vehicle reports, the cork-shell microcapsules described improve upon the prior art in two ways. First, release via a non-burst kinetic profile occurs in less than one minute, avoiding the need for continuous ultrasound ablation for controlled release while still providing the potential for tuning release rates. Second, the overall microcapsule integrity is maintained, offering further potential for control of the release rate even after activation (again unlike the pulsatile release observed with ultrasound triggered microbubble destruction).

Moving forward, additional studies associated with understanding the release kinetics and mechanism need to be performed. First, the effects of the duration of ultrasound activation, the intensity of the applied ultrasound (associated with the voltage), and the frequency of the ultrasound signal should be conducted to determine what level of control can be achieved over both the magnitude and rate of drug release. For example,

staged popping of corks as the intensity (modifiable by adjusting the voltage of the ultrasound generator used in this setup, as per Equation 3.3) is ramped may facilitate the delivery of tunable doses of drug over time or even a switching of the release mechanism between cork vibration (enabling on-off release) or cork popping (enabling triggered controlled release without requiring continuous ultrasound exposure).

Equation 3.3

$$I = \frac{p^2}{Z}, and\ I = \frac{V^2}{R}$$

The natural resonance of the glass microbeads is also likely different from that of the PLGA shell, which means that changing the ultrasonic frequency to match the microcorks rather than the polymer shell may lead to an alternate mode of release. Changing the material used to prepare the microcorks from silica to another degradable polymer also immiscible in the PLGA/chloroform pre-shell solution and the aqueous continuous phase but with a resonant frequency much closer to PLGA) would also be of interest to assess how the gradient of mechanical indices between the cork and the shell materials affects the release kinetics and/or the release mechanism.

Lastly, *in vitro* phantom studies and *in vivo* animal studies need to be performed to assess the potential translatability of the cork-shell microcapsules for practical drug delivery applications. There are two recommended approaches for the phantom study, as suggested in literature[113, 144]. One method recommends creating a cavity in an agar gel using a tube, which is then filled with the delivery vehicle, while the second method

suggests to make two pellets of a porous acrylic acid gel in which one pellet has the drug delivery vehicle dispersed and the other pellet is used as spacing agent to focus the ultrasound and study the release of the payload. The agar method will be used first to do such investigations. *In vivo* studies will be performed by encapsulating a fluorescent probe inside the microcapsules and using live imaging confocal equipment, such as an IVIS machine[149, 188], to track release. Alternatively, encapsulating copper into the microcapsule would enable *in situ* conversion of the loaded Cu to ^{64}Cu ($t_{1/2}$ ~ 12 h) upon neutron activation, enabling tracking of drug release using positron emission tomography (PET) scanning[158, 203].

3.6 References

1. Yun, Y.H., B.K. Lee, and K. Park, *Controlled Drug Delivery: Historical perspective for the next generation.* J Control Release, 2015. **219**: p. 2-7.
2. Hoffman, A.S., *The origins and evolution of "controlled" drug delivery systems.* J Control Release, 2008. **132**(3): p. 153-63.
3. *Controlled Release Drug Delivery Market Analysis Report*, in *Industry Report*. 2018, Grand View Research.
4. Zhang, Y., et al., *Mechanical Force-Triggered Drug Delivery.* Chem Rev, 2016. **116**(19): p. 12536-12563.
5. Hu, J., G. Zhang, and S. Liu, *Enzyme-responsive polymeric assemblies, nanoparticles and hydrogels.* Chem Soc Rev, 2012. **41**(18): p. 5933-49.
6. Hoare, T. and R. Pelton, *Highly pH and Temperature Responsive Microgels Functionalized with Vinylacetic Acid.* Macromolecules, 2004. **37**(7): p. 2544-2550.
7. Liu, J., et al., *pH-sensitive nano-systems for drug delivery in cancer therapy.* Biotechnol Adv, 2014. **32**(4): p. 693-710.
8. Simpson, M.J., et al., *Narrowly Dispersed, Degradable, and Scalable Poly(oligoethylene glycol methacrylate)-Based Nanogels via Thermal Self-Assembly.* Industrial & Engineering Chemistry Research, 2018. **57**(22): p. 7495-7506.

9. Felber, A.E., M.H. Dufresne, and J.C. Leroux, *pH-sensitive vesicles, polymeric micelles, and nanospheres prepared with polycarboxylates.* Adv Drug Deliv Rev, 2012. **64**(11): p. 979-92.
10. Cheng, W., et al., *pH-Sensitive Delivery Vehicle Based on Folic Acid-Conjugated Polydopamine-Modified Mesoporous Silica Nanoparticles for Targeted Cancer Therapy.* ACS Appl Mater Interfaces, 2017. **9**(22): p. 18462-18473.
11. Anderson, J.M., A. Rodriguez, and D.T. Chang, *Foreign body reaction to biomaterials.* Semin Immunol, 2008. **20**(2): p. 86-100.
12. Brazel, C.S., *Magnetothermally-responsive nanomaterials: combining magnetic nanostructures and thermally-sensitive polymers for triggered drug release.* Pharm Res, 2009. **26**(3): p. 644-56.
13. Volodkin, D.V., A.G. Skirtach, and H. Mohwald, *Near-IR remote release from assemblies of liposomes and nanoparticles.* Angew Chem Int Ed Engl, 2009. **48**(10): p. 1807-9.
14. Coussios, C.C. and R.A. Roy, *Applications of Acoustics and Cavitation to Noninvasive Therapy and Drug Delivery.* Annu Rev Fluid Mech, 2008. **40**(1): p. 395-420.
15. Schroeder, A., et al., *Controlling Liposomal Drug Release with Low Frequency Ultrasound: Mechanism and Feasibility.* Langmuir, 2007. **23**(7): p. 4019-4025.
16. Li, H.J., et al., *Smart Superstructures with Ultrahigh pH-Sensitivity for Targeting Acidic Tumor Microenvironment: Instantaneous Size Switching and Improved Tumor Penetration.* ACS Nano, 2016. **10**(7): p. 6753-61.
17. Yu, S., et al., *A novel pH-induced thermosensitive hydrogel composed of carboxymethyl chitosan and poloxamer cross-linked by glutaraldehyde for ophthalmic drug delivery.* Carbohydr Polym, 2017. **155**: p. 208-217.
18. Choi, S.W., Y. Zhang, and Y. Xia, *A temperature-sensitive drug release system based on phase-change materials.* Angew Chem Int Ed Engl, 2010. **49**(43): p. 7904-8.
19. Li, W., et al., *Gold nanocages covered with thermally-responsive polymers for controlled release by high-intensity focused ultrasound.* Nanoscale, 2011. **3**(4): p. 1724-30.
20. Mueller, E., et al., *Dynamically Cross-Linked Self-Assembled Thermoresponsive Microgels with Homogeneous Internal Structures.* Langmuir, 2018. **34**(4): p. 1601-1612.

21. Ta, T. and T.M. Porter, *Thermosensitive liposomes for localized delivery and triggered release of chemotherapy.* J Control Release, 2013. 169(1-2): p. 112-25.
22. Ulbrich, K., et al., *Targeted Drug Delivery with Polymers and Magnetic Nanoparticles: Covalent and Noncovalent Approaches, Release Control, and Clinical Studies.* Chem Rev, 2016. 116(9): p. 5338-431.
23. Zhang, H., et al., *High intensity focused ultrasound-responsive release behavior of PLA-b-PEG copolymer micelles.* J Control Release, 2009. 139(1): p. 31-9.
24. Hoare, T., et al., *Magnetically Triggered Composite Membrane for On-Demand Drug Delivery.* Nano Letters, 2009. 9(10): p. 3651-3657.
25. Gao, F., et al., *Preparation of aminated core-shell fluorescent nanoparticles and their application to the synchronous fluorescence determination of gamma-globulin.* Luminescence, 2008. 23(6): p. 392-6.
26. Mabrouk, M., et al., *The Influence of Lyophilized EmuGel Silica Microspheres on the Physicomechanical Properties, In Vitro Bioactivity and Biodegradation of a Novel Ciprofloxacin-Loaded PCL/PAA Scaffold.* Polymers, 2016. 8(6).
27. Nanaki, S., et al., *PLGA/SBA-15 mesoporous silica composite microparticles loaded with paclitaxel for local chemotherapy.* Eur J Pharm Sci, 2017. 99: p. 32-44.
28. Xu, W., et al., *A mesoporous silicon/poly-(DL-lactic-co-glycolic) acid microsphere for long time anti-tuberculosis drug delivery.* Int J Pharm, 2014. 476(1-2): p. 116-23.
29. Gao, Y., et al., *Optimising the shell thickness-to-radius ratio for the fabrication of oil-encapsulated polymeric microspheres.* Chem Eng J, 2016. 284: p. 963-971.
30. Li, Z. and C. Wang, *Effects of Working Parameters on Electrospinning*, in *One-Dimensional nanostructures*. 2013. p. 15-28.
31. Xu, Q., et al., *Coaxial electrohydrodynamic atomization process for production of polymeric composite microspheres.* Chem Eng Sci, 2013. 104.
32. Ito, F., H. Fujimori, and K. Makino, *Incorporation of water-soluble drugs in PLGA microspheres.* Colloids Surf B, 2007. 54(2): p. 173-8.
33. Agrahari, V., *Novel drug delivery systems, devices, and fabrication methods.* Drug Deliv Transl Res, 2018. 8(2): p. 303-306.

34. Sanjay, S.T., et al., *Controlled Drug Delivery Using Microdevices.* Curr Pharm Biotechnology, 2016. 17(9): p. 772-787.
35. Muanprasat, C. and V. Chatsudthipong, *Chitosan oligosaccharide: Biological activities and potential therapeutic applications.* Pharmacol Ther, 2017. 170: p. 80-97.
36. Figueiredo, M. and R. Esenaliev, *PLGA Nanoparticles for Ultrasound-Mediated Gene Delivery to Solid Tumors.* J Drug Deliv, 2012. 2012: p. 767839.
37. Luan, Y., et al., *Lipid shedding from single oscillating microbubbles.* Ultrasound Med Biol, 2014. 40(8): p. 1834-46.
38. Mikhaylov, G., et al., *Ferri-liposomes as an MRI-visible drug-delivery system for targeting tumours and their microenvironment.* Nat Nanotechnol, 2011. 6(9): p. 594-602.
39. Campbell, S.B., M. Patenaude, and T. Hoare, *Injectable superparamagnets: highly elastic and degradable poly(N-isopropylacrylamide)-superparamagnetic iron oxide nanoparticle (SPION) composite hydrogels.* Biomacromolecules, 2013. 14(3): p. 644-53.
40. Deng, W., et al., *Controlled gene and drug release from a liposomal delivery platform triggered by X-ray radiation.* Nat Commun, 2018. 9(1): p. 2713.
41. Park, J., et al., *Polydopamine-Based Simple and Versatile Surface Modification of Polymeric Nano Drug Carriers.* ACS Nano, 2014. 8(4): p. 3347-3356.
42. Lengert, E., et al., *Silver Alginate Hydrogel Micro- and Nanocontainers for Theranostics: Synthesis, Encapsulation, Remote Release, and Detection.* ACS Appl Mater Interfaces, 2017. 9(26): p. 21949-21958.
43. Ahmad, Z., et al., *Generation of multilayered structures for biomedical applications using a novel tri-needle coaxial device and electrohydrodynamic flow.* J R Soc Interface, 2008. 5(27): p. 1255-61.
44. Azizi, M., et al., *Fabrication of protein-loaded PLGA nanoparticles: effect of selected formulation variables on particle size and release profile.* J Polym Res, 2013. 20(4).
45. Ishak, R.A.H., N.M. Mostafa, and A.O. Kamel, *Stealth lipid polymer hybrid nanoparticles loaded with rutin for effective brain delivery - comparative study with the gold standard (Tween 80): optimization,*

characterization and biodistribution. Drug Deliv, 2017. **24**(1): p. 1874-1890.
46. Lussier, B. and A.A. Wilson, *Alpha-1 Antitrypsin: The Protein*, in *Alpha-1 Antitrypsin*. 2016. p. 17-30.
47. Kim, M.R., et al., *Golf ball-shaped PLGA microparticles with internal pores fabricated by simple O/W emulsion.* Chem Commun (Camb), 2010. **46**(39): p. 7433-5.
48. Cheng, J., et al., *Electrospinning versus microfluidic spinning of functional fibers for biomedical applications.* Biomaterials, 2017. **114**: p. 121-143.
49. Liechty, W.B., et al., *Polymers for drug delivery systems.* Annu Rev Chem Biomol Eng, 2010. **1**: p. 149-73.
50. Escoffre, J.M., et al., *Doxorubicin delivery into tumor cells with ultrasound and microbubbles.* Mol Pharm, 2011. **8**(3): p. 799-806.
51. Bakaic, E., N.M.B. Smeets, and T. Hoare, *Injectable hydrogels based on poly(ethylene glycol) and derivatives as functional biomaterials.* RSC Advances, 2015. **5**(45): p. 35469-35486.
52. Husseini, G.A., et al., *Investigating the acoustic release of doxorubicin from targeted micelles.* Colloids Surf B, 2013. **101**: p. 153-5.
53. Husseini, G.A. and W.G. Pitt, *Micelles and nanoparticles for ultrasonic drug and gene delivery.* Adv Drug Deliv Rev, 2008. **60**(10): p. 1137-52.
54. Fong, W.K., et al., *Responsive self-assembled nanostructured lipid systems for drug delivery and diagnostics.* J Colloid Interface Sci, 2016. **484**: p. 320-339.
55. Zhao, C.X., *Multiphase flow microfluidics for the production of single or multiple emulsions for drug delivery.* Adv Drug Deliv Rev, 2013. **65**(11-12): p. 1420-46.
56. Growney Kalaf, E.A., et al., *Characterization of slow-gelling alginate hydrogels for intervertebral disc tissue-engineering applications.* Mater Sci Eng C Mater Biol Appl, 2016. **63**: p. 198-210.
57. Sivakumaran, D., E. Mueller, and T. Hoare, *Temperature-Induced Assembly of Monodisperse, Covalently Cross-Linked, and Degradable Poly(N-isopropylacrylamide) Microgels Based on Oligomeric Precursors.* Langmuir, 2015. **31**(21): p. 5767-78.
58. Zhang, L., et al., *Co-delivery of hydrophobic and hydrophilic drugs from nanoparticle-aptamer bioconjugates.* Chem Med Chem, 2007. **2**(9): p. 1268-71.

59. Wang, H., et al., *Enhanced anti-tumor efficacy by co-delivery of doxorubicin and paclitaxel with amphiphilic methoxy PEG-PLGA copolymer nanoparticles.* Biomaterials, 2011. **32**(32): p. 8281-90.
60. Zhang, X.J., et al., *Preparation of thermo/pH-sensitive reduced graphene oxide interpenetrating hydrogel nanocomposites for co-delivery of paclitaxel and epirubicin.* Mater Technol, 2018. **33**(4): p. 245-252.
61. Kolesnichenko, I.V. and E.V. Anslyn, *Practical applications of supramolecular chemistry.* Chem Soc Rev, 2017. **46**(9): p. 2385-2390.
62. Liu, R., et al., *Core-shell Fe3O4 polydopamine nanoparticles serve multipurpose as drug carrier, catalyst support and carbon adsorbent.* ACS Appl Mater Interfaces, 2013. **5**(18): p. 9167-71.
63. de Gracia Lux, C., et al., *Biocompatible polymeric nanoparticles degrade and release cargo in response to biologically relevant levels of hydrogen peroxide.* J Am Chem Soc, 2012. **134**(38): p. 15758-64.
64. Li, H., et al., *Near-infrared light-triggered drug release from a multiple lipid carrier complex using an all-in-one strategy.* J Control Release, 2017. **261**: p. 126-137.
65. Griffin, W.C. and M.J. Lynch, *Surface Active Agents*, in *Handbook of Food Additives*, T. Furia, Editor. 1968.
66. Ltd., C.E., *Span and Tween*, C.E. Ltd., Editor. 2009: England.
67. Kanicky, J.R., et al., *Surface Chemistry in the Petroleum Industry*, in *Handbook of Applied Surface and Colloid Chemistry*, K. Holmberg, Editor. 2001, John Wiley & Sons, Ltd.
68. Salager, J.-L., *Surfactants - Types and Uses*, in *FIRP Booklet #E300-A*, FIRP, Editor. 2002: Venezuela.
69. Wang, F., et al., *Polyelectrolyte Complex Nanoparticles from Chitosan and Acylated Rapeseed Cruciferin Protein for Curcumin Delivery.* J Agric Food Chem, 2018. **66**(11): p. 2685-2693.
70. Liu, Y., H. Miyoshi, and M. Nakamura, *Encapsulated ultrasound microbubbles: therapeutic application in drug/gene delivery.* J Control Release, 2006. **114**(1): p. 89-99.
71. Makadia, H.K. and S.J. Siegel, *Poly Lactic-co-Glycolic Acid (PLGA) as Biodegradable Controlled Drug Delivery Carrier.* Polymers (Basel), 2011. **3**(3): p. 1377-1397.
72. Ortega-Oller, I., et al., *Bone Regeneration from PLGA Micro-Nanoparticles.* Biomed Res Int, 2015. **2015**: p. 415289.

73. Khvedelidze, M., et al., *Calorimetric and spectrophotometric investigation of PLGA nanoparticles and their complex with DNA*. Vol. 99. 2010. 337-348.
74. Mura, S., J. Nicolas, and P. Couvreur, *Stimuli-responsive nanocarriers for drug delivery.* Nat Mater, 2013. **12**(11): p. 991-1003.
75. Li, Y. and T.M. Liu, *Discovering Macrophage Functions Using In Vivo Optical Imaging Techniques.* Front Immunol, 2018. **9**: p. 502.
76. Ramsay, R.R., et al., *A perspective on multi-target drug discovery and design for complex diseases.* Clin Transl Med, 2018. **7**(1): p. 3.
77. Wang, C., et al., *Predicting target-ligand interactions using protein ligand-binding site and ligand substructures.* BMC Systems Biology, 2015. **9**(1): p. S2.
78. Matsumoto, A., et al., *Fabrication of Janus particles composed of poly (lactic-co-glycolic) acid and hard fat using a solvent evaporation method.* Drug Discov Ther, 2016. **10**(6): p. 307-313.
79. Yang, X., et al., *Superparamagnetic graphene oxide–Fe3O4 nanoparticles hybrid for controlled targeted drug carriers.* J Mater Chem, 2009. **19**(18).
80. Chowdhuri, A.R., et al., *Carbon Dots Embedded Magnetic Nanoparticles @Chitosan @Metal Organic Framework as a Nanoprobe for pH Sensitive Targeted Anticancer Drug Delivery.* ACS Appl Mater Interfaces, 2016. **8**(26): p. 16573-83.
81. Yarin, A.L., et al., *Material encapsulation and transport in core–shell micro/nanofibers, polymer and carbon nanotubes and micro/nanochannels.* J Mater Chem, 2007. **17**(25): p. 2585 - 2599.
82. Yang, Q., et al., *Facile Synthesis of Lipid-Perfluorocarbon Nanoemulsion Coated with Silica Shell as an Ultrasound Imaging Agent.* Adv Healthc Mater, 2018. **7**(4).
83. Li, J., et al., *Janus polymeric cages.* Polymer, 2012. **53**(17): p. 3712-3718.
84. Rao, K.J., et al., *A Force to Be Reckoned With: A Review of Synthetic Microswimmers Powered by Ultrasound.* Small, 2015. **11**(24): p. 2836-46.
85. Shemi, O. and M.J. Solomon, *Self-Propulsion and Active Motion of Janus Ellipsoids.* J Phys Chem B, 2018. **122**(44): p. 10247-10255.
86. Jiang, H.R., N. Yoshinaga, and M. Sano, *Active motion of a Janus particle by self-thermophoresis in a defocused laser beam.* Phys Rev Lett, 2010. **105**(26): p. 268302.

87. Moghaddam, M.K., S.M. Mortazavi, and T. Khaymian, *Micro/nano-encapsulation of a phase change material by coaxial electrospray method.* Iran Polym J, 2015. **24**(9): p. 759-774.
88. Hernot, S. and A.L. Klibanov, *Microbubbles in ultrasound-triggered drug and gene delivery.* Adv Drug Deliv Rev, 2008. **60**(10): p. 1153-66.
89. Mendelsohn, A.D., et al., *Patterning of mono- and multilayered pancreatic beta-cell clusters.* Langmuir, 2010. **26**(12): p. 9943-9.
90. Sadowski, L.P., et al., *Synthesis of Polyester Dendritic Scaffolds for Biomedical Applications.* Macromol Biosci, 2016. **16**(10): p. 1475-1484.
91. Pooja, D., et al., *Dendrimer-TPGS mixed micelles for enhanced solubility and cellular toxicity of taxanes.* Colloids Surf B, 2014. **121**: p. 461-8.
92. Zhou, M., et al., *Low density lipoprotein/pectin complex nanogels as potential oral delivery vehicles for curcumin.* Food Hydrocolloids, 2016. **57**: p. 20-29.
93. Steinhilber, D., et al., *A microgel construction kit for bioorthogonal encapsulation and pH-controlled release of living cells.* Angew Chem Int Ed Engl, 2013. **52**(51): p. 13538-43.
94. Taylor, G., *Disintegration of Water Drops in an Electric Field.* Proc R Soc Lond A Math Phys Sci, 1964. **280**(1382): p. 383-397.
95. Jaworek, A., *Electrospray droplet sources for thin film deposition.* J Mater Sci, 2006. **42**(1): p. 266-297.
96. Wang, F., et al., *Fabrication and Characterization of Prosurvival Growth Factor Releasing, Anisotropic scaffolds for Enhanced Mesenchymal Stem Cell Survival Growth and Orientation.* Biomacromolecules, 2009. **10**(9): p. 2609-2618.
97. D'Amore, A., et al., *Heart valve scaffold fabrication: Bioinspired control of macro-scale morphology, mechanics and micro-structure.* Biomaterials, 2018. **150**: p. 25-37.
98. Pena, B., et al., *Biomimetic Polymers for Cardiac Tissue Engineering.* Biomacromolecules, 2016. **17**(5): p. 1593-601.
99. Reuter, K.G., et al., *Targeted PRINT Hydrogels: The Role of Nanoparticle Size and Ligand Density on Cell Association, Biodistribution, and Tumor Accumulation.* Nano Lett, 2015. **15**(10): p. 6371-8.

100. Soukoulis, C. and T. Bohn, *A comprehensive overview on the micro- and nano-technological encapsulation advances for enhancing the chemical stability and bioavailability of carotenoids.* Crit Rev Food Sci Nutr, 2018. 58(1): p. 1-36.
101. Yuan, Y., et al., *Complex coacervation of soy protein with chitosan: Constructing antioxidant microcapsule for algal oil delivery.* LWT - Food Sci Technol, 2017. 75(Complete): p. 171 - 179.
102. Akbulut, M., et al., *Generic Method of Preparing Multifunctional Fluorescent Nanoparticles Using Flash NanoPrecipitation.* Adv Funct Mater, 2009. 19(5): p. 718-725.
103. Holowka, E.P. and S.K. Bhatia, *Controlled Release Systems*, in *Drug Delivery: Materials Design and Clinical Perspective*. 2014, Springer-Verlag: New York.
104. Fu, Y. and W.J. Kao, *Drug release kinetics and transport mechanisms of non-degradable and degradable polymeric delivery systems.* Expert Opin Drug Deliv, 2010. 7(4): p. 429-444.
105. Dash, S., et al., *KINETIC MODELING ON DRUG RELEASE FROM CONTROLLED DRUG DELIVERY SYSTEMS.* Acta Poloniae Pharmaceutica, 2010. 67(3): p. 217-223.
106. Yu, J., et al., *Stimuli-Responsive Delivery of Therapeutics for Diabetes Treatment.* Bioeng Transl Med, 2016. 1(3): p. 323-337.
107. Fischel-Ghodsian, F., et al., *Enzymatically controlled drug delivery.* Proc Natl Acad Sci U S A, 1988. 85(7): p. 2403-2406.
108. Napoli, A., et al., *Glucose-oxidase Based Self-Destructing Polymeric Vesicles.* Langmuir, 2004. 20(9): p. 3487-3491.
109. Di, J., et al., *Ultrasound-triggered noninvasive regulation of blood glucose levels using microgels integrated with insulin nanocapsules.* Nano Research, 2017. 10(4): p. 1393-1402.
110. Tan, H., et al., *Thermosensitive injectable hyaluronic acid hydrogel for adipose tissue engineering.* Biomaterials, 2009. 30(36): p. 6844-53.
111. Li, L., et al., *Enzymatic Hydrolysis and Simultaneous Extraction for Preparation of Genipin from Bark of Eucommia ulmoides after Ultrasound, Microwave Pretreatment.* Molecules, 2015. 20(10): p. 18717-31.
112. Li, Y., et al., *Enzyme-Responsive Polymeric Vesicles for Bacterial-Strain-Selective Delivery of Antimicrobial Agents.* Angew Chem Int Ed Engl, 2016. 55(5): p. 1760-4.

113. Phillips, L.C., et al., *Phase-shift perfluorocarbon agents enhance high intensity focused ultrasound thermal delivery with reduced near-field heating.* J Acoust Soc Am, 2013. **134**(2): p. 1473-82.
114. Liu, H., et al., *Hydrophobic interaction-mediated capture and release of cancer cells on thermoresponsive nanostructured surfaces.* Adv Mater, 2013. **25**(6): p. 922-7.
115. Ferrara, K.W., *Driving delivery vehicles with ultrasound.* Adv Drug Deliv Rev, 2008. **60**(10): p. 1097-102.
116. Gao, Z., et al., *Drug-loaded nano/microbubbles for combining ultrasonography and targeted chemotherapy.* Ultrasonics, 2008. **48**(4): p. 260-70.
117. Hoare, T., et al., *Magnetically triggered nanocomposite membranes: a versatile platform for triggered drug release.* Nano Lett, 2011. **11**(3): p. 1395-400.
118. Lafond, M., et al., *Cavitation-threshold Determination and Rheological-parameters Estimation of Albumin-stabilized Nanobubbles.* Sci Rep, 2018. **8**(1): p. 7472.
119. Moyer, L.C., et al., *High-intensity focused ultrasound ablation enhancement in vivo via phase-shift nanodroplets compared to microbubbles.* J Ther Ultrasound, 2015. **3**: p. 7.
120. Suzuki, T., et al., *Experimental studies of moderate temperature burns.* Burns, 1991. **17**(6): p. 443-451.
121. Dai, T., et al., *Chitosan Acetate Bandage as a Topical Antimicrobial Dressing for Infected Burns.* Antimicrob Agents Chemother, 2009. **53**(2): p. 393.
122. Laurent, S., et al., *Superparamagnetic iron oxide nanoparticles for delivery of therapeutic agents: opportunities and challenges.* Expert Opin Drug Deliv, 2014. **11**(9): p. 1449-70.
123. Vallooran, J.J., R. Negrini, and R. Mezzenga, *Controlling anisotropic drug diffusion in lipid-Fe3O4 nanoparticle hybrid mesophases by magnetic alignment.* Langmuir, 2013. **29**(4): p. 999-1004.
124. Shah, S.A., et al., *Mixed Brownian alignment and Neel rotations in superparamagnetic iron oxide nanoparticle suspensions driven by an ac field.* Phys Rev B Condens Matter Mater Phys, 2015. **92**(9).
125. Liu, T.-Y., et al., *Influence of magnetic nanoparticle arrangement in ferrogels for tunable biomolecule diffusion.* RSC Advances, 2015. **5**(109): p. 90098-90102.

126. Miao, X., et al., *Application of Dye-coated Ultrasmall Gadolinium Oxide Nanoparticles for Biomedical Dual Imaging.* Bull Korean Chem, 2017. **38**(9): p. 1058-1068.
127. Fedoryshin, L.L., et al., *Near-infrared-triggered anticancer drug release from upconverting nanoparticles.* ACS Appl Mater Interfaces, 2014. **6**(16): p. 13600-6.
128. Goodman, A.M., et al., *Near-infrared remotely triggered drug-release strategies for cancer treatment.* Proc Natl Acad Sci U S A, 2017. **114**(47): p. 12419-12424.
129. Song, G., et al., *Perfluorocarbon-Loaded Hollow Bi2Se3 Nanoparticles for Timely Supply of Oxygen under Near-Infrared Light to Enhance the Radiotherapy of Cancer.* Adv Mater, 2016. **28**(14): p. 2716-23.
130. Farag, M.M., W.M. Abd-Allah, and A.M. Ibrahim, *Effect of gamma irradiation on drug releasing from nano-bioactive glass.* Drug Deliv Transl Res, 2015. **5**(1): p. 63-73.
131. Caruso, M.M., et al., *Mechanically-induced chemical changes in polymeric materials.* Chem Rev, 2009. **109**(11): p. 5755-98.
132. Hu, Y., J.M. Wan, and A.C. Yu, *Cytomechanical perturbations during low-intensity ultrasound pulsing.* Ultrasound Med Biol, 2014. **40**(7): p. 1587-98.
133. Li, J., C. Nagamani, and J.S. Moore, *Polymer mechanochemistry: from destructive to productive.* Acc Chem Res, 2015. **48**(8): p. 2181-90.
134. Feigenbaum, H., W.F. Armstrong, and T. Ryan, *Feigenbaum's Echocardiography*. 2005: Lippincott Williams & Wilkins.
135. Prince, J.L. and J.M. Links, *Medical Imaging Signals and Systems*, in *Medical Imaging Signals and Systems*. 2006, Pearson Prentice Hall.
136. Sakai, S., *Chapter 2*.
137. Chen, X., et al., *Single-site sonoporation disrupts actin cytoskeleton organization.* J R Soc Interface, 2014. **11**(95): p. 20140071.
138. D'Onofrio, M., et al., *Acoustic radiation force impulse of the liver.* World J Gastroenterol, 2013. **19**(30): p. 4841-9.
139. Kang, M., G. Huang, and C. Leal, *Role of lipid polymorphism in acoustically sensitive liposomes.* Soft Matter, 2014. **10**(44): p. 8846-54.
140. ter Haar, G. and C. Coussios, *High Intensity Focused Ultrasound: Past, present and future.* Int. J. Hyperthermia, 2009. **23**(2): p. 85-87.

141. Kawabata, K.-i., et al., *Nanoparticles with Multiple Perfluorocarbons for Controllable Ultrasonically Induced Phase Shifting.* Jpn J Appl Phys, 2005. **44**(6B): p. 4548-4552.
142. Jablonowski, L.J., et al., *Shell effects on acoustic performance of a drug-delivery system activated by ultrasound.* J Biomed Mater Res A, 2017. **105**(11): p. 3189-3196.
143. Li, G., et al., *Spatial and temporal control of shape memory polymers and simultaneous drug release using high intensity focused ultrasound.* J Mater Chem, 2012. **22**(16).
144. Tang, J., et al., *Controlled drug release from ultrasound-visualized elastic eccentric microcapsules using different resonant modes.* J Mater Chem B, 2018. **6**(13): p. 1920-1929.
145. Deckers, R., et al., *New insights into the HIFU-triggered release from polymeric micelles.* Langmuir, 2013. **29**(30): p. 9483-90.
146. Arpicco, S., et al., *Recent studies on the delivery of hydrophilic drugs in nanoparticulate systems.* J Drug Deliv Sci Technol, 2016. **32**: p. 298-312.
147. Seip, R., et al., *Targeted ultrasound-mediated delivery of nanoparticles: on the development of a new HIFU-based therapy and imaging device.* IEEE Trans Biomed Eng, 2010. **57**(1): p. 61-70.
148. Menon, J.U., et al., *Effects of surfactants on the properties of PLGA nanoparticles.* J Biomed Mater Res A, 2012. **100**(8): p. 1998-2005.
149. Fokong, S., et al., *Image-guided, targeted and triggered drug delivery to tumors using polymer-based microbubbles.* J Control Release, 2012. **163**(1): p. 75-81.
150. Barz, M., et al., *P(HPMA)-block-P(LA) copolymers in paclitaxel formulations: polylactide stereochemistry controls micellization, cellular uptake kinetics, intracellular localization and drug efficiency.* J Control Release, 2012. **163**(1): p. 63-74.
151. Seo, M. and N. Matsuura, *Monodisperse, submicrometer droplets via condensation of microfluidic-generated gas bubbles.* Small, 2012. **8**(17): p. 2704-14.
152. Birajdar, M.S. and J. Lee, *Nanoscale Bumps and Dents on Nanofibers Enabling Sonication-Responsive Wetting and Improved Moisture Collection.* Macromol Mater Eng, 2015. **300**(11): p. 1108-1115.
153. Gao, Y., et al., *Tuning Microparticle Porosity during Single Needle Electrospraying Synthesis via a Non-Solvent-Based Physicochemical Approach.* Polymers, 2015. **7**(12): p. 2701-2710.

154. Ghayempour, S. and S.M. Mortazavi, *Fabrication of micro–nanocapsules by a new electrospraying method using coaxial jets and examination of effective parameters on their production.* J Electrostat, 2013. 71(4): p. 717-727.
155. Jaworek, A. and A.T. Sobczyk, *Electrospraying route to nanotechnology: An overview.* J Electrostat, 2008. 66(3-4): p. 197-219.
156. M, J.C., et al., *Mimicking Hierarchical Complexity of the Osteochondral Interface Using Electrospun Silk-Bioactive Glass Composites.* ACS Appl Mater Interfaces, 2017. 9(9): p. 8000-8013.
157. Xu, Y. and M.A. Hanna, *Electrospray encapsulation of water-soluble protein with polylactide. Effects of formulations on morphology, encapsulation efficiency and release profile of particles.* Int J Pharm, 2006. 320(1-2): p. 30-6.
158. Vasquez, K.O., C. Casavant, and J.D. Peterson, *Quantitative whole body biodistribution of fluorescent-labeled agents by non-invasive tomographic imaging.* PLoS One, 2011. 6(6): p. e20594.
159. Latham, J. and I.W. Roxburgh, *Disintegration of Pairs of Water Drops in an Electric Field.* Proc R Soc Lond A Math Phys Sci, 1966. 295(1440): p. 84-97.
160. Loeb, L.B., et al., *Pulses in Negative Point-to-Plane Corona.* Physical Review, 1941. 60(10): p. 714-722.
161. Davoodi, P., et al., *Coaxial electrohydrodynamic atomization: microparticles for drug delivery applications.* J Control Release, 2015. 205: p. 70-82.
162. Zhang, L., et al., *Coaxial electrospray of microparticles and nanoparticles for biomedical applications.* Expert Rev Med Devices, 2012. 9(6): p. 595-612.
163. Fujimoto, K.L., et al., *An elastic, biodegradable cardiac patch induces contractile smooth muscle and improves cardiac remodeling and function in subacute myocardial infarction.* J Am Coll Cardiol, 2007. 49(23): p. 2292-300.
164. Li, M., et al., *Culturing primary human osteoblasts on electrospun poly(lactic-co-glycolic acid) and poly(lactic-co-glycolic acid)/nanohydroxyapatite scaffolds for bone tissue engineering.* ACS Appl Mater Interfaces, 2013. 5(13): p. 5921-6.
165. Jaworek, A., *Micro- and nanoparticle production by electrospraying.* Powder Technology, 2007. 176(1): p. 18-35.

166. Lee, Y.H., et al., *Release profile characteristics of biodegradable-polymer-coated drug particles fabricated by dual-capillary electrospray.* J Control Release, 2010. **145**(1): p. 58-65.
167. Rasekh, M., et al., *Hollow-layered nanoparticles for therapeutic delivery of peptide prepared using electrospraying.* J Mater Sci Mater Med, 2015. **26**(11): p. 256.
168. Xie, J. and C.H. Wang, *Electrospray in the dripping mode for cell microencapsulation.* J Colloid Interface Sci, 2007. **312**(2): p. 247-55.
169. Kishan, A.P. and E.M. Cosgriff-Hernandez, *Recent advancements in electrospinning design for tissue engineering applications: A review.* J Biomed Mater Res A, 2017. **105**(10): p. 2892-2905.
170. Wu, Y. and R.L. Clark, *Controllable porous polymer particles generated by electrospraying.* J Colloid Interface Sci, 2007. **310**(2): p. 529-35.
171. Casper, C.L., et al., *Controlling Surface Morphology of Electrospun Polystyrene Fibers: Effect of Humidity and Molecular Weight in the Electrospinning Process.* Macromolecules, 2004. **37**(2): p. 573-578.
172. Mit-uppatham, C., M. Nithitanakul, and P. Supaphol, *Ultrafine Electrospun Polyamide-6 Fibers: Effect of Solution Conditions on Morphology and Average Fiber Diameter.* Macromol Chem Phys, 2004. **205**(17): p. 2327-2338.
173. McDonagh, P.F. and S.K. Williams, *The Preparation and Use of FluorescentProtein Conjugates for Microvascular Research.* Microvasc Res, 1984. **27**(1): p. 14-27.
174. Wischke, C. and H.-H. Borchert, *Fluorescein isothiocyanate labelled bovine serum albumin (FITC-BSA) as a model protein drug: opportunities and drawbacks.* Pharmazie, 2005. **61**(9): p. 770-774.
175. Salomi, B.S.B., C.K. Mitra, and L. Gorton, *Electrochemical and spectrophotometric studies on dyes and proteins labelled with dyes.* Synthetic Metals, 2005. **155**(2): p. 426-429.
176. Wu, F., et al., *Grafting polymerization of polylactic acid on the surface of nano-SiO2and properties of PLA/PLA-grafted-SiO2nanocomposites.* J Appl Polym Sci, 2013. **129**(5): p. 3019-3027.
177. Lee, Y.-C., et al., *Optical Properties of Fluorescein labeled Organoclay.* Photochem Photobiol, 2010. **86**(3): p. 520-527.
178. Mei, F. and D.R. Chen, *Operational modes of dual-capillary electrospraying and the formation of the stable compound cone-jet mod.* Aerosol and Air Quality Research, 2008. **8**(2): p. 218-232.

179. Torza, S. and S.G. Mason, *Three-phase interactions in shear and electrical fields.* J Colloid Interface Sci, 1970. **33**(1): p. 67-83.
180. Gennes, P.-G.d., F. Brochard-Wyart, and D. Quere, *Drops, Bubbles, Pearls, Waves*, in *Capillarity and Wetting Phenomena*. 2004, Springer-Verlag New York.
181. Smallwood, I.M., *Handbook of Organic Solvent Properties*. 1996, New York: Halsted Press.
182. Company, D.C., *Tergitol NP-4 Surfactant*, D.C. Company, Editor.
183. Chitkara, D. and N. Kumar, *BSA-PLGA-based core-shell nanoparticles as carrier system for water-soluble drugs.* Pharm Res, 2013. **30**(9): p. 2396-409.
184. Li, M., et al., *Cisplatin crosslinked pH-sensitive nanoparticles for efficient delivery of doxorubicin.* Biomaterials, 2014. **35**(12): p. 3851-64.
185. Aggells, D.G. and T. Shlotani, *Repair evaluation of concrete cracks using surface and through-transmission wave measurements.* Cement Concrete Comp, 2007. **29**(9): p. 700-711.
186. Quiviger, A., et al., *Effect of the presence and size of a real macro-crack on diffuse ultrasound in concrete.* Ndt & E International, 2012. **45**(1): p. 128-132.
187. Chemat, F., et al., *Ultrasound assisted extraction of food and natural products. Mechanisms, techniques, combinations, protocols and applications. A review.* Ultrason Sonochem, 2017. **34**: p. 540-560.
188. McClure, A., *Using High-Intensity Focused Ultrasound as a Means to Provide Targeted Drug Delivery.* J Diagn Med Sonogr, 2016. **32**(6): p. 343-350.
189. ter Haar, G., et al., *Guidance on reporting ultrasound exposure conditions for bio-effects studies.* Ultrasound Med Biol, 2011. **37**(2): p. 177-83.
190. Asfaram, A., M. Ghaedi, and A. Goudarzi, *Optimization of ultrasound-assisted dispersive solid-phase microextraction based on nanoparticles followed by spectrophotometry for the simultaneous determination of dyes using experimental design.* Ultrason Sonochem, 2016. **32**: p. 407-417.
191. Ellens, N.P., et al., *The targeting accuracy of a preclinical MRI-guided focused ultrasound system.* Med Phys, 2015. **42**(1): p. 430-9.
192. Mougenot, C., et al., *Quantification of near-field heating during volumetric MR-HIFU ablation.* Med Phys, 2011. **38**(1): p. 272-82.

193. Bekeredjian, R., et al., *Augmentation of cardiac protein delivery using ultrasound targeted microbubble destruction.* Ultrasound Med Biol, 2005. 31(5): p. 687-91.
194. Oerlemans, C., et al., *Evidence for a new mechanism behind HIFU-triggered release from liposomes.* J Control Release, 2013. 168(3): p. 327-33.
195. Hoogenboom, M., et al., *Mechanical high-intensity focused ultrasound destruction of soft tissue: working mechanisms and physiologic effects.* Ultrasound Med Biol, 2015. 41(6): p. 1500-17.
196. Rodriguez-Frutos, B., et al., *Enhanced brain-derived neurotrophic factor delivery by ultrasound and microbubbles promotes white matter repair after stroke.* Biomaterials, 2016. 100: p. 41-52.
197. Nance, E., et al., *Non-invasive delivery of stealth, brain-penetrating nanoparticles across the blood-brain barrier using MRI-guided focused ultrasound.* J Control Release, 2014. 189: p. 123-132.
198. Tipler, P.A. and G. Mosca, *Physics for Scientists and Engineers*. 2008: Macmillan Higher Education.
199. Park, P.I.P. and S. Jonnalagadda, *Predictors of glass transition in the biodegradable poly-lactide and poly-lactide-co-glycolide polymers.* J Appl Polym Sci, 2006. 100(3): p. 1983-1987.
200. Zolnik, B.S., P.E. Leary, and D.J. Burgess, *Elevated temperature accelerated release testing of PLGA microspheres.* J Control Release, 2006. 112(3): p. 293-300.
201. Avramov, I., T. Vassilev, and I. Penkov, *The glass transition temperature of silicate and borate glasses.* J Non-Cryst Solids, 2005. 351(7): p. 472 - 476.
202. Xu, J.S., et al., *Synthesizing and binding dual-mode poly (lactic-co-glycolic acid) (PLGA) nanobubbles for cancer targeting and imaging.* Biomaterials, 2010. 31(7): p. 1716-22.
203. Peng, F., F. Xie, and O. Muzik, *Alteration of Copper Fluxes in Brain Aging: A Longitudinal Study in Rodent Using (64)CuCl2-PET/CT.* Aging Dis, 2018. 9(1): p. 109-118.

Chapter 4 – Conclusions and Recommendations

4.1 Conclusions

Targeted, and controlled drug delivery may be activated by many different factors, ranging from changes in microenvironments to externally applied stimulus. Of these activation methods, ultrasound is of particular interest because its mechanism of activation does not strictly rely on the material's chemical properties (pKa, LCST, etc.). Instead, acoustic waves travel longitudinally to and through the drug delivery vehicle, and either induce cavitation, shear stress, and localized heating, which will result in either the destruction of the delivery vehicle, increased permeability of the shell material through mechanical agitation, or the melting the delivery vehicle. These activation mechanisms are all initiated through different US modalities and have their benefits and drawbacks. Although it is possible to have effective dosage control using ultrasound via the increased permeation of the shell, constant ultrasound must be applied. Rapid drug release and uptake is possible by ultrasound triggered microparticle destruction, but the administered concentration may exceed the minimal toxic concentration threshold and may also damage healthy cells in the process. As such, the development of a US triggered delivery vehicle that overcomes the issues associated with prolonged ultrasound exposure while maintaining microcapsule integrity would be beneficial to the field.

In this thesis, a drug delivery vehicle consisting of a microcapsule with a complex polymer shell in which an additional phase (referred to as corks) is incorporated was proposed, fabricated, and validated.

Chapter 2 describes the fabrication of this product using electrohydrodynamic fabrication, specifically electrospraying. A coaxial needle was used in which the inner phase consisted of an aqueous solution containing BSA and a fluorescent label and the outer shell phase consisted of microcorks suspended in a PLGA/DCM solution. The continuous phase for the collection of the samples was an aqueous solution containing PVA. However, surface tensions between the air/water and PLGA/air/water interface were too high, resulting in film formation instead of capsular product. To overcome this issue, the coaxial needle was submerged in the continuous phase, forcing the formation of spherical and symmetric microcapsules. An increase in voltage decreased the size of the microcapsules while an increase in extrusion speed increased the size of the microcapsules, both consistent with literature; the concentration of the PVA in the continuous phase and the effects of different surfactants replacing BSA in the inner core were also assessed but, provided that microcapsules could still be formed, these variables had less significant effects.

Microcapsules with corks were then successfully fabricated and analyzed under confocal microscopy. The density of corks in the microcapsules was inconsistent between the start and finish of the electrospray process, with the maximum cork density observed in the first five minutes of fabrication and the lowest cork density observed during the last five minutes of fabrication. However, varying the collection time could thus enable the collection of microcapsules with varying cork densities within a single electrospray process.

The major contribution of this thesis involves the first reported fabrication of complex hollow spherical cork-shell delivery vehicles. The only previous literature with comparable

properties involved the use of two separate conductive capillaries for the fabrication of cork-shell microfibres. The developed work improves on the prior art by the creation of controlled, spherical cork shell microcapsules that are injectable and thus more amenable to potential clinical translation while also using a simpler fabrication technique.

Chapter 3 describes the ultrasound-mediated release of a fluorescent probe (either rhodamine 123 or fluorescein) from the cork-shell microcapsules. Drug release studies were performed using a sonication bath and a focused ultrasound probe. Sonication bath studies suggested that there is a direct correlation between the release of Rhd123 in corked microcapsules and the duration of ultrasound. However, comparing the release observed as a function of shell thickness and the presence or absence of corks suggested that the sonication bath was an insufficiently controlled experimental setup due to inconsistent ultrasound geometries and localized heating beyond the glass transition temperature of the PLGA shell material.

Instead a focused ultrasound probe was used together with a latex-based sample holder that could permit control over the focus distance but remain highly permeable to ultrasound while not significantly changing the wave path due to reflections. Release studies using this approach showed that corked microcapsules exhibited significantly higher drug release compared to the uncorked microcapsules, which together with corked or uncorked microcapsules in the absence of ultrasound did not show any significant release. Similar amounts of drug were also released whether the duration of ultrasound exposure was 1 minute, 5 minutes, or 10 minutes, suggesting that the initial pulse of

ultrasound plays a key (but, given continual slower release observed after the ultrasound is switched off, non-exclusive) role in regulating the release kinetics. The cork density was also determined to play a role in the release, whereby microcapsules supersaturated with corks displayed minimal release while subsequent reductions in cork presence resulted in increased release, hypothesized to be related to reduced attenuation of the ultrasound vibrations by the corks at the frequency used for ablation; however, in the absence of corks, no payload is released from the microcapsules. This suggests that there is an optimal cork concentration in the shell for facilitating controlled release.

Our initial mechanism hypothesis was that some population of corks would be irreversibly popped out the shell in the presence of ultrasound, resulting in the formation of a permanent pore that would enable continuous drug release until the delivery vehicle emptied. However, there was also a discernable plateau after all of the release studies at a drug concentration well below the total concentration anticipated if all the microcapsule payload was released; furthermore, small but significant increases in cumulative drug release were observed over time. This suggests that there could be an additional mechanism of release that is occurring by which the corks vibrate enough to deform the shell and create temporary pores without causing irreversible removal of the corks from the shell. In this case, in the absence of ultrasound, the vibrational stimulus would be removed and release would be significantly suppressed if not stopped. In order to determine which of these mechanisms is occurring, it would be useful to perform secondary and tertiary US activations. If no additional release occurs, this would suggest that all of the corks have been popped from the microcapsules on the initial ultrasound

burst; if additional release of a payload occurs, the vibrational mechanism is at least important if not dominant. The two potential mechanisms are depicted in Figure 4.1.

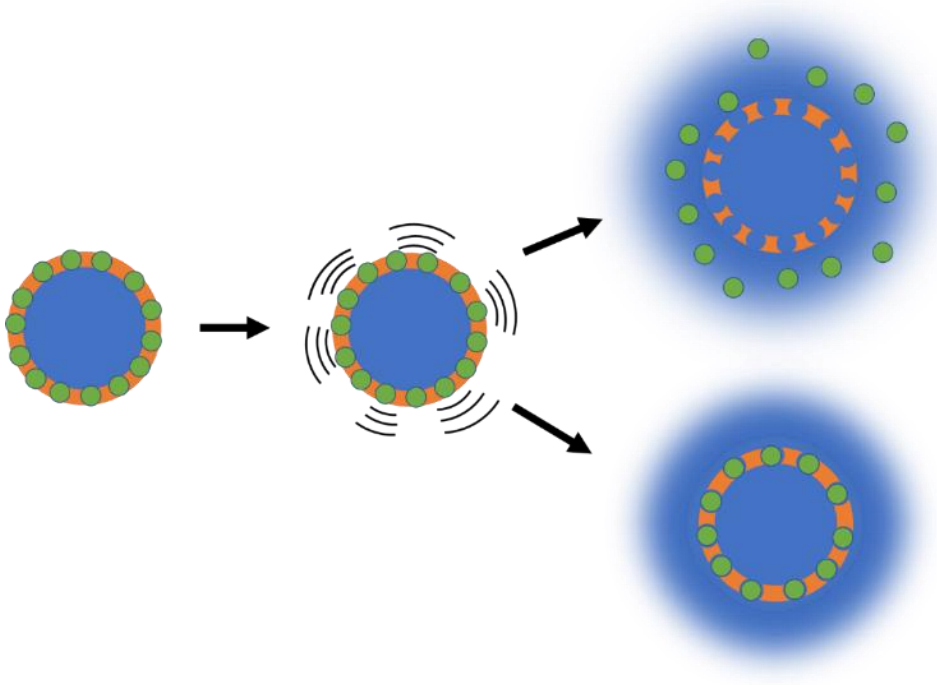

Figure 4.1: Potential release mechanisms of ultrasound triggered release of corked microcapsules. Blue – aqueous phase with dissolved model drug; orange – PLGA shell; green – microcorks

The cork shell microcapsules may employ one or both of these two potential mechanisms to release its contents, and the initial release data presented in this thesis suggests that both mechanisms may be at play. This is a unique combination relative to previously reported delivery vehicles, given that the integrity of the shell is maintained while under US for both corked and uncorked shells. Specifically, our cork-shell microcapsules can provide some control in the release kinetics by avoiding UTMD while also not requiring excessive exposure periods to US in order to begin the degradation/dissociation of the

microcoks in the shell. Additionally, in comparison to soft and more elastic polymers that release drug in the presence of US, the PLGA microcorks do not leak in the absence of ultrasound, overcoming an issue associated with soft particles.

4.2 Recommendations

Going forward, it is recommended that the fabrication process be modified in order to (1) manage the size and thickness of the microcapsules, and (2) to maintain constant cork density in all of the microcapsules. To do so, it can be suggested that a pneumatically manipulated extruder be used, which would allow for the integration of a continuously stirred tank reactor (CSTR) in the process to ensure uniform cork concentrations throughout the fabrication process and avoid the issues around cork settling observed in this work. Also, changing the aforementioned fabrication parameters may have a positive impact on controlling the size of the microcapsule, the shell thickness, the cork density, and the drug encapsulation efficiency.

For better controlling the drug release kinetics, the effects of varying the ultrasound frequencies and intensities should be investigated to determine (1) the lowest intensity resulting in a significant drug release, (2) determining an optimal frequency for resonating the corks instead of the microcapsules, (3) determining the time and acoustic energy required to remove only the corks from the shell. Such studies would also further clarify the mechanism of release under different microcapsule fabrication and triggering conditions, enabling better design of drug release kinetics as desired for a particular therapeutic or clinical application. Similarly, studying the release of different drugs (in particular, by varying drug size from the current small molecules all the way up to drug-loaded nanoparticles) would be useful to understand the scope of potential payloads and

the mechanism of release (cork vibration or cork popping) that predominates. Finally, performing *in vitro* phantom studies using agar gels would help to demonstrate the release of the drug in a tissue mimicking medium, paving the way for *in vivo* models for release to confirm the potential clinical relevance of these triggered release vehicles.